The People's Democratic Republic of Algeria
Ministry of Higher Education and Scientific Research

Dr Yahia Fares University, Medea
Faculty of Technology

Master's dissertation

In Electrical engineering
Specialization:
Renewable Energy in electrotechnics
Electrical Control

Entitled

MPPT-Remora control of a pumping photovoltaic system

Presented by:
Medani Safaa Yasmine
Bachene Youcef

under the guidance and supervision of
Pr. HAMIDIA.Fethia
Dr.ABBADI.Amel

Jun 2024

Acknowledgments

First and foremost, we would like to thank "Allah" for giving us the courage, patience, and strength to carry out this work during all these years of study.

First, we would like to express our deepest gratitude to our professors Pr F. Hamidia, and Dr A.Abbadi for their availability, guidance, invaluable advice, and unprecedented kindness.

We extend our sincere gratitude to the committee members Dr Y.TAMI and Dr A.MORSLI, for dedicating their time and agreeing to examine and evaluate this modest work.

Thanks are also offered to all teachers of the electrical engineering department for their invaluable ..

Especially teacher Bouguirat for her moral and practical support throughout our academic career.

We would like to express our sincere thanks to all those who have helped us from near and far, and to all those who have given us so much of their time.

Dedication

With all my feelings of respect, With the experience of my gratitude, I dedicate, my graduation and my joy

To my paradise, to the apple of my eye, to the source of my joy and happiness, my moon and the thread of hope that lights my way, my other half, Whatever I may say or write, I cannot express my great affection and deep gratitude. I hope never to disappoint you or betray your trust and your sacrifices.

To my Princess Mommy

To the one who made me a woman, my source of life, love and affection, To my support who was always by my side to support and encourage me, to my prince Daddy. Of all fathers, you are the best, and no dedication can express my gratitude and deep love.

To my Superhero Daddy

To my brother Wael, my right-hand man thanks for the support and love that you reserve for me

To my twin, my dear sister Wafaa who shared with me happy memories, experiences, and difficult moments,

You are my luck

To my adorable little sister Anfel who always brings joy and happiness to the whole family

To all my family

The day has come to say I love you ...

Safaa

Dedication

I dedicate this humble work to:

To my dear mother, may Allah protect and preserve her,

To my father, may Allah have mercy on his soul,

To my small and large family,

To all my friends and everyone who has helped me in completing my studies.

Youcef

ملخص

في الوقت الحاضر، تُستخدم الطاقة الشمسية على نطاق واسع في ضخ المياه. تُظهر خاصية الجهد الكهربائي للوحة الكهروضوئية في حالة التظليل الجزئي عدة نقاط محلية، مما يجعل من الصعب على التقنيات التقليدية التقارب إلى النقطة الاعظمية الكبرى، مما يؤد ي إلى فقدان الطاقة.

سوف يقترح هذا العمل طريقة خوارزمية التحسين من ريمورا من أجل تحسين أداء نظام الضخ الكهروضوئي لدينا بحيث يعمل بأقصى طاقة ويضمن الحفاظ على ثبات الجهد الذي يوفره النظام الكهروضوئي لتغذية الآلة غير المتزامنة التي يتم التحكم فيها عن طريق التحكم المباشر في عزم الدوران .أظهرت نتائج المحاكاة فعالية التقنية المقترحة لإيجاد النقطة الاعظمية الكبرى.

الكلمات المفتاحية: المولد الكهروضوئي، تتبع اقصى نقطة بتقنية ريمورا، آلة غير متزامنة، التحكم المباشر في عزم الدوران، التظليل الجزئي.

Abstract

Nowadays, solar energy is widely used to pump water. The power-voltage characteristic of a photovoltaic panel in the case of partial shading shows several local points, and it is difficult for conventional techniques to converge to the global point, resulting in a loss of power.

This work will propose the maximum power point tracking (MPPT) method based on the Remora optimization algorithm to improve the performance of our photovoltaic pumping system so that it operates at its maximum power and ensures that the voltage delivered by the photovoltaic system remains constant, to feed the induction machine which is controlled by direct torque control (DTC). Simulation results demonstrated the effectiveness of the proposed technique for finding the global maximum power point (GMPP).

.**Keywords:** PVG, Remora, MPPT, Induction machine, Direct Torque Control (DTC), GMPP, partial shading.

Résumé

De nos jours, l'énergie solaire est largement utilisée dans le pompage de l'eau. La caractéristique, puissance-tension, d'un panneau photovoltaïque dans le cas d'ombrage partiel montre plusieurs points locaux, il est difficile aux techniques classiques de converger vers le point global entrainant ainsi une perte de puissance.

Ce travail proposera la méthode suivre le point de puissance maximal basé sur l'algorithme d'optimisation Remora afin d'améliorer les performances de notre système de pompage photovoltaïque pour qu'il fonctionne à sa puissance maximale et assure le maintien de la tension délivrée par le système photovoltaïque constante, pour alimenter la machine asynchrone qui est contrôlée par la commande directe du couple. Les résultats de simulation ont démontré l'efficacité de la technique proposée pour trouver le point de puissance global.

Mots-clés : PVG, Remora, MPPT, machine à induction, contrôle direct du couple (DTC), GMPP, ombrage partiel.

Summary

Abstract .....

List of Figures .....

List of Tables .....

Notations and Abbreviations .....

General Introduction 1

Chapter I: Overview of photovoltaic systems

I.1 Introduction 3

I.2 Definition of Photovoltaic 3

I.3 Photovoltaic cell 3

I.4 Principle of photovoltaic effect 3

I.5 Type of photovoltaic cell 4

I.5.1 Mono-crystalline Silicon 4

I.5.2 Poly-crystalline Silicon 5

I.5.3 Amorphous Silicon 5

I.6 Efficiency 6

I.7 Perovskite solar cells 6

I.8 Photovoltaic cell model 7

I.9 The parameters of a photovoltaic cell 8

I.9.1 The short-circuit current Isc 8

I.9.2 The open-circuit voltage Voc 8

I.9.3 The maximum power point mpp 9

I.9.4 The fill factor 9

I.9.5 Efficiency 9

I.10 Electrical characteristic 9

I.10.1 Current-voltage characteristic 9

I.10.2 Power-voltage characteristic 10

I.11 Climatic effect on PV cell 11

I.11.1 Temperature Influence 11

I.11.2 Irradiation influence 13

I.12 Association of PV cells 14

I.12.1 Serial association 14

I.12.2 Parallel association 15

I.12.3 Series-parallel association 15

I.13 Photovoltaic generator 16
I.14 Protection of photovoltaic system 17
I.15 Conclusion 18

II Chapter II: DC-DC Converter and MPPT control

II.1 Introduction 19
II.2 Adapting stage 19
II.3 Definition of the DC-DC Converter (chopper) 20
II.4 DC-DC Converter types 20
II.4.1 Boost Converter 20
II.4.2 Buck Converter 23
II.4.3 Buck-Boost Converter 26
II.5 MPPT control of DC-DC converters 28
II.6 MPPT Control classification 29
II.6.1 The indirect MPPT methods 29
II.6.2 The direct MPPT methods 30
II.7 Tracking the maximum power point of the photovoltaic generator 30
II.8 Conclusion 31

III Chapter III: Modeling of Induction Machine

III.1 Introduction 32
III.2 Description of the induction machine 32
III.3 Induction machine modeling 33
III.3.1 Simplifying assumptions 33
III.3.2 Machine model 33
III.3.3 Setting up equations 34
III.4 Transformation of PARK 37
III.4.1 Electrical equations 39
III.4.2 Magnetic equations 40
III.4.3 Expressions of electromagnetic torque 40
III.5 Choice of reference frame 40
III.5.1 Choice of reference frame orientation 40
III.5.2 Model expressed in the reference frame (**d**,**q**) related to the rotating field 41
III.6 Inverter modelling **43**
III.6.1 Voltages in the phases of the induction machine 44

III.6.2 PWM (Pulse width modulation) voltage inverter....44
III.7 Simulation results with and without inverter....45
III.7.1 IM results without inverter....46
III.7.2 IM results with inverter....47
III.7.3 Comparison of results obtained with and without inverter....49
III.8 Conclusion....49

IV Chapter IV: Direct Torque Control (DTC)

IV.1 Introduction....50
IV.2 Principle of DTC control....51
IV.3 Operation of a three-phase voltage inverter....51
IV.4 Control of stator flux and electromagnetic torque....52
IV.4.1 Stator flux control principle....52
IV.4.2 Principle of electromagnetic torque control....54
IV.4.3 Voltage vector selection....54
IV.5 Estimators....56
IV.5.1 Stator flux estimation....56
IV.5.2 Electromagnetic torque estimation....57
IV.6 Development of the control vector....57
IV.6.1 Flux corrector....57
IV.6.2 Torque corrector....58
IV.7 Development of switching table:....59
IV.8 Advantages and Drawbacks of DTC control....60
IV.8.1 The advantages of Direct Torque Control....60
IV.8.2 Drawbacks of Direct Torque Control....60
IV.9 Simulation results for DTC of IM....60
IV.10 Interpretation of results....62
IV.11 Conclusion....62

V Chapter V: PV pumping system-DTC based on MPPT-Remora

V.1 Introduction....63
V.2 The proposed photovoltaic system....63
V.3 Overview of pumps....64
V.3.1 Positive displacement pump....65
V.3.2 Centrifugal pump....65

V.3.3 Modeling pump 66
V.4 MPPT Based on Remora Algorithm 67
V.5 Remora optimization principle 68
V.5.1 Initialization 68
V.5.2 Free travel (Exploration) 68
V.5.3 Eat thoughtfully (Exploitation) 69
V.6 Proposed ROA-MPPT 70
V.7 Simulation results 71
V.8 Conclusion 77

General Conclusion 78
Appendix .....
REFERENCES .....

List of Figures

Chapter I

Figure I-1: Photovoltaic effect 4
Figure I-2: Mono-crystalline cell 4
Figure I-3: Poly-crystalline cell 5
Figure I-4: Amorphous cell 5
Figure I-5: Electrical circuit of PV cell 7
Figure I-6: Current-voltage characteristic of PV module I=f(V) 10
Figure I-7: Power-Voltage characteristic of PV module P=f(V) 11
Figure I-8: Current-Voltage characteristics of a module for different temperatures I(V) 12
Figure I-9: Power-Voltage characteristics of a module for different temperatures P(V) 12
Figure I-10: Current-Voltage characteristics of a module for different illuminations I(V) 13
Figure I-11: Power-Voltage characteristics of a PV module for different illuminations P(V) . 13
Figure I-12: PV cell in series 14
Figure I-13: PV cell in parallel 15
Figure I-14: Series-parallel association of PV cell 16
Figure I-15: Photovoltaic generator 17
Figure I-16: Modules protected by by-pass and blocking diodes. 18

Chapter II

Figure II-1: Block diagram of PV system with MPPT 19
Figure II-2: Chopper symbol 20
Figure II-3: The equivalent circuit diagram of a boost converter 21
Figure II-4: Electrical diagram of a closed boost converter 21
Figure II-5: Electrical diagram of an opened boost converter 22
Figure II-6: Voltage and current characteristics of the boost converter**.** 23
Figure II-7: The equivalent circuit diagram of a buck converter 24
Figure II-8: Electrical diagram of a closed buck converter 24
Figure II-9: Electrical diagram of an opened buck converter 25
Figure II-10: Voltage and current characteristics of the buck converter. 26
Figure II-11: Electrical diagram of a buck-boost converter 27
Figure II-12: Voltage and current characteristics of the buck-boost converter. 28
Figure II-13: Principle of MPPT control 29

Chapter III

Figure III-1: Three-phase induction machine 32
Figure III-2: Definition of the windings of the three-phase induction machine. 34
Figure III-3: Angular location of axis systems in electrical space (reference d,q). 38

Figure III-4 : Representation of the two-level inverter feeding an IM. 43
Figure III-5: Principle of current control by PWM 45
Figure III-6: Simulation results of an induction machine without PWM 46
Figure III-7: Simulation results of an induction machine with PWM 48

Chapter IV

Figure IV-1: General structure of direct torque control. 50
Figure IV-2:Operating sequences of a two-level voltage inverter 52
Figure IV-3:Evolution of the end of vector φ_s. 53
Figure IV-4:Selection of voltages corresponding to stator flux amplitude control. 58
Figure IV-5:The two-level torque corrector 59
Figure IV-6:Evolution of torque, stator flux and IM-DTC current [(A):open loop,(B):closed loop] 61

Chapter V

Figure V-1: The proposed System 64
Figure V-2: Positive displacement pump 65
Figure V-3: Centrifugal pump 66
Figure V-4: The individual remora 67
Figure V-5: Remora parasitizes on different hosts 68
Figure V-6: Flowchart of ROA. 70
Figure V-7: Impact of partial shading on the P(V) characteristic at T=25 °C 72
Figure V-8: PV power and duty cycle responses of the PV-resistance load controlled by Remora-MPPT without and under shading with MPPT 73
Figure V-9: Flux ,torque and current response without shading 74
Figure V-10:Performance of the photovoltaic system (PV-IM-Pump) using MPPT-Remora without shading 75
Figure V-11: Flux ,torque and current response under PSC 75
Figure V-12:Performance of the photovoltaic system (PV-IM-Pump) using MPPT-Remora under PSC 76

List of Tables

Chapter I

Table I-1: Efficiency of different types of photovoltaic cells 6

Chapter V

Table IV-1: Evolution of the flux and torque quantities 55
Table IV-2: Different strategies of switching table 59
Table IV-3: Control strategy with a two-level hysteresis comparator. 60

Notations And Abbreviations

I	The current supplied by the cell when operating as a generator (A).
V	The terminal voltage of the same cell (V).
I_s	Saturation current (A).
I_{ph}	The photocurrent of the cell depends (A).
R_{se}	Series resistance (Ω) of the photovoltaic cell.
R_{sh}	The shunt resistance (Ω) of the photovoltaic cell.
K	Boltzmann's constant (1.3819×10^{-23}J/K).
T	The effective cell temperature in Kelvin (K).
q	The electron charge (q = 1.6×10^{-19} C)
n	The ideality factor of the junction (1 < n < 2).
I_{sc}	The short circuit current (A).
V_{oc}	The open circuit voltage (V).
P_{mpp}	The maximum power (W).
V_{mpp}	Maximum voltage (V)
I_{mpp}	Maximum current (A)
FF	The fill factor.
ɳ	The efficiency.
P_L	Power of the incident light on the cell.
N_s	Number of series cells.
N_p	Number of parallel cells.
α	The duty cycle.
T_s	The impulse period.
L	The inductor of the DC-DC converter.
K	The switch of the DC-DC converter.
D	The diode of the DC-DC converter.
$C_1; C_2$	The two capacitors of the DC-DC converter.
V_i	The input voltage on the DC-DC converter.
V_o	The output voltage on the DC-DC converter.
I_i	The input current on the DC-DC converter.
I_o	The output current on the DC-DC converter.
ω_s	The stator pulsation (rad/sec).
ω_r	The rotor pulsation (rad/sec).
P_n	The number of pole pairs.
Ω_s	Slip speed.
V_{sa}, V_{sb}, V_{sc}	Simple stator voltages (V).

V_{ra}, V_{rb}, V_{rc}	Simple rotor voltages (V).
φ_s	The stator flux (Wb).
φ_r	The rotor flux (Wb).
R_s	Stator resistance (Ω).
R_r	Rotor resistance (Ω).
I_s	Stator current (A).
I_r	Rotor current (A).
L_s, L_r	stator and rotor inductance matrices (H).
M_{sr}, M_{rs}	Mutual inductance matrices between stator and rotor (H).
l_s, l_r	Stator and rotor inductance coefficients (H).
m_s, m_r	Maximum values of mutual inductance between stator and rotor (H).
T_e	Electromagnetic torque (N.m).
T_R	Resistive torque (N.m).
J	The moment of inertia of the rotating parts (Kg.$m2$).
f	Coefficient of friction (N.m sec/rad).
$P(\theta)$	Park's transformation matrix.
V_{sdq0}, V_{rdq0}	The stator and rotor voltage in the (d, q,0) reference frame.
I_{sdq0}, I_{rdq0}	The stator and rotor currents in the (d, q, 0) frame.
L_{s0}, L_{r0}	Coefficient of stator and rotor zero sequence inductance.
P_{elec}	Electrical power (W).
θ_s	Stator position (rad).
θ_r	Rotor position (rad).
d	Direct axis index.
q	Quadrature axis index.
o	Homopolar axis index.
σ	Coefficient of magnetic dispersion.

GPV	Photovoltaic generator.
MPPT	Maximum Power Point Tracking.
AC	Alternating current.
DC	Direct current.
IM	Induction machine
PWM	Pulse width modulation.
ROA	Remora optimization algorithm
GMPP	Global maximum power point
LMPP	Local maximum power point
WOA	Whale optimization algorithm
SFO	Swordfish optimization algorithm
PSC	Partial shading condition

General Introduction

General introduction

Energy production is a major challenge for the future. Energy needs are constantly increasing. What's more, emerging countries will need more and more energy to drive their development.

The move towards renewable energies offers a promising solution to energy problems. Our future energy needs must be met by combining sustainable technologies with minimal environmental impact and renewable sources such as solar energy, which is one of the viable solutions. It has the potential to generate electricity free of charge and is seen as the way forward to a cleaner, sustainable energy future that is resilient to climate change.

Since the first installations at the end of the 1970s, photovoltaic pumping systems have played a major role in photovoltaic energy application projects, and today they are among the most significant applications of photovoltaic energy. This can be attributed mainly to the fact that connecting such remote sites to the electricity grid is not economically feasible.

Induction machines are widely used in applications requiring considerable power. They are characterized by their robustness, durability, and ability to offer a wide range of speed variations. To obtain performance similar to that of a DC machine, it is essential to achieve effective decoupling between flux and electromagnetic torque. With this in mind, the DTC (Direct Torque Control) control technique was developed, offering numerous advantages such as natural decoupling, elimination of the PWM (Pulse Width Modulation) block, excellent torque response, and much more. Unlike other control methods, DTC does not aim to determine the voltages to be applied to the machine, but rather to find the best switching state for the inverter to meet the user's requirements.

The characteristics of the PV module are considerably influenced by environmental conditions and shading phenomena, as multiple peaks are observed in the PV characteristics, with a global peak (GMPP) and other local peaks (LMPPs). Consequently, many studies have been proposed to combat the impact of shading phenomena to capture the maximum available power from the PV system in the best possible way. The efficiency of PV systems can then be improved using methods known as Maximum Power Point Tracking (MPPT) techniques. These methods, as their name suggests, track the MPP over time that the panel is capable of producing.

Despite the strengths of the many traditional optimization techniques (P&O; INC) none of them can solve all optimization problems. for this reason, Human beings have always used nature as a source of inspiration for solving complex problems, given its highly diverse, dynamic, adaptive, and robust phenomena. Nature always finds the optimal solution to solve its problems and maintains the perfect balance between its components. Bio-inspired algorithms are stochastic meta-heuristics for optimization, inspired by different phenomena in the natural world, particularly by the social behavior of animals and insects, the evolution of species, or the intelligent behavior of certain organisms.

The objective of our work is to propose one of the very promising meta-heuristics algorithms called Remora. This technique is utilized to demonstrate the effectiveness of the proposed method in achieving the Global Maximum Power Point (GMPP).

This study is discussed in five chapters:

The first chapter addresses the study of PV cells, the principle of their work, their mathematical modelization, and their different characteristics to simulate it on MATLAB.

In the second chapter, we will present a preliminary study of the main DC-DC converters, focusing on the Boost converter. The algorithms to find the maximum power point for the photovoltaic source are provided in this chapter as well.

The third chapter will be devoted to modeling the induction machine fed by an PWM. voltage inverter, using the Park transformation (three-phase to two-phase transition), all of which will be simulated in MATLAB-SIMULINK.

In the fourth chapter, we will present direct torque and flux control and the application of this technique to an induction machine.

In the last chapter, we will present a pumps overview. Then we will propose a new MPPT algorithm using the Remora optimization method to improve the performance of the PV-IM-Pump hybrid system. Followed by simulation results.

Finally, ending up with a general conclusion discussing the obtained results and the system's effectiveness.

Chapter I:

Overview of photovoltaic systems

I.1 Introduction

Renewable energy comes from natural resources such as the sun, also called green energies or clean energies, in contrast to energy derived from finite resources based on fossil fuels like coal and oil which sooner or later will be exhausted.

The use of photovoltaic systems is becoming the optimal solution to meet energy needs, especially with the continuous increase in demand for electrical energy over the years.

The photovoltaic cell transforms light directly into electrical energy based on the photovoltaic effect. In this chapter, we explained photovoltaic cells and the different generalities of photovoltaic systems and their performances.

I.2 Definition of Photovoltaic

The term «photovoltaic», often abbreviated by the letters PV, was formed from the words «photo» is a Greek word meaning light and «Volta» is the name of the Italian physicist Alessandro Volta, who invented the electrochemical battery in 1800.

The photovoltaic effect was discovered by the physicist French Edmon BECQUEREL in 1839. **[AGH 22]**

I.3 Photovoltaic cell

The photovoltaic cell is an electronic component made from semiconductor materials that exposed to sunlight (photons) generates an electrical voltage. This process is called the photovoltaic effect. **[AGH 22]**

A PV cell is made from two layers of silicon doped P (doped by boron) and the other doped N (doped by phosphorus) thus creating a PN junction with a potential barrier. **[YEK 23]**

I.4 Principle of photovoltaic effect

A photovoltaic effect is a physical phenomenon that can produce electricity by a direct process, when the cell is exposed to sunlight (excited) and the photons are absorbed by the semiconductor, their energy is transmitted to the atom at the PN junction so the electrons (charge N) and holes (charge P) then create a potential difference between the two layers, here is the principle of operation of a photovoltaic cell. **[YEK 23]**

The voltage generated can vary between 0.3 V and 0.7 V depending on the material used and its arrangement as well as the temperature and aging of the cell.

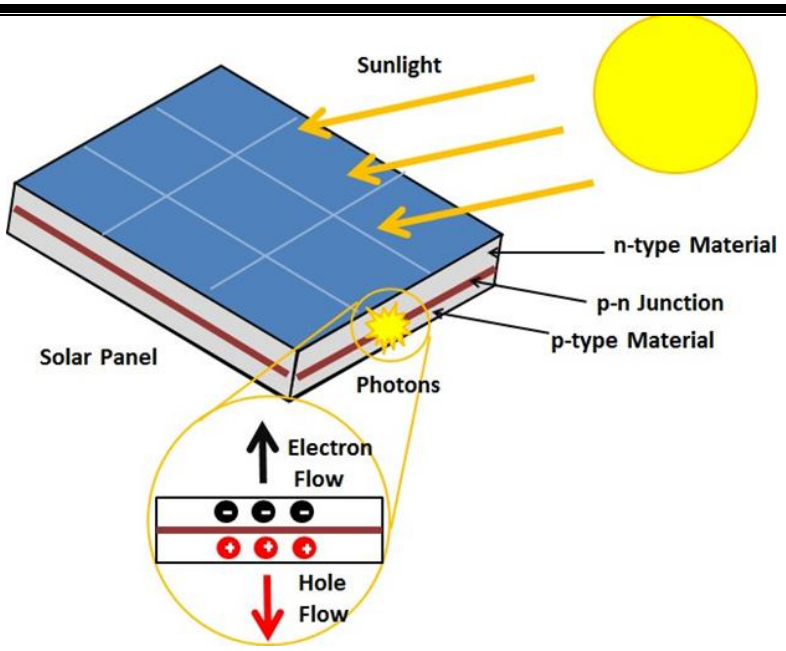


Figure I-1: Photovoltaic effect

I.5 Type of photovoltaic cell

There are different types of PV cells and different generations, they are made from semiconductor materials (monocrystalline silicon, polycrystalline silicon, amorphous silicon).

The efficiency of a semiconductor material is of great importance because, on an equal surface, it can be of different interest from one material to another. They are many, but silicon, present in large quantities on the Earth's surface is the second most abundant element after oxygen and is the most widely used. **[GRA 18]**

I.5.1 Mono-crystalline Silicon

Monocrystalline silicon also called single-Crystal Silicon, is the result of molten silicon cooling. Once solidified, it becomes a uniform crystal that is cut into thin slices to form the photovoltaic cell. Monocrystalline cells are recognized by their very dark blue color, without any trace of crystals or other. **[DAN 19]**



Figure I-2: Mono-crystalline cell

I.5.2 Poly-crystalline Silicon

Globally, in the world, it is the most used type of photovoltaic cell, because offering the best price/quality until now compared with monocrystalline silicon. These cells are composed of crystals oriented in different directions.

To obtain polycrystalline silicon also known as Multicrystalline, the silicon is melted in a square metal mold. The color of this type of cell is blue and dotted with patterns left by the crystals. This feature allows us to recognize this photovoltaic cell easily. **[DAN 19]**

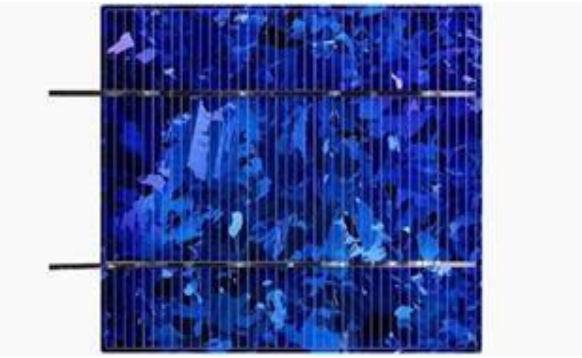


Figure I-3: Poly-crystalline cell

I.5.3 Amorphous Silicon

They are the cheapest photovoltaic cells to make. They are much finer than monocrystalline or crystalline polys. It is mainly used for low-power equipment.

Amorphous silicon is obtained from silicon gas. This gas is vaporized on a support, made of glass, flexible plastic, or metal, using a vacuum spraying process. These photovoltaic cells are dark gray**. [GRA 18]**

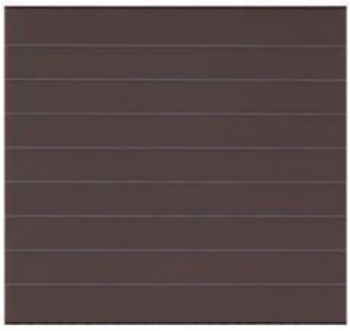


Figure I-4: Amorphous cell

I.6 Efficiency

Cell type	Efficiency	Lifetime	Characteristics
Mono-crystalline Silicon	17-22 %	20 to 30 years	• Very good performance. • High cost. • Low efficiency under reduced illumination.
Polycrystalline Silicon	16-18 %	20 to 30 years	• Performance/price ratio. • Low efficiency under reduced illumination.
Amorphous Silicon	6 -11 %	(+/- 10 years)	• Operate with low illumination • Low manufacturing cost

Table I-1: Efficiency of different types of photovoltaic cells **[SIT 20]**

I.7 Perovskite solar cells

Perovskite solar cells have a higher energy conversion efficiency than other types of solar cells. They have achieved efficiencies of more than 20 to 25 percent in laboratory settings. Perovskite solar cells have several advantages, including high absorption, good energy conversion efficiency, long carrier lifetime, tunable bandgap width, and relatively low manufacturing cost. These features make them an interesting emerging photovoltaic technology.

While perovskite solar cells have potential in terms of efficiency, silicon solar cells are currently more stable and mature for commercial applications. The disadvantage of perovskite cells is their instability and low resistance to external agents like water and temperature. However, promising research is currently underway, which should make this type of cell more attractive soon. **[WEN 24]**

One area of particular interest in photovoltaic research is combining perovskite with another technology, typically silicon, to improve cell efficiency. A cell that combines perovskite

with silicon can achieve higher efficiency over a wider range of wavelengths. In June 2018, these tandem cells achieved an efficiency of 25.2% for a perovskite-silicon cell.

In the future, as technology improves, perovskite solar cells may make greater breakthroughs in energy efficiency. **[DOU 24]**

I.8 Photovoltaic cell model

Under illumination, the photovoltaic cell can be represented by an equivalent electrical circuit schematized by the figure (I-5)

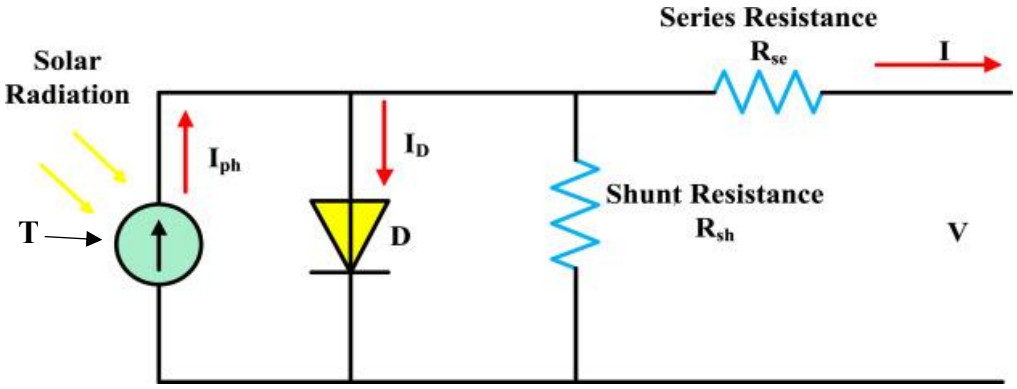


Figure I-5: Electrical circuit of PV cell

The photovoltaic cell is represented by the "standard" model with one diode, it corresponds to a current generator $\mathbf{I_{ph}}$ connected in parallel with a diode. It comprises a series resistor $\mathbf{(R_{se})}$ and a shunt resistor $\mathbf{(R_{sh})}$. These resistors have a certain influence on the cell's $\mathbf{I = f(V)}$ characteristic.

The $\mathbf{R_{se}}$ and $\mathbf{R_{sh}}$ resistors allow for losses due to manufacturing defects.

$\mathbf{R_{se}}$: represents the various contact and connection resistors.

$\mathbf{R_{sh}}$: characterizes the leakage currents due to diode and the edge effects of the junction

The current-voltage characteristic is expressed by the relationship **[HAI 17]**

$$\mathbf{I = I_{ph} - I_s\left(exp^{\frac{q(V+(R_{se}I))}{nKT}} - 1\right) - \frac{(V+(R_{se}I))}{R_{sh}}} \qquad \mathbf{(I.1)}$$

With

$\mathbf{I_s}$: Saturation current (A).

K: Boltzmann's constant (1.3819×10^{-23} J/K).

T: The effective cell temperature in Kelvin (K).

q: The electron charge ($q = 1.6 \times 10^{-19}$ C)

n: The ideality factor of the junction ($1 < n < 2$).

I: The current supplied by the cell when operating as a generator.

V: The terminal voltage of the same cell.

$\mathbf{I_{ph}}$: The photocurrent of the cell depends on the illumination and temperature or short-circuit current.

I.9 The parameters of a photovoltaic cell

The performance of a photovoltaic cell is characterized by a certain number of key parameters. The value of these parameters varies more or less according to a certain number of external parameters, including the cell lighting level and temperature.

I.9.1 The short-circuit current I_{sc}

This value represents the current generated by an illuminated cell when it is short-circuited (connected to itself). This is the highest value of the current generated by a cell. It is produced under short-circuit conditions: V = 0. **[HAI 17]**

In the ideal case **($\mathbf{R_{se} = 0}$, $\mathbf{R_{sh} = \infty}$)**.

$$\mathbf{I_{sc} = I_{ph} - I_s\left(exp^{\frac{q(R_{se}\, I_{sc})}{nKT}} - 1\right) - \frac{(V+(R_{se}\, I))}{R_{sh}}} \quad \textbf{(I.2)}$$

For most cells (with low series resistance), the term can be neglected:

$$\mathbf{I_s\left(exp^{\frac{q(R_{se}\, I_{sc})}{nKT}} - 1\right)} \quad \textbf{(I.3)}$$

And

$$\mathbf{\frac{V+(R_{se}\, I)}{R_{sh}}} \quad \textbf{(I.4)}$$

the approximate expression for the short-circuit current is :

$$\mathbf{I_{sc} = I_{ph}} \quad \textbf{(I.5)}$$

I.9.2 The open-circuit voltage V_{oc}

The open-circuit voltage is the maximum voltage generated by the photovoltaic cell. It represents the voltage measured at the terminals of the cell under illumination without a load circuit when the current flowing through the cell is zero**.**

It can be calculated from the relationship as follows **[HAI 17]**

$$\mathbf{0 = I_{ph} - I_s\left(\exp\frac{qV_{oc}}{nKT} - 1\right) - \frac{V_{oc}}{R_{sh}}} \quad \textbf{(I.6)}$$

In the ideal case, the value of $\boldsymbol{V_{oc}}$ is

$$\mathbf{V_{oc} = V_T.\left(\ln\left(\frac{I_{ph}}{I_s}\right) + 1\right)} \quad \textbf{(I.7)}$$

With $\mathbf{V_T = \frac{nKT}{q}}$ is known as thermal voltage

I.9.3 The maximum power point $\mathbf{P_{mpp}}$

This is the relationship between maximum voltage $\mathbf{V_{mpp}}$ and maximum current $\mathbf{I_{mpp}}$ under standard sunshine conditions (Temperature= 25° and Illuminance =1000 w/ m^2 **[LYU 24]**

it is given by the relationship $\mathbf{P_{mpp} = V_{mpp}.I_{mpp}}$ **(I.8)**

I.9.4 The fill factor

The fill factor is an important metric used to evaluate the performance and electrical characteristics of a photovoltaic cell. It is defined as the ratio between the maximum power and the product of the cell's current ($\mathbf{I_{sc}}$) and voltage ($\mathbf{V_{oc}}$), **[AGH 22]** which can be expressed as follows:

$$\mathbf{FF = \frac{P_{mpp}}{I_{sc}.V_{oc}} = \frac{I_{mpp}.V_{mpp}}{I_{sc}.V_{oc}}} \quad \textbf{(I.9)}$$

I.9.5 Efficiency

It is defined as the ratio between the maximum power produced by the cell $\mathbf{P_{mpp}}$ and the power of the incident light on the cell $\mathbf{P_L}$. **[AGH 22]**

$$\eta = \frac{\mathbf{P_{mpp}}}{\mathbf{P_L}} \quad \textbf{(I.10)}$$

I.10 Electrical characteristic

I.10.1 Current-voltage characteristics

The photovoltaic cell has a non-linear $\boldsymbol{I}(\boldsymbol{V})$ characteristic, the electrical power delivered by

a photovoltaic cell is the product of the voltage by the current it generates. These two quantities, current and voltage, depend at the same time on the electrical properties of the cell but also on the electric charge at its terminals. They are synthesized in a graph called characteristic current-voltage. At a fixed temperature and illumination, the current/voltage characteristic of a cell looks like the following:

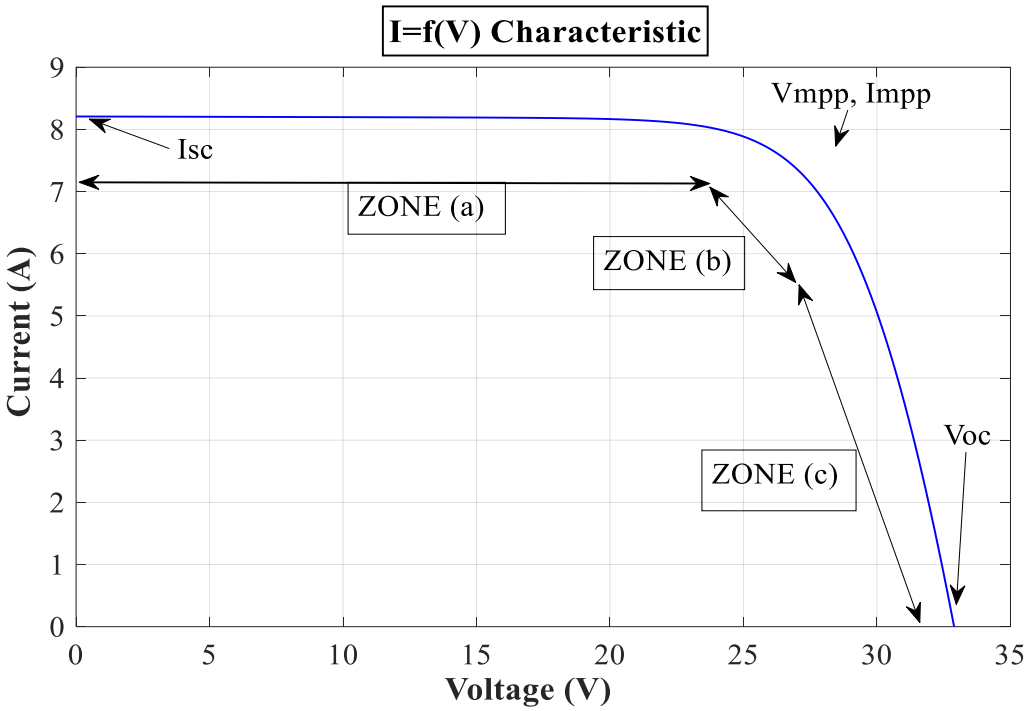


Figure I-6: Current-Voltage characteristic of PV module I=f(V)

The characteristic is divided into three parts:

- **Zone (a):** where the current remains constant, the photovoltaic generator operates as a current generator.
- **Zone (b):** represents the preferred region for generator operation, where the optimum point (characterized by maximum power) can be determined.
- **Zone (c):** distinguished by a current variation corresponding to an almost constant voltage, in which case the generator can be likened to a voltage generator.

I.10.2 Power-voltage characteristic

To determine the power output of a solar cell, one can simply multiply the current (**I**) flowing through it by the voltage (**V**) across it. This results in the expression for power (**P**), which is represented by the formula $\mathbf{P = V.I}$

By applying this formula and mapping the resulting values of **P** against **V** on a graph, a clear representation of the relationship between the two can be obtained. In this diagram **P = f(V).**

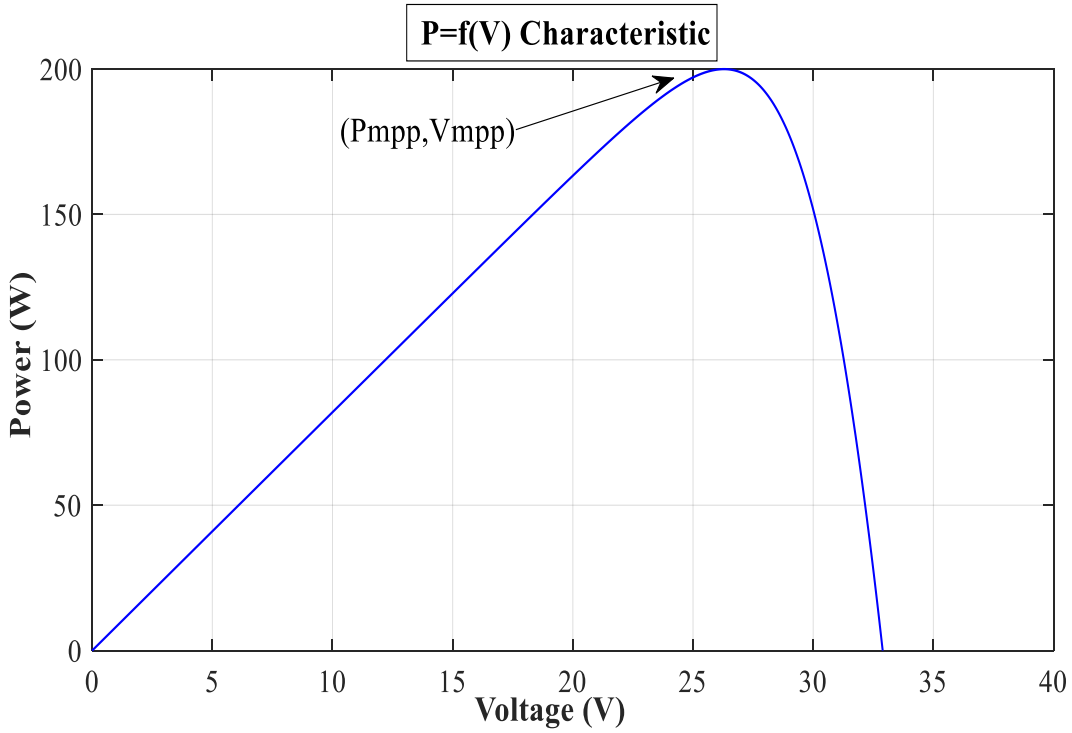


Figure I-7: Power-Voltage Characteristic of PV module P=f(V)

I.11 Climatic effect on PV cell

The characteristic of a PV cell is directly dependent on illumination and temperature

I.11.1 Temperature Influence

Temperature is an important parameter in the behavior of cells. Here the illumination is fixed at (G=1000 W/m²).Figure (I-8) show the current-voltage I(V) characteristics for different temperatures (T=0∘C,25∘C,50∘C,75∘C). The open-circuit voltage decreases with increasing temperature, while the short-circuit current increases slightly with increasing temperature so the influence of temperature on I_{sc} can be neglected in most cases.

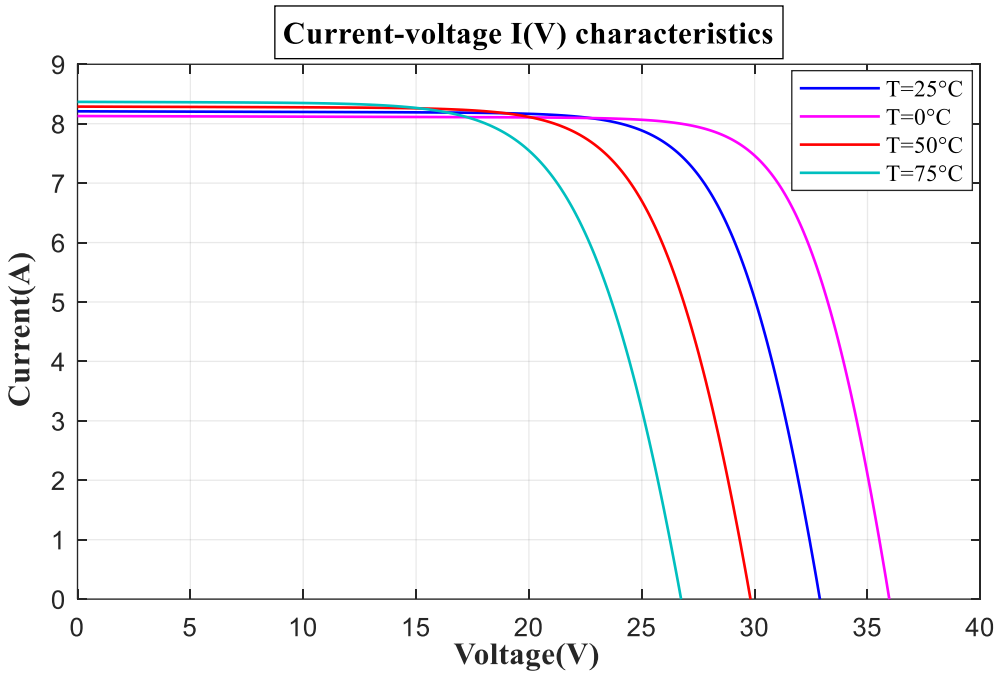


Figure I-8: Current-Voltage characteristics of a module for different temperatures I(V)

In Figure I-9, the maximum power decreases as open-circuit voltage decreases due to an increase in temperature. It can be concluded that temperature has a negative influence on open-circuit voltage.

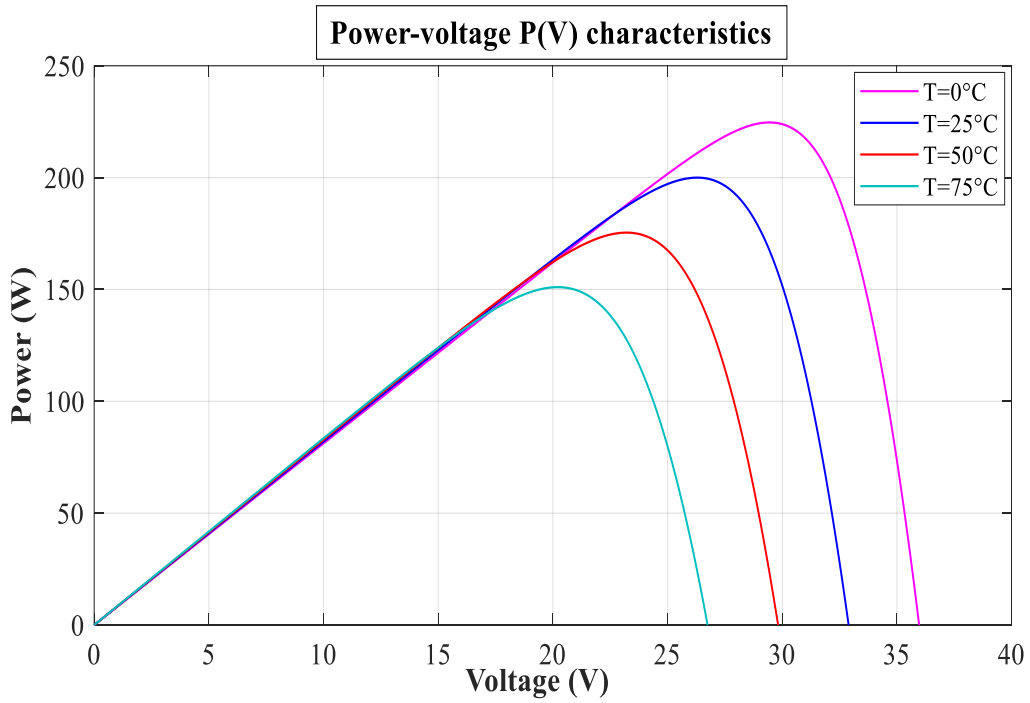


Figure I-9: Power-Voltage characteristics of a module for different temperatures P(V)

I.11.2 Irradiation influence

The main source of energy for PV modules is radiation from the sun. The amount of solar radiation that a PV module receives depends on various factors such as the module's angle and orientation, the location's latitude and longitude, and the time of day and year. Figures (I-10, I-11) show the influence of different illuminances on the characteristic I = f(V) and P = f(V). At a constant temperature (T = 25∘C),

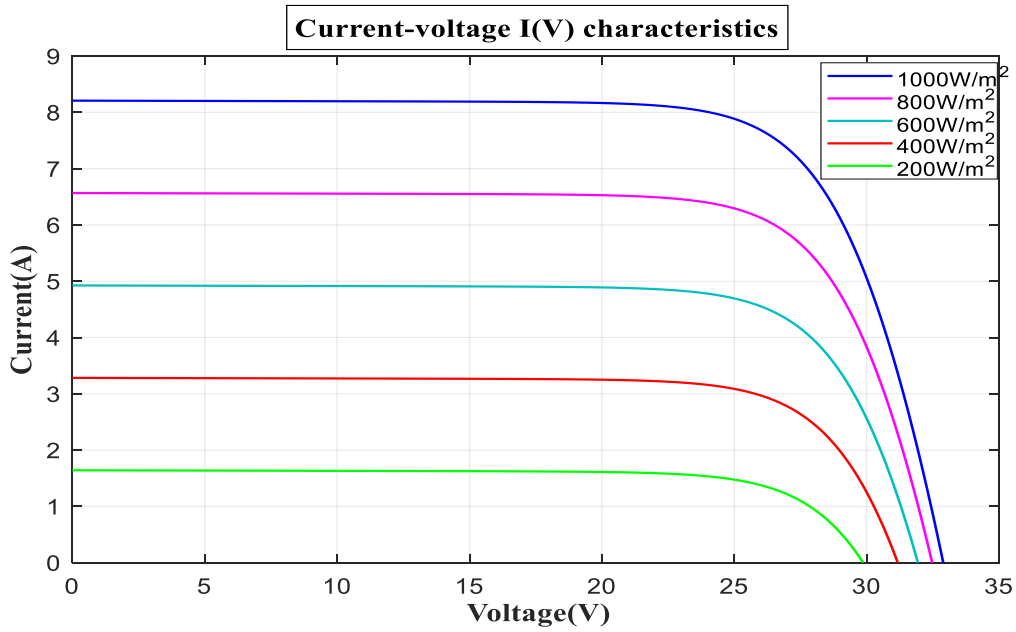


Figure I-10: Current-Voltage characteristics of a module for different illuminations I(V)

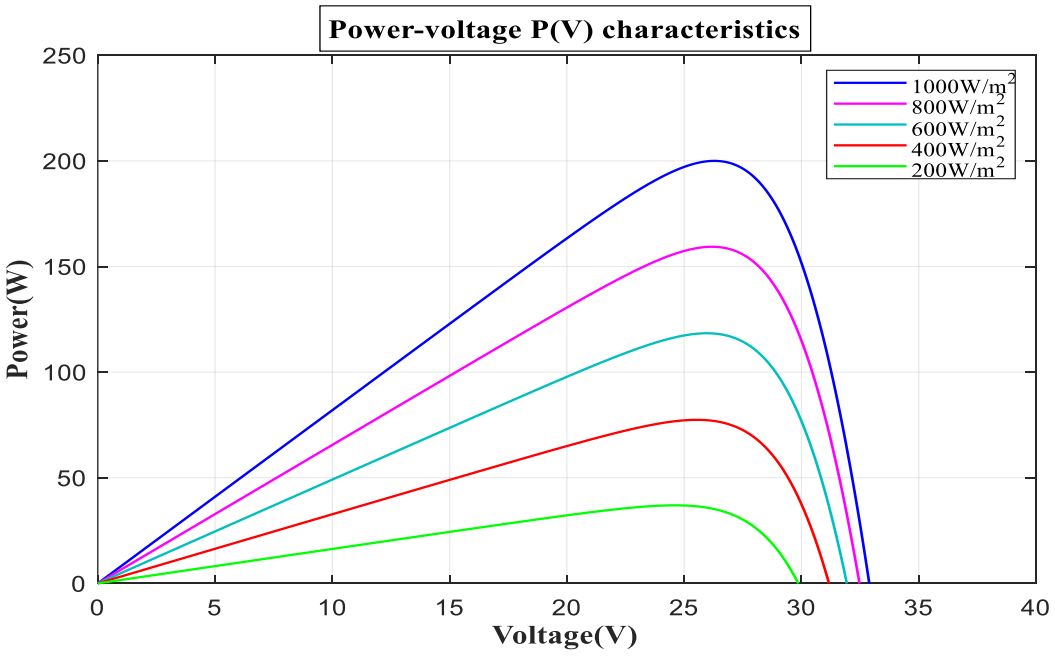


Figure I-11 : Power-Voltage characteristics of a PV module for different illuminations P(V)

The increase in irradiation causes an increase in the maximum power as a current increase significantly but the voltage changes very little. Because The photocurrent is directly proportional to the irradiance level, while the open-circuit voltage is a logarithmic function and is usually ignored.

Temperature and irradiation are therefore the two main parameters that will change the characteristics of a PV generator. These two parameters should therefore be carefully considered in the sizing of PV installation.

I.12 Association of PV cells

I.12.1 Serial association

A combination of N_s cells in series increases the voltage of the photovoltaic module. The cells are then crossed by the same current and the characteristic resulting from the serial grouping is obtained by adding the elementary voltages of each cell. The equation summarizes the electrical characteristics of a series of N_s cells. **[MAH 21]**

$$V_{oc}' = N_s \times V_{oc} \quad \textbf{(I.11)}$$

$\mathbf{V_{oc}}$: open circuit voltage

$\mathbf{N_s}$: number of series cells

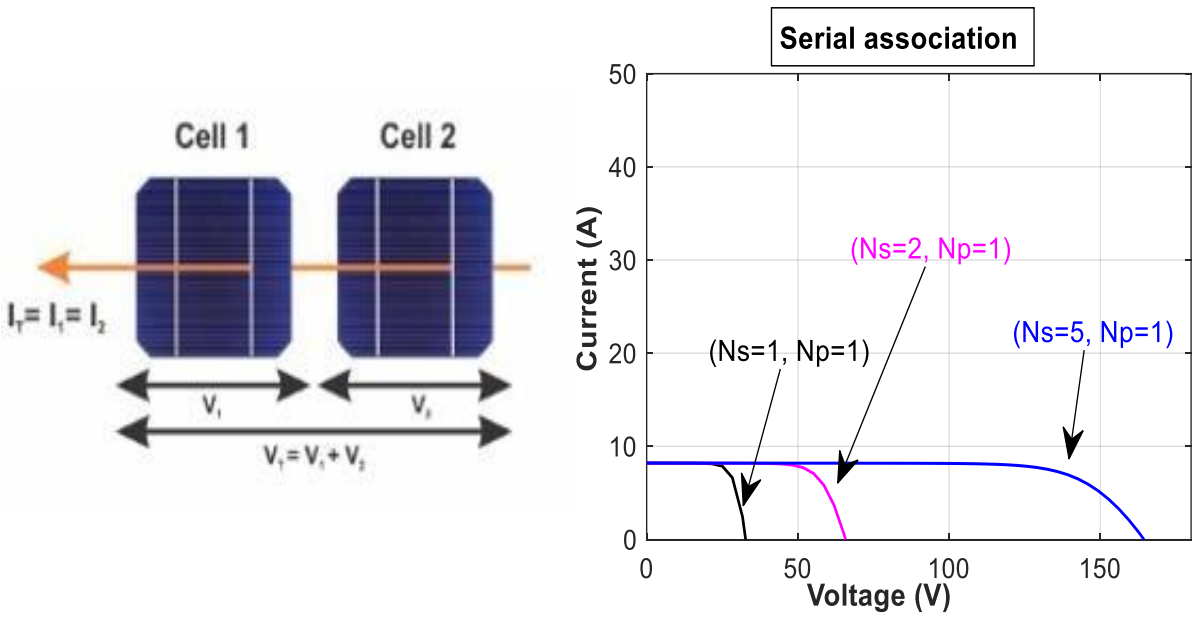


Figure I-12: PV cell in series

I.12.2 Parallel association

A parallel association of N_p cells is possible and allows to increase the output current of the module thus created. In a group of identical cells connected in parallel, the cells are subjected to the same voltage, and the characteristic resulting from the group is obtained by the addition of currents, The equation in turn summarizes the electrical characteristics of a parallel association of N_p cells.

$$I_{sc}' = N_p \times I_{sc} \quad \text{(I.12)}$$

I_{sc} : short circuit current

N_p: number of parallel cells

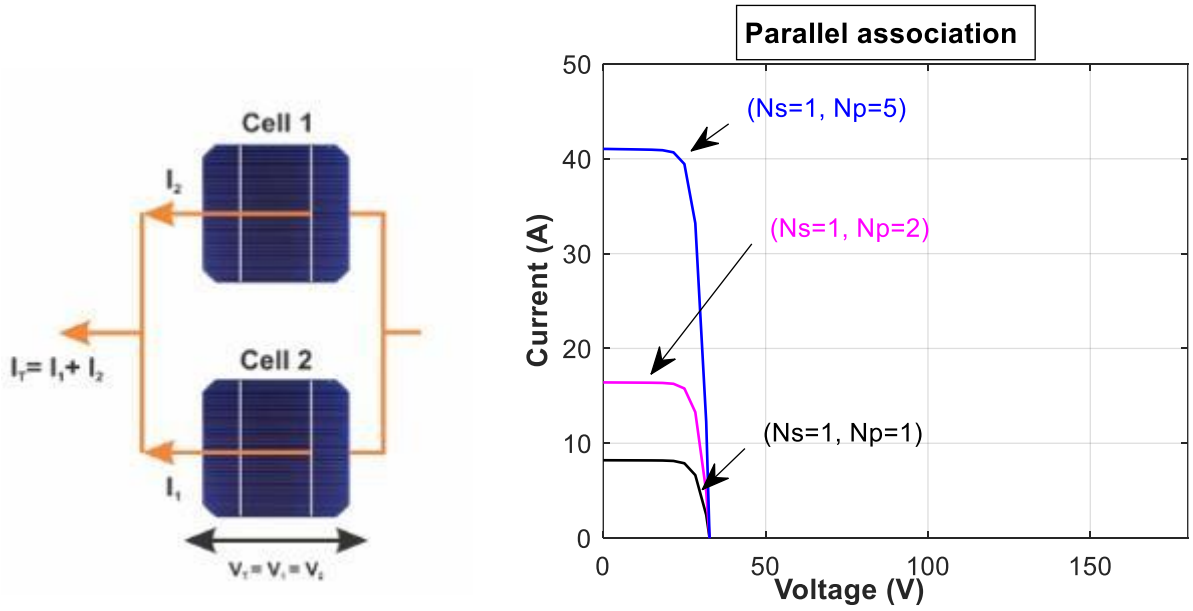


Figure I-13: PV cell in parallel

I.12.3 Series-parallel association

Connecting several cells in series forms a cell string, which increases the voltage for the same current while assembling several cell strings in parallel forms a module, which increases current and maintains voltage. An association of several modules in the same plane is called a panel, and the assembly of several panels in rows of series and parallel panels forms a photovoltaic field. **[MAH 21]**

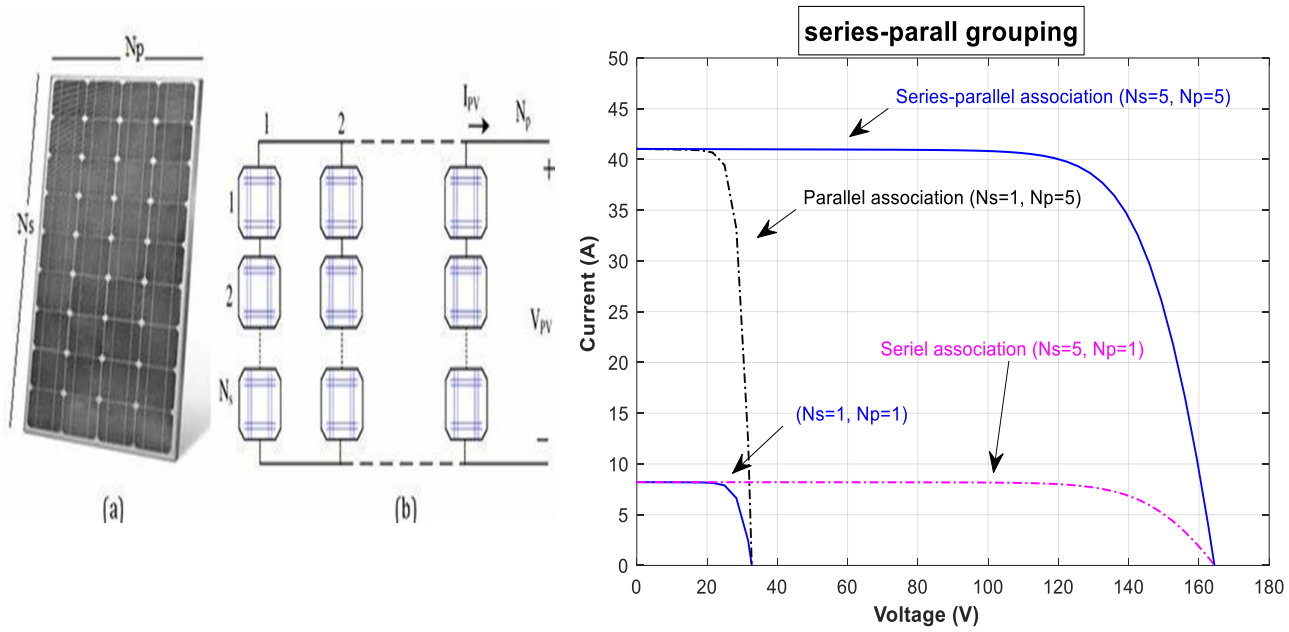


Figure I-14: Series-parallel association of PV cell

Note:

To function optimally a PV module, it is important to select the most identical cells possible when making a module, that is, the cells series-parallel (N_s, N_p) all behave in the same way. They must come from the same technology, the same operating conditions (illumination, temperature, ageing and inclination).

I.13 Photovoltaic generator

To produce more power, solar cells are assembled to form a module and modules are assembled in PV array.

By associating the PV modules in series (sum of the voltages of each cell) or in parallel (sum of the intensities of each cell), a PV generator can be formed as needed. Thus, for N_s module in series, constituting branches themselves N_p in parallel, the available output power of the PV generator is given by: **[MAH 21]**

$$P_{pv} = N_s \times V_{pv} \times N_p \times I_{pv} \quad \textbf{(I.13)}$$

P_{pv}: the available power of the PV array output

V_{pv} : the voltage at the output of the PV array

I_{pv} : the output current of the PV array

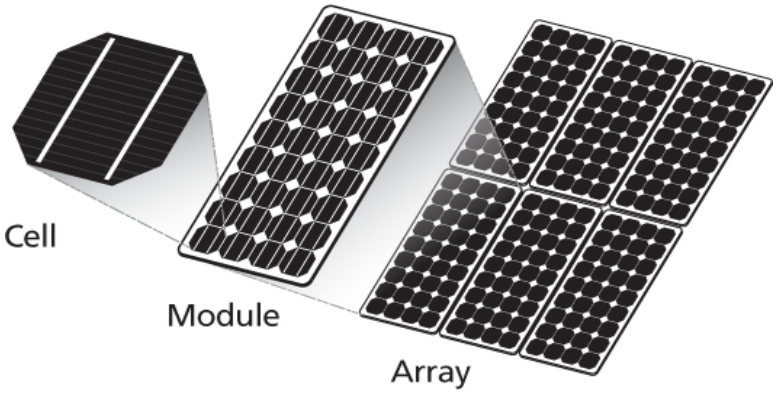


Figure I-15: Photovoltaic generator

I.14 Protection of photovoltaic system

The protection of PV systems is important to ensure the continuity in service, increase its lifespan, in particular by avoiding destructive breakdowns related to the association of cells, their functions, and protect PV panels against lightning.

Solar panels are often subjected to environmental conditions, such as temperature variations, humidity, strong winds, bad weather and the risk of vandalism or theft.

When installing solar panels, it is important to ensure that they are able to withstand extreme weather conditions such as high winds. Additionally, a secure fastening system should be put in place to prevent the panels from becoming detached or falling off, which could cause damage to property or individuals. Electrical connections should also be protected using waterproof connectors and suitable cables to prevent short circuits or damage caused by moisture. Lightning and overvoltage protection devices should be utilized to prevent damage from electrical discharges. Furthermore, security measures should be taken to prevent vandalism or theft, such as installing security fencing, surveillance cameras or alarms. Effective protection measures ensure the safety of people and property while also ensuring reliable and stable energy production over the long term.

The main enemy of PV systems is darkness, whether it is shadow or night time. The key to both of these impacts::

- Hot-spot phenomenon: is a phenomenon that occurs when a shadow on one of the photovoltaic panel's cells or on part of it (the main cause is the shading effect).

Shading in one part of the module causes it to function as a receiver, so then the current of the string comes to this panel which results in an explosion or a combustion of this panel. The ideal solution to eliminate this phenomenon is bypass diode. **[MAH 21]**

- Overnight to avoid battery discharge in the reverse direction is important to place a blocking diode, blocking diode prevents current from flowing in the reverse direction. It is an essential component in solar panels that stops your solar array from discharging at night or when the batteries are full. Blocking diodes are also known as ‘rectifiers' because they allow current to flow in one direction and prevent the reverse flow. **[SIT 01]**

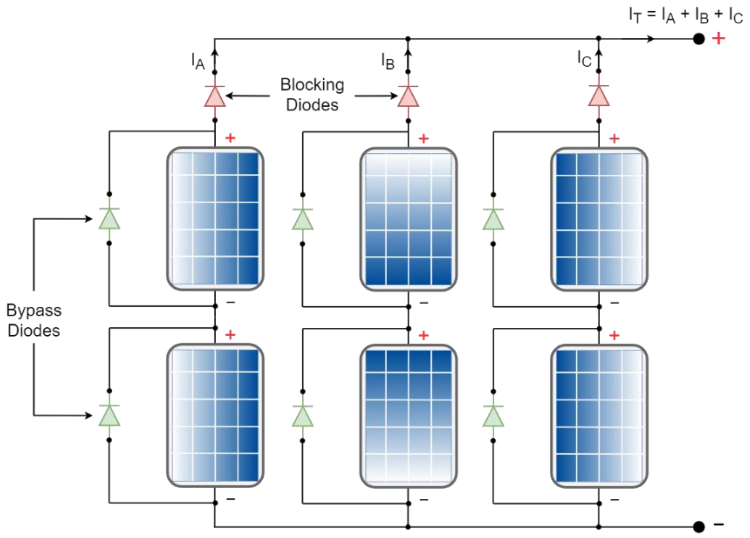


Figure I-16: Modules protected by by-pass and blocking diodes.

I.15 Conclusion

In this chapter, we have presented the principle of converting solar energy directly into electrical energy by photovoltaic effect and the various technologies of PV cells, as well as the mathematical model of photovoltaic cells with different parameters that can defined by the current-voltage I(V) and power-voltage P(V) characteristics were strongly influenced by climatic conditions, particularly solar irradiation and temperature.

We finished this part with the different methods of combining cells to create a photovoltaic generator and the essential safety measures to ensure the optimal performance of the PV system.

In the next chapter, we will present a study of DC-DC converters (choppers) and their MPPT control to find the point at which the power of the photovoltaic generator is at its maximum.

Chapter II:

DC-DC Converter And MPPT Control

II.1 Introduction

The current-voltage characteristic of a photovoltaic generator GPV is non-linear and varies as a function of irradiance and temperature. It is important to note that the generator's operating point is directly impacted by the load being supplied. To achieve maximum power output, it is necessary to insert an adapting stage between the power supply and the load.

To optimize solar power generation an algorithm known as MPPT (Maximum Power Point Tracking) is used. The principle of this control is to automatically adjust the duty cycle **α** of a DC-DC converter to maximize the power output of the PV panel.

This chapter presents the MPPT control algorithm. By understanding the operating principles of these converters, we can gain a better understanding of how MPPT algorithms work to optimize solar power generation.

II.2 Adapting stage

When connecting a photovoltaic generator to a DC load directly, it is important to find the operating point that intersects the I(V) characteristic of the generator and the I(V) characteristic of the load. To achieve this, a DC-DC converter can be placed between the generator and the load, which is controlled by a maximum power point (MPP) tracker. This converter is known as a maximum power point tracker (MPPT) and is managed by a PPM tracker algorithm. As illustrated in Figure (II-1), the input of the DC-DC converter is the photovoltaic array (GPV), and the output is the load. The main function of the MPPT is to ensure that the PV array operates at its PPM, thus extracting the maximum available power. **[SAD 23]**

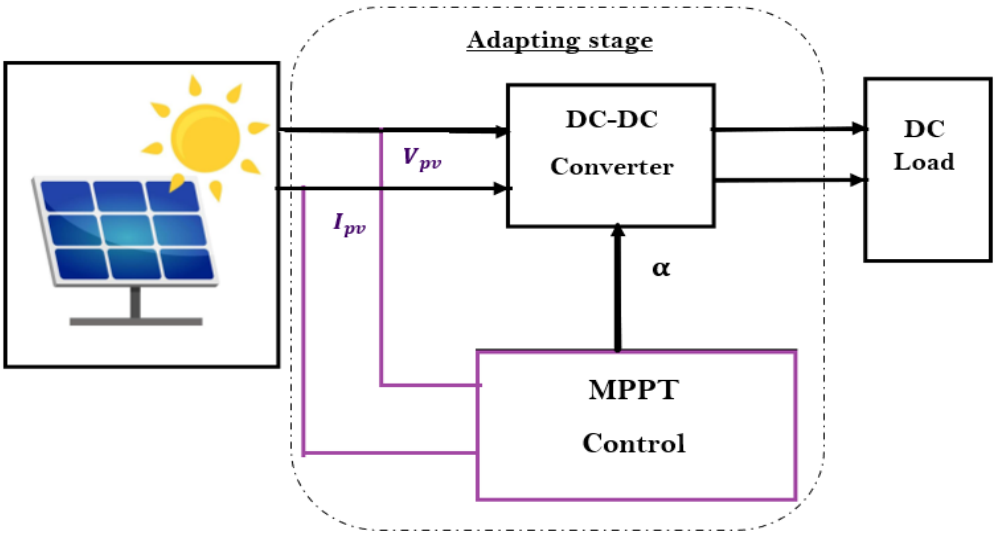


Figure II-1: Block diagram of PV system with MPPT

II.3 Definition of the DC-DC converter (chopper)

Choppers are static DC-DC converters that convert a fixed voltage source into a variable DC voltage. They consist of capacitors, inductors, and switches. In the ideal case, these components consume no power, resulting in high efficiency for choppers.

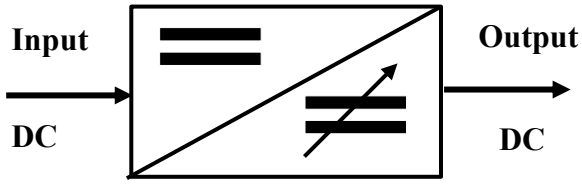


Figure II-2: Chopper symbol

II.4 DC-DC Converter types

There are several DC-DC converter topologies. In practice, they are characterized by two main topologies: isolated topology and Fly Back topology.

Isolated topology, requires an isolation transformer operating at high frequency and it is mainly used for switch-mode power supplies. **[FOR 17]**

The Fly Back topology, on the other hand, is non-isolated and does not use an isolation transformer, is mainly used in DC machine drives and the chains of control systems and photovoltaic power supply systems. In photovoltaic (PV) applications grid-coupled systems often use these types of topologies when electrical isolation is preferred for safety reasons.

Non-isolated topology converters are classified into three categories:

- Buck
- Boost
- Buck-Boost

II.4.1 Boost Converter

The boost chopper or step-up chopper, is shown in (figure II-3), it is generally used to convert a low input voltage to a high output voltage. It consists of a source of DC input voltage (Vi), an inductor (L), a switch (K), a diode (D), and two capacitors (C_1 and C_2). **[FOR 17]**

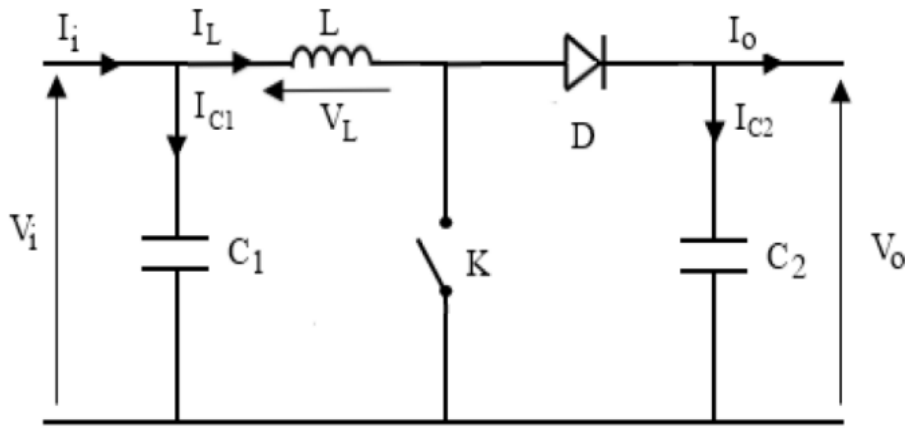


Figure II-3: The equivalent circuit diagram of a boost converter

To summarize the functions of the boost chopper in a steady state, it is necessary to present the equivalent circuit diagrams for each position of the switch K.

Figure II-4 shows the equivalent boost circuit when K is closed, between [0, αTs].

- In the first stage [0, αTs]: the transistor switch is closed, and the current in the inductor increases progressively and stores energy, until the end of the first period when the transistor opens and the energy is stored.

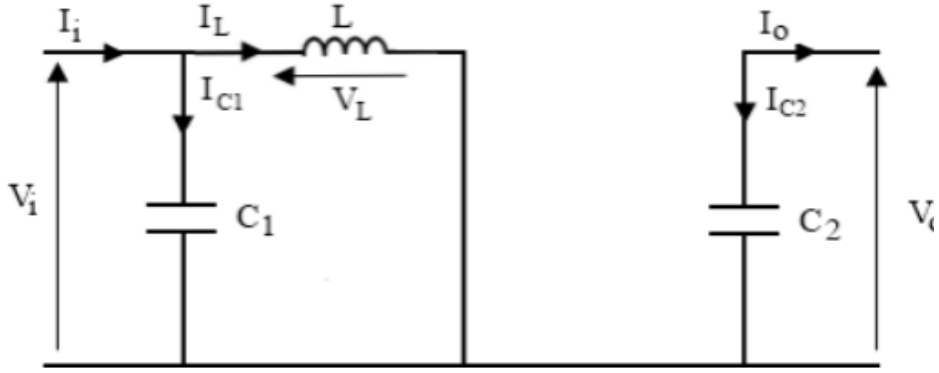


Figure II-4: Electrical diagram of a closed boost converter

$$\mathbf{I_{C_1} = C_1 . \frac{dV_i}{dt} = I_i - I_L} \quad \textbf{(II.1)}$$

$$\mathbf{I_{C_2} = C_2 . \frac{dV_0}{dt} = -I_0} \quad \textbf{(II.2)}$$

$$\mathbf{V_L = L . \frac{dV_L}{dt} = V_i} \quad \textbf{(II.3)}$$

- In the second stage [αTs, Ts]: the transistor switch opens and the inductance (L) opposes the decrease in current (I), thus it generates a voltage in addition to the source voltage, which is applied to the load (R) through the diode.

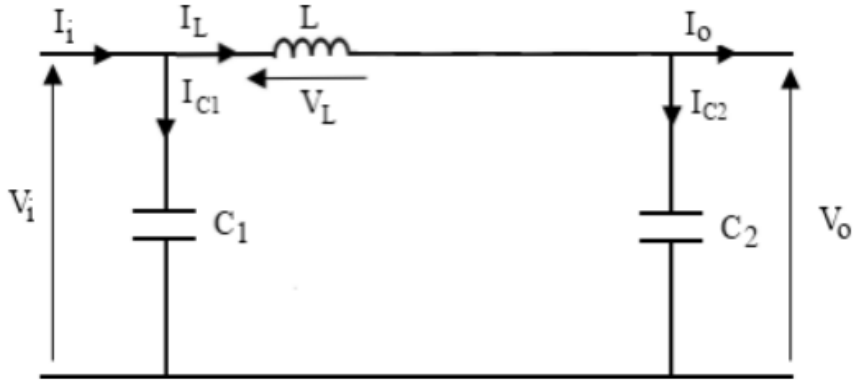


Figure II-5: Electrical diagram of an opened boost converter

$$\mathbf{I_{C_1} = C_1 . \frac{dV_i}{dt} = I_i - I_L} \quad \textbf{(II.4)}$$

$$\mathbf{I_{C_2} = C_2 . \frac{dV_0}{dt} = I_L - I_0} \quad \textbf{(II.5)}$$

$$\mathbf{V_L = L . \frac{dV_L}{dt} = V_i - V_0} \quad \textbf{(II.6)}$$

To simplify the study of boost converters, we are interested in the continuous regime. This is obtained by eliminating the derivatives of the dynamic variables and replacing these signals with their mean values. The resulting equations are:

$$\mathbf{I_L = I_i} \quad \textbf{(II.7)}$$

$$\mathbf{I_0 = (1 - \alpha)\, I_L} \quad \textbf{(II.8)}$$

$$\mathbf{V_i = (1 - \alpha) V_0} \quad \textbf{(II.9)}$$

This results in:

$$\mathbf{M(\alpha) = \frac{V_0}{V_i} = \frac{1}{1-\alpha}} \quad \textbf{(II.10)}$$

Figure II.6 shows how the load voltage varies with the load current, i.e. the current and voltage characteristics representing the operation of the chopper

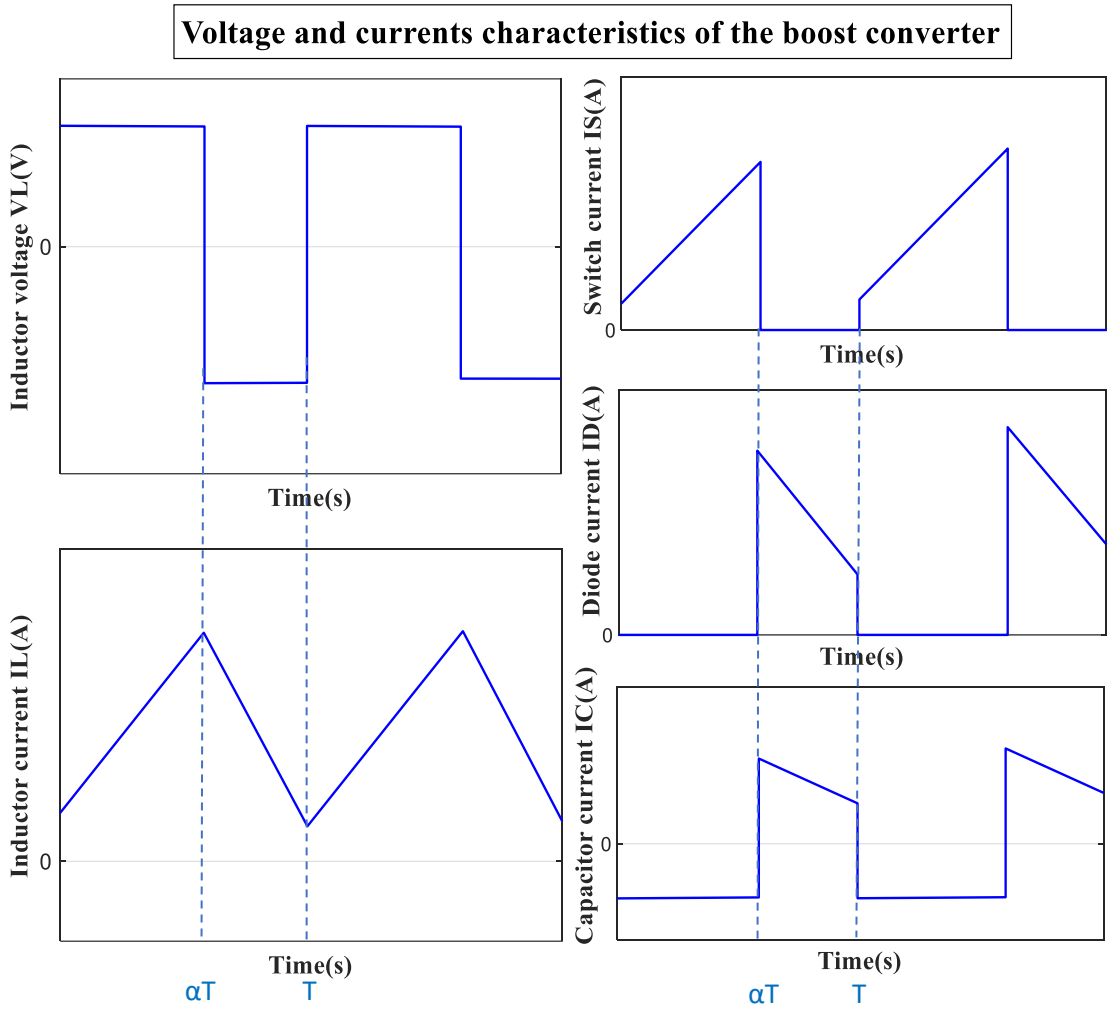


Figure II-6: Voltage and current characteristics of the boost converter**.**

II.4.2 Buck Converter

The buck converter, also known as a Buck chopper or step-down chopper, is a switch that can connect only two sources with different current/voltage types or vice versa. It is suitable for use in photovoltaic conversion systems since a photovoltaic generator is a source of direct current rather than voltage. The receiver, usually a battery, is a voltage source. The buck chopper's primary function is to convert the input voltage into a lower output voltage, where the conversion ratio M = Vo /Vi changes with the duty cycle α of the switch. **[FOR 17]**

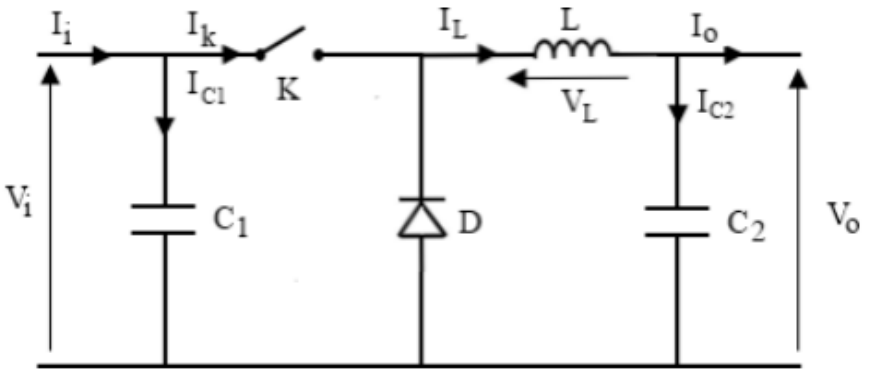


Figure II-7: The equivalent circuit diagram of a buck converter

To find out the actual behavior, we need to represent the equivalent circuit by the two states of the switch and then draw the mathematical model linking the input/output variables.

Figure II.8 shows the equivalent circuit diagram of a flyback converter with the switch closed,

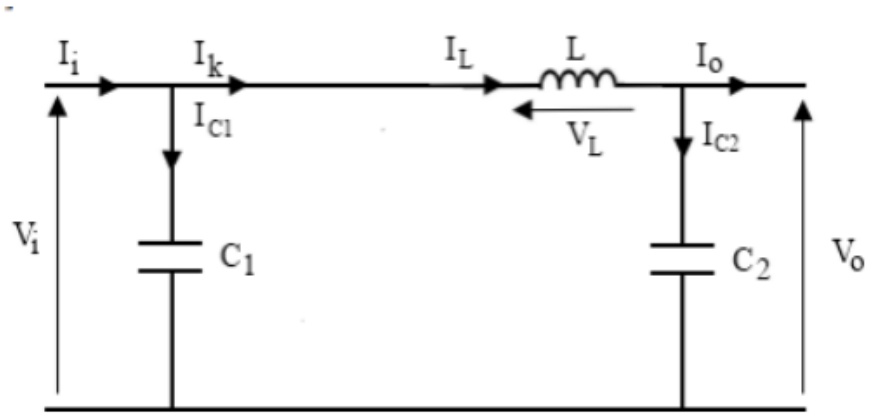


Figure II-8: Electrical diagram of a closed buck converter

When we apply Kirchhoff's law to the above circuit, we get the following equivalent equations:

$$\mathbf{I_{C_1} = C_1 . \frac{dV_i}{dt} = I_i - I_L} \qquad \textbf{(II.11)}$$

$$\mathbf{I_{C_2} = C_2 . \frac{dV_0}{dt} = I_L - I_0} \qquad \textbf{(II.12)}$$

$$\mathbf{V_L = L . \frac{dV_L}{dt} = V_i - V_0} \qquad \textbf{(II.13)}$$

while Figure II.9 shows the flyback converter with the switch open for (1 - α) Ts.

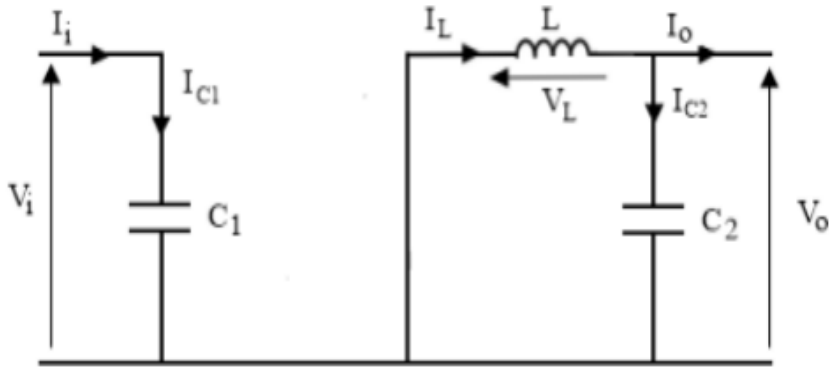


Figure II-9: Electrical diagram of an opened buck converter

$$\mathbf{I_{C_1} = C_1 . \frac{dV_i}{dt} = I_i} \quad \textbf{(II.14)}$$

$$\mathbf{I_{C_2} = C_2 . \frac{dV_0}{dt} = I_L - I_0} \quad \textbf{(II.15)}$$

$$\mathbf{V_L = L . \frac{dV_L}{dt} = -V_0} \quad \textbf{(II.16)}$$

During the first phase, the electronic switch is closed, allowing current to flow through the inductor. The inductor stores energy in the form of a magnetic field.

Next, the switch is quickly opened, which interrupts the current in the inductor. The energy that was stored in the inductor tries to keep the current flowing, causing the voltage across the inductor to decrease.

The capacitor is connected in parallel with the load and supplies energy to the load while maintaining a stable voltage. As a result, the output voltage is lower than the input voltage.

The resulting equations are:

$$\mathbf{I_i = \alpha I_L} \quad \textbf{(II.17)}$$

$$\mathbf{I_0 = I_L} \quad \textbf{(II.18)}$$

$$\mathbf{V_0 = \alpha V_i} \quad \textbf{(II.19)}$$

This results in:

$$\mathbf{M(\alpha) = \frac{V_0}{V_i} = \alpha} \quad \textbf{(II.20)}$$

The Buck converter current and voltage waveforms are shown in the figure below:

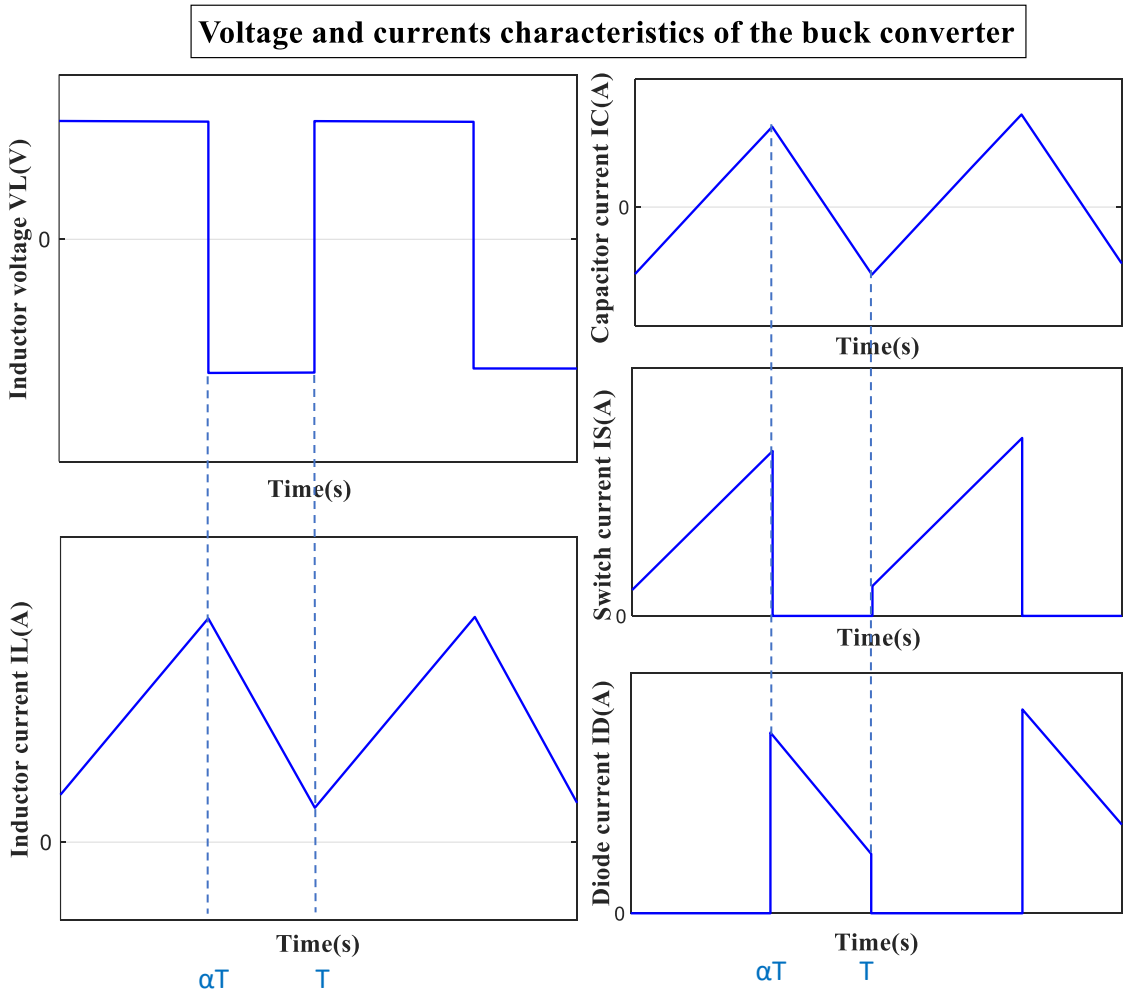


Figure II-10: Voltage and current characteristics of the buck converter.

II.4.3 Buck-Boost Converter

The buck-boost converter combines the properties of buck and boost configurations. It can be used to ideally transform any DC input voltage into any desired DC output voltage. **[FOR 17]**

The equivalent circuit diagram of a Buck-Boost converter is shown in Figure II-11

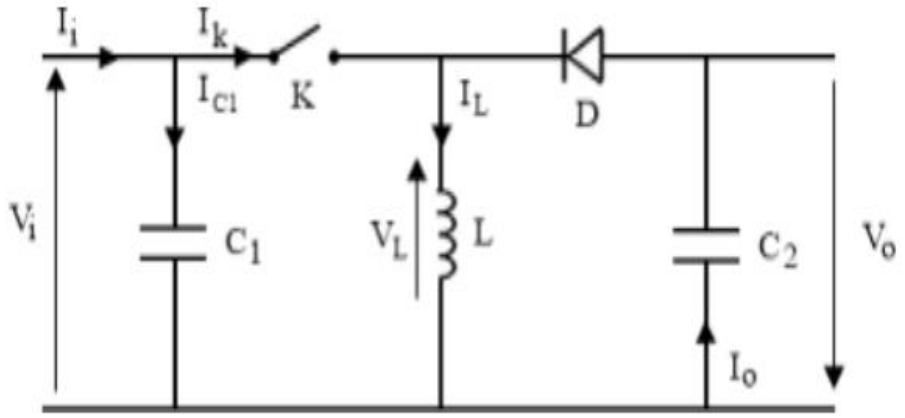


Figure II-11: Electrical diagram of a buck-boost converter

- In the first stage [0, αTs]: when the switch is closed, the current increases linearly. The voltage is equal to Vi

$$\mathbf{V_L = V_i} \quad \textbf{(II.21)}$$

- When the switch is opened the voltage across the inductor is reversed, and the stored energy is transferred to the load through the diode. That:

$$\mathbf{V_L = (1-\alpha)V_0} \quad \textbf{(II.22)}$$

As a result $$\mathbf{\alpha V_i = (1-\alpha)V_0} \quad \textbf{(II.23)}$$

Then, the conversion ratio is defined as follows:

$$\mathbf{M(\alpha) = \frac{V_0}{V_i} = \frac{\alpha}{1-\alpha}} \quad \textbf{(II.24)}$$

Figure II-12 shows the current and voltage characteristics representing the operation of the Buck-Boost chopper:

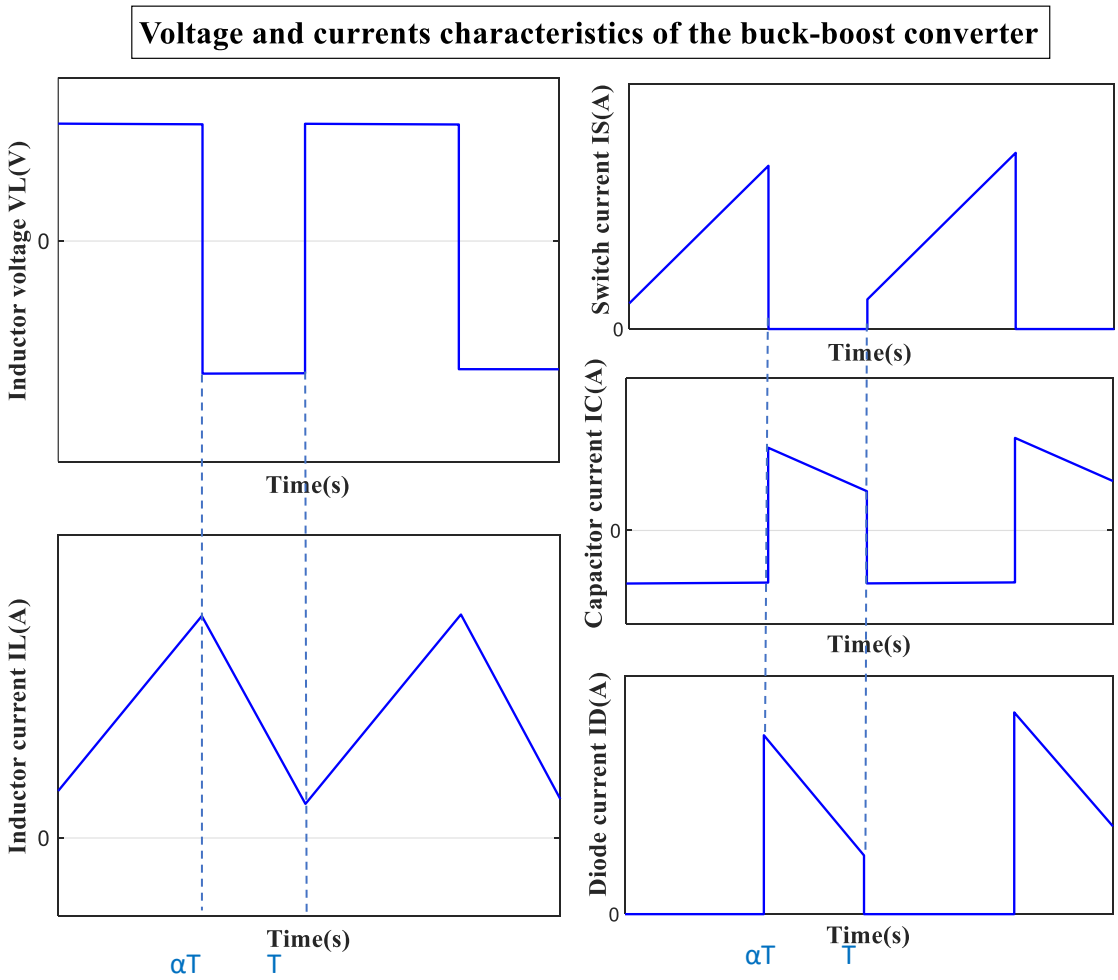


Figure II-12: Voltage and current characteristics of the buck-boost converter.

II.5 MPPT control of DC-DC converters

MPPT control maximizes the energy extraction from solar panels, improving the overall efficiency and performance of the PV system. It adapts to changing environmental conditions, ensuring optimal power output throughout the day and across different seasons. This control system is used in DC-DC converters that automatically adjust the duty cycle α to the optimum value, there by maximizing the power output of the PV panel. **[DEG 24]**

The MPPT algorithm can be simple or complex depending on the method used to find the MPP (Maximum Power Point). For this reason, the most popular control algorithms are presented and discussed below.

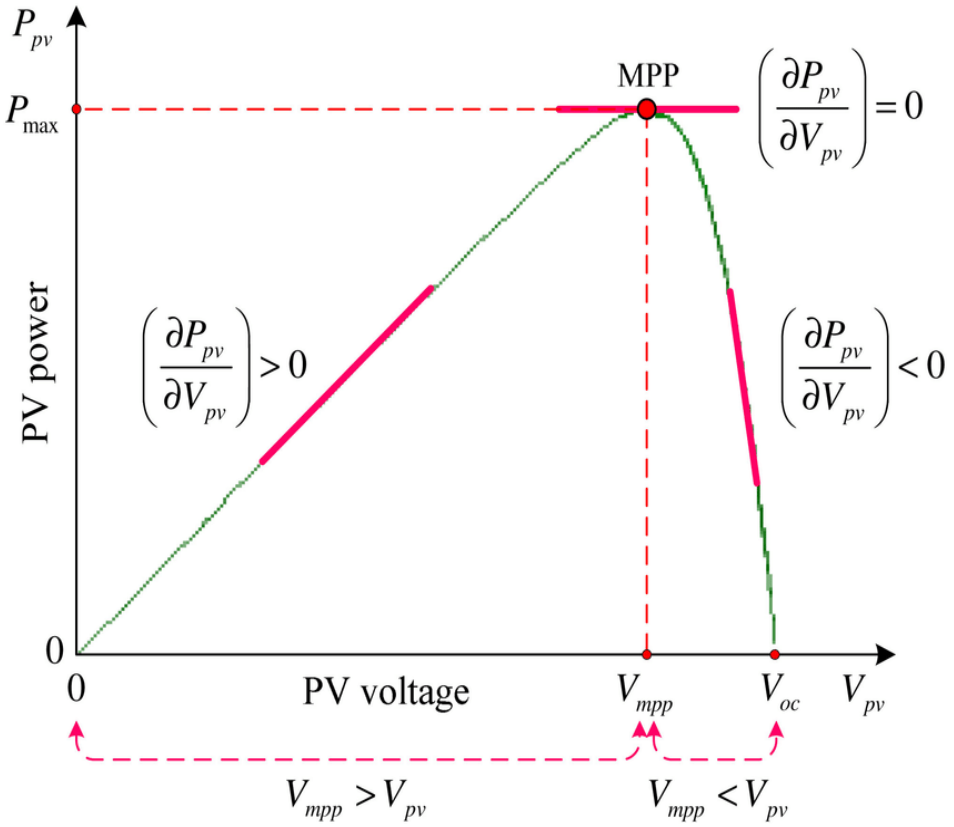


Figure II-13: Principle of MPPT control

II.6 MPPT Control classification

The classification of follower algorithms can be categorized into two groups based on the techniques or strategies used: direct and indirect methods.

II.6.1 The indirect MPPT methods

Indirect MPPT control methods rely on prior knowledge or modeling of the PV system based on proportional relationships between the optimum parameters characterizing the maximum power point ($\mathbf{V_{MPP}}$ and $\mathbf{I_{MPP}}$) and the characteristic parameters of the PV module ($\mathbf{V_{OC}}$ and $\mathbf{I_{SC}}$) to estimate the MPP without directly measuring the PV system's voltage and current. These methods typically use alternative measurements or environmental parameters.

These methods are often specific to each panel type and therefore difficult to generalize, some examples of indirect MPPT control methods include the "look up table" method, the open circuit voltage method, and the short-circuit method. **[SAD 23]**

II.6.2 The direct MPPT methods

Direct MPPT control methods have the distinct advantage of being able to track the maximum power point (MPP) of a PV system without requiring any prior knowledge or modeling of the PV system characteristics. These methods rely on real-time measurements of the PV system's voltage and current to determine the MPP. Examples of direct MPPT control methods include: Perturb and Observe (P&O), Incremental Conductance (IncCond), Fuzzy Logic Control (FLC)… **[SAD 23]**

Both methods aim to maximize the energy output from PV systems by continuously tracking the MPP as environmental conditions change. The choice between direct and indirect methods depends on factors like system complexity, cost, and the specific application requirements.

II.7 Tracking the maximum power point of the photovoltaic generator

The choice of MPP tracking method depends on factors such as the desired accuracy, computational resources, system complexity, and the availability of sensors or environmental data. In practice, a combination of these methods or hybrid approaches may be used to achieve better performance and reliability in tracking the MPP of a PV generator under various operating conditions**. [DEG 24]**

These techniques differ in terms of complexity, number of sensors required, speed of convergence, cost, performance and field of application:

Classical MPPT techniques:

- Constant Voltage (CV) algorithm
- Constant Current algorithm
- Perturb and Observe P&O,
- Incremental Conductance INC,
- Hill Climbing, ...

MPPT techniques based on artificial intelligence:

- MPPT based on fuzzy logic,
- MPPT based on neural networks,

- MPPT based on intelligent hybrid systems...

MPPT techniques based on metaheuristic optimization:

- MPPT based on Ant Colony Algorithm ACO
- MPPT based on Salp Swarm Optimization SSO
- MPPT based on Crow Search Algorithm-CSA
- MPPT based on Remora algorithm…

In our work we propose Remora optimization algorithm

II.8 Conclusion

In this chapter, we have explored several basic DC-DC converter topologies (Buck, Boost, and Buck-Boost), focusing on boost chopper operation as they are the most widely used in photovoltaic systems.

We also defined MPPT (Maximum Power Point Tracking) control and examined various techniques, both classic and modern, used to optimize the efficiency of photovoltaic systems and finding the operating point of the maximum power.

Chapter III:

Modeling of Induction machine

III.1 Introduction

Induction machine modeling is based on the use of equivalent schemes derived from rotating field theory. This approach is complemented by the development of matrix methods, which have become the basis for the modeling, simulation, identification and control of induction machine.

The first part of this chapter will deal with the modeling of the induction motor, based on the Park transformation which relates the stator and rotor electrical equations to electrically perpendicular axes called d, for direct, and q, for quadrature. The second part will be devoted to a detailed presentation of the modelling of the three-phase, two-level voltage inverter.

III.2 Description of the induction machine

An induction machine takes the form of a housing surrounding the stator magnetic circuit, which accommodates the three-phase stator winding in slots. The rotor magnetic circuit turns inside this magnetic circuit, which takes the form of a hollow cylinder. The rotor can be a squirrel-cage or wound. The shaft passes through the rotor magnetic circuit, resting on bearings mounted in flanges attached to the housing.

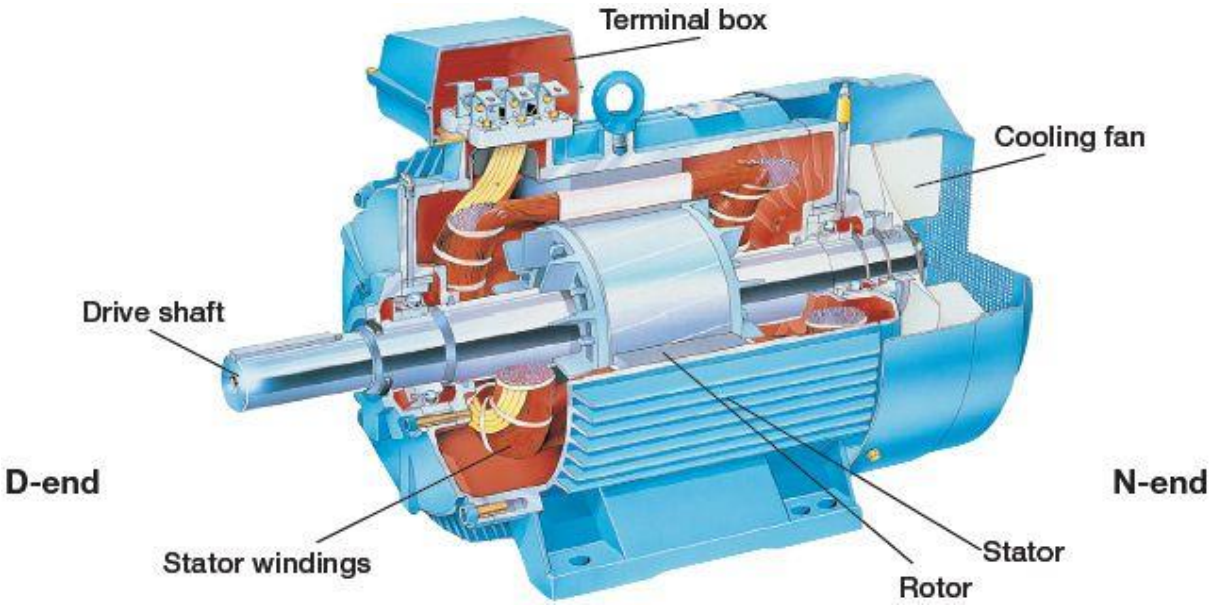


Figure III-1: Three-phase induction machine

III.3 Induction machine modeling

III.3.1 Simplifying assumptions

Modeling the induction machine is based on a number of assumptions:

- The three-phase motor is symmetrical; **[RAF 15]**
- The absence of saturation and losses in the magnetic circuit (hysteresis and Foucault current are negligible);
- Sinusoidal spatial distribution of magneto-motor air forces; **[BEL 23]**
- Winding resistances do not vary with operating temperature, and the skin effect is also neglected;
- The power supply is provided by a system of symmetrical three-phase voltages;
- The cage is assimilated to a short-circuited three-phase winding of the same number;
- The current density can be considered uniform throughout the cross-section of the elementary conductors;

Thus, among the important consequences of these assumptions are:

- Flux additivity;
- The self-inductances constancy; **[BEL 23]**

The law of sinusoidal variation of mutual inductances between static and rotor windings as a function of the angle between their magnetic axes.**[HAN 21]**

III.3.2 Machine model

For more information on the equation, see each time, we mention the decisions specific to this course in relation to what is usually done. **[VAS 90]**

The schematic representation of the induction machine in reference frame (abc) is shown in figure (III.2)

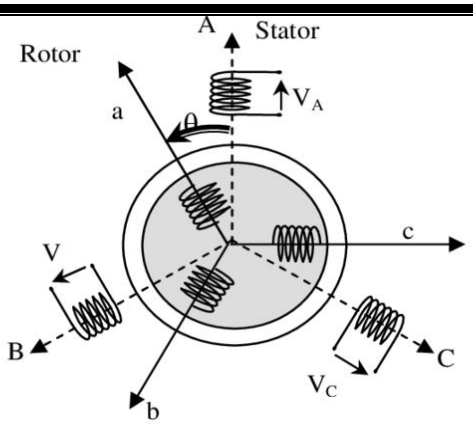


Figure III-2: Definition of the windings of the three-phase induction machine.

III.3.3 Setting up equations

Assuming certain conditions and for a balanced star-coupled induction machine, the equations describing the operation of the machine are as follows:

III.3.3.1 Electrical equations of the machine

The voltage equations for the three stator phases and the three rotor phases are :

$$\begin{cases} \mathbf{V_{sa}} = \mathbf{R_s i_{sa}} + \dfrac{\mathbf{d}}{\mathbf{dt}}\boldsymbol{\varphi}_{\mathbf{sa}} \\ \mathbf{V_{sb}} = \mathbf{R_s i_{sb}} + \dfrac{\mathbf{d}}{\mathbf{dt}}\boldsymbol{\varphi}_{\mathbf{sb}} \\ \mathbf{V_{sc}} = \mathbf{R_s i_{sc}} + \dfrac{\mathbf{d}}{\mathbf{dt}}\boldsymbol{\varphi}_{\mathbf{sc}} \end{cases} \quad (\mathbf{III.1})$$

$$\begin{cases} \mathbf{V_{ra}} = \mathbf{R_r i_{ra}} + \dfrac{\mathbf{d}}{\mathbf{dt}}\boldsymbol{\varphi}_{\mathbf{ra}} \\ \mathbf{V_{rb}} = \mathbf{R_r i_{rb}} + \dfrac{\mathbf{d}}{\mathbf{dt}}\boldsymbol{\varphi}_{\mathbf{rb}} \\ \mathbf{V_{rc}} = \mathbf{R_r i_{rc}} + \dfrac{\mathbf{d}}{\mathbf{dt}}\boldsymbol{\varphi}_{\mathbf{rc}} \end{cases} \quad (\mathbf{III.2})$$

[IKR 22]

Equations (III. 1) and (III. 2) are naturally presented in matrix form:

For the stator:

$$\begin{bmatrix} \mathbf{V_{sa}} \\ \mathbf{V_{sb}} \\ \mathbf{V_{sc}} \end{bmatrix} = \begin{bmatrix} \mathbf{R_s} & \mathbf{0} & \mathbf{0} \\ \mathbf{0} & \mathbf{R_s} & \mathbf{0} \\ \mathbf{0} & \mathbf{0} & \mathbf{R_s} \end{bmatrix} \begin{bmatrix} \mathbf{i_{sa}} \\ \mathbf{i_{sb}} \\ \mathbf{i_{sc}} \end{bmatrix} + \frac{\mathbf{d}}{\mathbf{dt}} \begin{bmatrix} \boldsymbol{\varphi}_{\mathbf{sa}} \\ \boldsymbol{\varphi}_{\mathbf{sb}} \\ \boldsymbol{\varphi}_{\mathbf{sc}} \end{bmatrix} \quad (\mathbf{III.3})$$

$$[\mathbf{V_{sabc}}] = [\mathbf{R_s}][\mathbf{i_{sabc}}] + \frac{\mathbf{d}}{\mathbf{dt}}[\boldsymbol{\varphi}_{\mathbf{sabc}}]$$

For the rotor:

$$\begin{bmatrix} V_{ra} \\ V_{rb} \\ V_{rc} \end{bmatrix} = \begin{bmatrix} R_r & 0 & 0 \\ 0 & R_r & 0 \\ 0 & 0 & R_r \end{bmatrix} \begin{bmatrix} i_{ra} \\ i_{rb} \\ i_{rc} \end{bmatrix} + \frac{d}{dt} \begin{bmatrix} \varphi_{ra} \\ \varphi_{rb} \\ \varphi_{rc} \end{bmatrix} \qquad (III.4)$$

$$[0] = [R_r][i_{rabc}] + \frac{d}{dt}[\varphi_{rabc}]$$

We pose:

$$[R_s] = \begin{bmatrix} R_s & 0 & 0 \\ 0 & R_s & 0 \\ 0 & 0 & R_s \end{bmatrix} \quad ; \quad [R_r] = \begin{bmatrix} R_r & 0 & 0 \\ 0 & R_r & 0 \\ 0 & 0 & R_r \end{bmatrix}$$

$[R_s]$: Resistance of a stator phase.

$[R_r]$: Resistance of a rotor phase.

$$[V_s] = \begin{bmatrix} V_{sa} \\ V_{sb} \\ V_{sc} \end{bmatrix}$$

$[V_s]$: Stator voltage vector.

$$[I_s] = \begin{bmatrix} I_{sa} \\ I_{sb} \\ I_{sc} \end{bmatrix} \quad ; \quad [I_r] = \begin{bmatrix} I_{ra} \\ I_{rb} \\ I_{rc} \end{bmatrix}$$

$[I_s]$: Stator current vector.

$[I_r]$: Rotor current vector.

$$[\varphi_s] = \begin{bmatrix} \varphi_{sa} \\ \varphi_{sb} \\ \varphi_{sc} \end{bmatrix} \quad ; \quad [\varphi_r] = \begin{bmatrix} \varphi_{ra} \\ \varphi_{rb} \\ \varphi_{rc} \end{bmatrix}$$

$[\varphi_s]$: Stator flux vector.

$[\varphi_r]$: Rotor flux vector.

III.3.3.2 Magnetic equations

The flux-current equations can be rewritten using the inductance matrix. This matrix is made up of 36 non-zero coefficients, half of which depend on the time through the electric angle θ.

$$\begin{bmatrix} \varphi_{sa} \\ \varphi_{sb} \\ \varphi_{sc} \\ \varphi_{ra} \\ \varphi_{rb} \\ \varphi_{rc} \end{bmatrix} = \begin{bmatrix} l_s & M_s & M_s & M_1 & M_2 & M_3 \\ M_s & l_s & M_s & M_2 & M_1 & M_3 \\ M_s & M_s & l_s & M_3 & M_2 & M_1 \\ M_1 & M_2 & M_3 & l_r & M_r & M_r \\ M_3 & M_1 & M_2 & M_r & l_r & M_r \\ M_2 & M_3 & M_1 & M_r & M_r & l_r \end{bmatrix} \begin{bmatrix} i_{sa} \\ i_{sb} \\ i_{sc} \\ i_{ra} \\ i_{rb} \\ i_{rc} \end{bmatrix} \quad (\mathbf{III.5})$$

Such as:

- ls: The self-inductance of a stator phase;
- lr: The self-inductance of a rotor phase;
- Ms: Mutual inductance between stator phases;
- Mr: Mutual inductance between rotor phases

With :

- $M_1 = M_{rs}\cos(\theta)$
- $M_2 = M_{rs}\cos(\theta - 2\pi/3)$
- $M_3 = M_{rs}\cos(\theta + 2\pi/3)$

Where :

- Msr: this is the maximum value of the mutual inductance between a stator phase and a rotor phase.

The matrix equation that summarizes the static and rotor flux equations

$$\begin{bmatrix} \varphi_s \\ \varphi_r \end{bmatrix} = \begin{bmatrix} [L_s] & [M_{sr}] \\ [M_{rs}] & [L_r] \end{bmatrix} \begin{bmatrix} i_s \\ i_r \end{bmatrix} \quad (\mathbf{III.6})$$

With :

- $[L_s]$: The stator inductance matrix :

$$[L_s] = \begin{bmatrix} l_s & M_s & M_s \\ M_s & l_s & M_s \\ M_s & M_s & l_s \end{bmatrix} \quad (\mathbf{III.7})$$

- $[L_r]$: The rotor inductance matrix :

$$[L_r] = \begin{bmatrix} l_r & M_r & M_r \\ M_r & l_r & M_r \\ M_r & M_r & l_r \end{bmatrix} \quad (\mathbf{III.8})$$

- $[M_{sr}]$: The stator rotor mutual inductance matrix.
- $[M_{rs}]$: The rotor stator mutual inductance matrix.

$$[\mathbf{M_{sr}}] = [\mathbf{M_{rs}}]' = \mathbf{M_{sr}}\begin{bmatrix} \cos(\theta) & \cos(\theta+\frac{2\pi}{3}) & \cos(\theta-\frac{2\pi}{3}) \\ \cos(\theta-\frac{2\pi}{3}) & \cos(\theta) & \cos(\theta+\frac{2\pi}{3}) \\ \cos(\theta+\frac{2\pi}{3}) & \cos(\theta-\frac{2\pi}{3}) & \cos(\theta) \end{bmatrix} \quad (\mathbf{III.9})$$

III.3.3.3 Mechanical equation

The mechanical equation is given by equation :

$$J\frac{d\Omega}{dt} = T_e - T_R - f.\Omega \quad (\mathbf{III.10})$$

The torque is given by the following expression, taken from considerations on electromechanical energy conversion,

$$T_e = P_n[i_s]\frac{d}{dt}([M_{sr}][i_r]) \quad (\mathbf{III.11})$$

The previous equations are difficult to solve because :

- The order of the system is high.
- The inductance matrix is a function of time.

So, we're looking for a transformation that reduces the order of the system and eliminates this time dependence.**[RAF 15]**

III.4 Transformation of PARK

The Park transformation consists of a three-phase - two-phase transformation followed by a rotation. The dq frame is movable relative to the abc frame.

Let's come back to the choice of these transformation angles for each set of quantities (stator and rotor). If we denote by φ_s (resp. by φ_r) the angle of the Park transformation of the stator (resp. rotor) quantities, there is a relationship between them which simplifies the equations and, by the same token, the final model.

In order to simplify these equations, the reference points for the Park transformation of the stator and rotor quantities must coincide.to simplify these equations (Figure III.3). This is done by linking the angles θ_s and θ_r by the relationship:

$$\theta_s = \theta + \theta_r$$

This transformation reduces the complexity of the system. The reference frame position can be fixed according to the three referential :

• Reference system linked to the rotating field.

• Referential linked to the stator.

• Reference system linked to the rotor. **[BEL 23]**

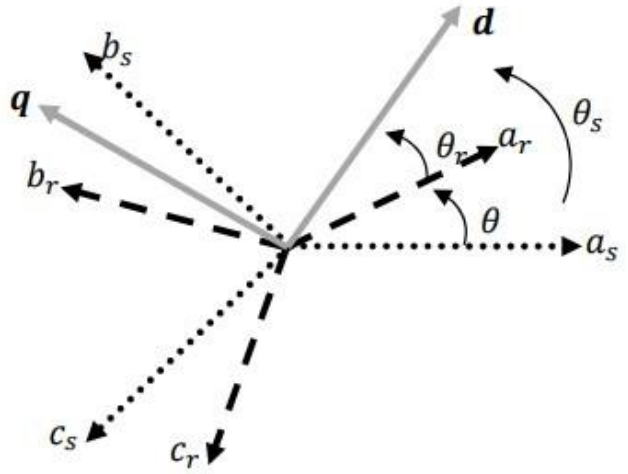


Figure III-3: Angular location of axis systems in electrical space (reference d,q).

The following equation describes the transformation of a three-phase system [a,b,c] into a two-phase system [d,q]: $\mathbf{X_{dq} = [P(\theta)]X_{abc}}$

Such as:

X : may be : voltage, current or flux ;

[P(θ)] : is the matrix of the Park transformation defined by :

$$\left[\mathbf{P_{(\theta)}}\right] = \sqrt{\frac{2}{3}}\begin{bmatrix} \cos(\theta) & \cos(\theta - \frac{2\pi}{3}) & \cos(\theta - \frac{4\pi}{3}) \\ -\sin(\theta) & -\sin\left(\theta - \frac{2\pi}{3}\right) & -\sin\left(\theta - \frac{4\pi}{3}\right) \\ \frac{1}{\sqrt{2}} & \frac{1}{\sqrt{2}} & \frac{1}{\sqrt{2}} \end{bmatrix} \qquad (\mathbf{III.12})$$

$\left[P_{(\theta)}\right]^{-1}$: Is the inverse Park matrix defined by :

$$\left[\mathbf{P}_{(\theta)}\right]^{-1} = \sqrt{\frac{2}{3}}\begin{bmatrix} \cos(\theta) & -\sin(\theta) & \frac{1}{\sqrt{2}} \\ \cos(\theta - \frac{2\pi}{3}) & -\sin\left(\theta - \frac{2\pi}{3}\right) & \frac{1}{\sqrt{2}} \\ \cos(\theta - \frac{4\pi}{3}) & -\sin\left(\theta - \frac{4\pi}{3}\right) & \frac{1}{\sqrt{2}} \end{bmatrix} \quad (\mathbf{III.13})$$

With :

The angle θ corresponds to the position of the reference frame chosen for the transformation.

- θ = θs for the stator (angle between sa and d).
- θ = θr for the rotor (angle between ra and d).

The change in variables relating to currents, voltages and flows is defined by :

$$\begin{bmatrix} \mathbf{X_d} \\ \mathbf{X_q} \\ \mathbf{X_0} \end{bmatrix} = \left[\mathbf{P}_{(\theta)}\right]\begin{bmatrix} \mathbf{X_a} \\ \mathbf{X_b} \\ \mathbf{X_c} \end{bmatrix}$$

The inverse transformation is obtained by :

$$\begin{bmatrix} \mathbf{X_a} \\ \mathbf{X_b} \\ \mathbf{X_c} \end{bmatrix} = \left[\mathbf{P}_{(\theta)}\right]^{-1}\begin{bmatrix} \mathbf{X_d} \\ \mathbf{X_q} \\ \mathbf{X_0} \end{bmatrix}$$

If we assume that the [abc] system is balanced and symmetrical (i.e. there is no disturbance), then the zero-sequence component has a value of zero. Under these conditions, the electrical, magnetic and mechanical equations simplify and become :

III.4.1 Electrical equations

Applying the PARK transformation to the electrical equations and assuming that the rotor is short-circuited, the result is :

$$\begin{cases} \mathbf{V_{sd}} = \mathbf{R_s i_{sd}} + \dfrac{\mathbf{d}}{\mathbf{dt}}\boldsymbol{\varphi}_{\mathbf{sd}} - \boldsymbol{\omega_s}\boldsymbol{\varphi}_{\mathbf{sq}} \\ \mathbf{V_{sq}} = \mathbf{R_s i_{sq}} + \dfrac{\mathbf{d}}{\mathbf{dt}}\boldsymbol{\varphi}_{\mathbf{sq}} - \boldsymbol{\omega_s}\boldsymbol{\varphi}_{\mathbf{sd}} \\ \mathbf{V_{rd}} = \mathbf{0} = \mathbf{R_r i_{sd}} + \dfrac{\mathbf{d}}{\mathbf{dt}}\boldsymbol{\varphi}_{\mathbf{rd}} - (\boldsymbol{\omega_s} - \boldsymbol{\omega_r})\boldsymbol{\varphi}_{\mathbf{rq}} \\ \mathbf{V_{rq}} = \mathbf{0} = \mathbf{R_r i_{sq}} + \dfrac{\mathbf{d}}{\mathbf{dt}}\boldsymbol{\varphi}_{\mathbf{rq}} - (\boldsymbol{\omega_s} - \boldsymbol{\omega_r})\boldsymbol{\varphi}_{\mathbf{rd}} \end{cases} \quad (\mathbf{III.14})$$

With :

$$(\boldsymbol{\omega_s} - \boldsymbol{\omega}) = \boldsymbol{\omega_r}$$

$$\omega_s = \frac{d\theta_s}{dt}$$

$$\omega_r = \frac{d\theta_r}{dt}$$

$$(\omega_s - \omega) = \frac{d\theta}{dt} = P\Omega$$

III.4.2 Magnetic equations

Applying Park's transformation to equation (III. 3) gives :

$$\begin{cases} \varphi_{sd} = L_s i_{sd} + M i_{sd} \\ \varphi_{sq} = L_s i_{sq} + M i_{sq} \end{cases} \quad (III.15)$$

$$\begin{cases} \varphi_{rd} = L_r i_{rd} + M i_{rd} \\ \varphi_{rq} = L_r i_{rq} + M i_{rq} \end{cases} \quad (III.16)$$

III.4.3 Expressions of electromagnetic torque

$$\begin{bmatrix} T_e = \frac{3}{2} P_n (\varphi_{sd} i_{sq} - \varphi_{sq} i_{sd}) \\ T_e = \frac{3}{2} P_n (\varphi_{rq} i_{rd} - \varphi_{rd} i_{rq}) \\ T_e = \frac{3}{2} P_n L_m (\varphi_{sq} i_{rd} - \varphi_{sd} i_{rq}) \end{bmatrix} \quad (III.17)$$

$$T_e = P_n \frac{M_{sr}}{L_r} (\varphi_{rd} i_{sq} - \varphi_{rq} i_{sd}) \quad (III.18)$$

III.5 Choice of reference frame

III.5.1 Choice of reference frame orientation

The orientation of the (d,q) axis is chosen according to the application's objective, as follows :

Stator mark : $\frac{d\theta s}{dt} = 0$ et $\omega = \frac{d\theta}{dt} = -\omega_r$ **.** This frame of reference is often used in the study of observers.

Rotor mark : $\frac{d\theta s}{dt} = \omega_r$ et $\omega = \frac{d\theta}{dt} = 0$. This choice is widely used to study the transient regimes of asynchronous machines.

Rotary field marker : $\frac{d\theta s}{dt} = \omega_s$ et $\omega = \frac{d\theta}{dt} = \omega_s - \omega_r$. This frame of reference is often used in the study and synthesis of control laws.

Where :

- ω_s is the stator pulsation,
- ω_r is the mechanical pulsation
- ω is the sliding pulsation.

III.5.2 Model expressed in the reference frame (d,q) related to the rotating field

If the reference frame is linked to the rotating field, the equations linking the voltage components to those of the currents and fluxes can be written as follows for the stator and rotor:

$$\begin{bmatrix} V_{sd} \\ V_{sq} \end{bmatrix} = \begin{bmatrix} R_s & 0 \\ 0 & R_s \end{bmatrix} \begin{bmatrix} i_{sd} \\ i_{sq} \end{bmatrix} + \frac{d}{dt} \begin{bmatrix} \varphi_{sd} \\ \varphi_{sq} \end{bmatrix} + \begin{bmatrix} 0 & -\omega_s \\ \omega_s & 0 \end{bmatrix} \begin{bmatrix} \varphi_{sd} \\ \varphi_{sq} \end{bmatrix}$$

$$\begin{bmatrix} V_{rd} \\ V_{rq} \end{bmatrix} = \begin{bmatrix} R_r & 0 \\ 0 & R_r \end{bmatrix} \begin{bmatrix} i_{rd} \\ i_{rq} \end{bmatrix} + \frac{d}{dt} \begin{bmatrix} \varphi_{rd} \\ \varphi_{rq} \end{bmatrix} + \begin{bmatrix} 0 & -\omega_r \\ \omega_r & 0 \end{bmatrix} \begin{bmatrix} \varphi_{rd} \\ \varphi_{rq} \end{bmatrix} \qquad (III.19)$$

The total fluxes through the four fictitious coils have the values (III. 15) and (III. 16).

From equation (III. 16), we obtain the following equation:

$$\begin{cases} i_{rd} = \dfrac{\varphi_{rd} - M_{sr} i_{ds}}{L_r} \\ i_{rq} = \dfrac{\varphi_{rq} - M_{sr} i_{qs}}{L_r} \end{cases} \qquad (III.20)$$

If we replace the expressions for the i_{rd} and i_{rq} currents in equation (III.20) with their values in equations (III. 15), we obtain :

$$\begin{cases} \varphi_{sd} = \left(L_s - \dfrac{M_{sr}^2}{L_r} \right) i_{sd} + \dfrac{M_{sr}}{L_r} \varphi_{rd} \\ \varphi_{sq} = \left(L_s - \dfrac{M_{sr}^2}{L_r} \right) i_{sq} + \dfrac{M_{sr}}{L_r} \varphi_{rq} \end{cases} \qquad (III.21)$$

Deriving the latter as a function of time, we find :

$$\begin{cases} \dfrac{d\varphi_{sd}}{dt} = \left(L_s - \dfrac{M_{sr}^{\,2}}{L_r}\right)\dfrac{di_{sd}}{dt} + \dfrac{M_{sr}}{L_r}\dfrac{d\varphi_{rd}}{dt} \\ \dfrac{d\varphi_{sq}}{dt} = \left(L_s - \dfrac{M_{sr}^{\,2}}{L_r}\right)\dfrac{di_{sq}}{dt} + \dfrac{M_{sr}}{L_r}\dfrac{d\varphi_{rq}}{dt} \end{cases} \quad \textbf{(III. 22)}$$

For the rotor, from equations (III. 19) we obtain :

$$\begin{cases} \dfrac{d\varphi_{rd}}{dt} = -R_r i_{rd} + \omega\varphi_{rq} \\ \dfrac{d\varphi_{rq}}{dt} = -R_r i_{rq} + \omega\varphi_{rd} \end{cases} \quad \textbf{(III. 23)}$$

By replacing i_{rd} and i_{rd} with their expressions obtained in (III. 20), the following expressions are obtained :

$$\begin{cases} \dfrac{d\varphi_{rd}}{dt} = \dfrac{M_{sr}R_r}{L_r} i_{sd} - \dfrac{R_r}{L_r}\varphi_{rd} + \omega\varphi_{rq} \\ \dfrac{d\varphi_{rq}}{dt} = \dfrac{M_{sr}R_r}{L_r} i_{sq} - \dfrac{R_r}{L_r}\varphi_{rq} + \omega\varphi_{rd} \end{cases} \quad \textbf{(III. 24)}$$

From equations (III. 15), (III. 21), (III. 22) and (III. 24) we finally obtain :

$$\begin{cases} \dfrac{di_{sd}}{dt} = \dfrac{1}{\sigma L_s} V_{sd} - \left(\dfrac{R_s}{\sigma L_s} + \dfrac{M_{sr}^{\,2} R_r}{\sigma L_s L_r^{\,2}}\right) i_{sd} + \omega_s i_{sq} + \dfrac{M_{sr}R_r}{\sigma L_s L_r^{\,2}}\varphi_{rd} + \dfrac{M_{sr}}{\sigma L_s L_r}\omega\varphi_{rq} \\ \dfrac{di_{sq}}{dt} = \dfrac{1}{\sigma L_s} V_{sq} - \left(\dfrac{R_s}{\sigma L_s} + \dfrac{M_{sr}^{\,2} R_r}{\sigma L_s L_r^{\,2}}\right) i_{sq} + \omega_s i_{sd} + \dfrac{M_{sr}R_r}{\sigma L_s L_r^{\,2}}\varphi_{rq} + \dfrac{M_{sr}}{\sigma L_s L_r}\omega\varphi_{rd} \end{cases} \quad \textbf{(III. 25)}$$

The equations can be written as equations of state such as

$$\begin{bmatrix} i_{sd} \\ i_{sq} \\ \varphi_{rd} \\ \varphi_{rq} \end{bmatrix} = \begin{bmatrix} -\left(\frac{1}{T_r\sigma} + \frac{1}{T_r}\frac{1-\sigma}{\sigma}\right) & \omega_s & \frac{1-\sigma}{\sigma}\frac{1}{M_{sr}T_r} & \frac{1-\sigma}{\sigma}\frac{1}{M_{sr}}\omega \\ -\omega_s & -\left(\frac{1}{T_r\sigma} + \frac{1}{T_r}\frac{1-\sigma}{\sigma}\right) & -\frac{1-\sigma}{\sigma}\frac{1}{M_{sr}}\omega & \frac{1-\sigma}{\sigma}\frac{1}{M_{sr}T_r} \\ \frac{M_{sr}}{T_r} & 0 & -\frac{1}{T_r} & \omega_{sl} \\ 0 & \frac{M_{sr}}{T_r} & -\omega_{sl} & -\frac{1}{T_r} \end{bmatrix} \begin{bmatrix} i_{sd} \\ i_{sq} \\ \varphi_{rd} \\ \varphi_{rq} \end{bmatrix} + \begin{bmatrix} \frac{1}{\sigma L_s} & 0 \\ 0 & \frac{1}{\sigma L_s} \\ 0 & 0 \\ 0 & 0 \end{bmatrix} \quad \textbf{(III. 26)}$$

$$\dot{X} = \frac{dX}{dt} = QX + BU \quad \textbf{(III. 27)}$$

$T_r = \frac{L_r}{R_r}$; $T_s = \frac{L_s}{R_s}$: Rotor and stator time constants.

$\sigma = 1 - \frac{{M_{sr}}^2}{L_s L_r}$: Dispersion coefficient.

The electromagnetic torque can then be expressed as follows :

$$\begin{cases} T_e = P_n \frac{M}{L_r}(\varphi_{rd} i_{sq} - \varphi_{rq} i_{sd}) \\ J\frac{d\Omega}{dt} + \Omega f = T_e - T_R \end{cases} \quad (III.28)$$

III.6 Inverter modelling

The conversion of DC-AC energy using static converters such as voltage inverters is an essential function in the growing field of power electronics. They can be found in the widest range of applications, the best known of which are undoubtedly AC motor speed control, safety power supplies, etc.**[ABA 23]**

The inverter mounting consists of six bidirectional switches, with a recovery diode mounted in the head-to-head and a transistor.

Switch pairs (Sa, Sb, Sc) are controlled in a complementary manner, to ensure continuity of currents in the machine's stator phases, and to avoid short-circuiting the source.

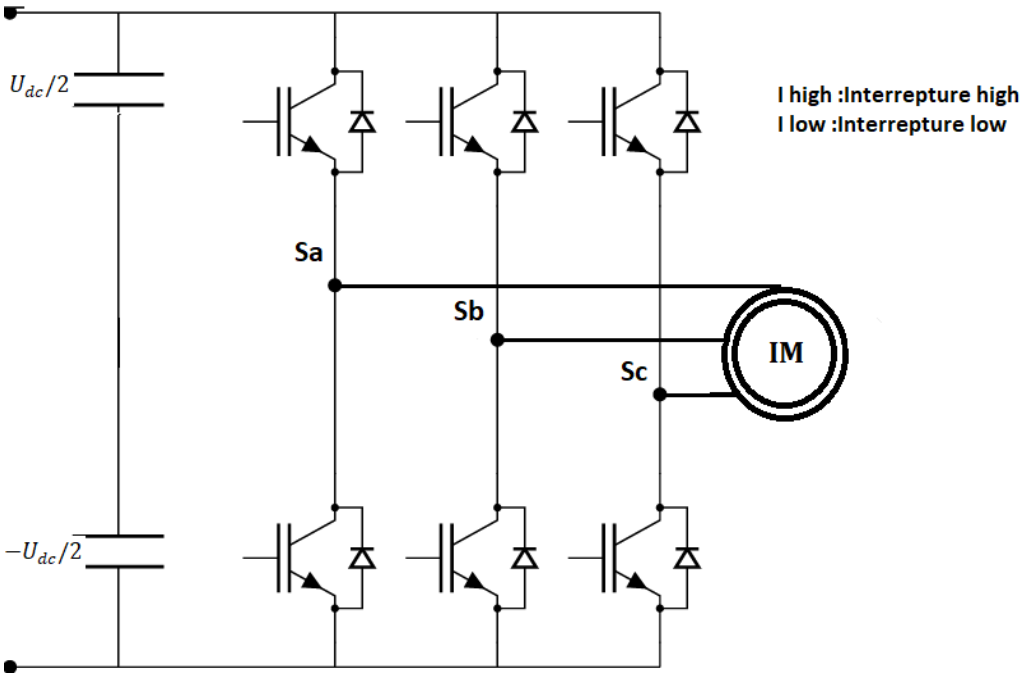


Figure III-4 : Representation of the two-level inverter feeding an IM**.**

III.6.1 Voltages in the phases of the induction machine

To simplify the study, it is assumed that switching of the switches is instantaneous and that voltage drops across the switches are negligible.

Compound voltages are given by :

$$\begin{cases} \mathbf{U_{AB} = V_{ao} - V_{bo}} \\ \mathbf{U_{BC} = V_{bo} - V_{co}} \\ \mathbf{U_{CA} = V_{co} - V_{ao}} \end{cases} \quad \mathbf{(III.30)}$$

V_{ao} V_{bo} V_{co} are the inverter output voltages relative to reference 'o'. The phase voltages are given by

$$\begin{cases} \mathbf{V_{as} = V_{ao} - V_{no}} \\ \mathbf{V_{bs} = V_{bo} - V_{no}} \\ \mathbf{V_{cs} = V_{co} - V_{no}} \end{cases} \quad \mathbf{(III.31)}$$

V_{no} : is the load neutral voltage with respect to point "o".

We have: $V_{as} + V_{bs} + V_{cs} = 0$

So we shoot:

$$\mathbf{V_{no} = {}^{1}/_{3}\,(V_{ao} + V_{bo} + V_{co})} \quad \mathbf{(III.32)}$$

Replacing (III.32) in (III.31) gives:

$$\begin{cases} \mathbf{V_{as} = \frac{2}{3}V_{ao} + \frac{1}{3}V_{bo} + \frac{1}{3}V_{co}} \\ \mathbf{V_{as} = \frac{1}{3}V_{ao} + \frac{2}{3}V_{bo} + \frac{1}{3}V_{co}} \\ \mathbf{V_{as} = \frac{1}{3}V_{ao} + \frac{1}{3}V_{bo} + \frac{2}{3}V_{co}} \end{cases} \quad \mathbf{(III.33)}$$

Matrix form :

$$\begin{bmatrix} \mathbf{V_{an}} \\ \mathbf{V_{bn}} \\ \mathbf{V_{cn}} \end{bmatrix} \mathbf{\frac{1}{3}U_{DC}} \begin{pmatrix} \mathbf{2} & \mathbf{-1} & \mathbf{-1} \\ \mathbf{-1} & \mathbf{2} & \mathbf{-1} \\ \mathbf{-1} & \mathbf{-1} & \mathbf{2} \end{pmatrix} \begin{bmatrix} \mathbf{S_a} \\ \mathbf{S_b} \\ \mathbf{S_c} \end{bmatrix} \quad \mathbf{(III.34)}$$

III.6.2 PWM (Pulse width modulation) voltage inverter

This technique (natural PWM) is one of the best known and simplest of the other types of control and is based on the comparison between two signals See Figure III.5 :

- the first, called the reference signal, represents the image of the sinusoid we want at the output of the inverter. output of the inverter. This signal can be modulated in amplitude and frequency. change these characteristics to control our machine.
- the second, called the carrier signal, defines the switching rate of the inverter's static switches. It is a high-frequency (HF) signal compared to the reference signal.

The pulse wave is better than the rectangular wave if :

$$f_{carrier} > 20 f_{reference}$$

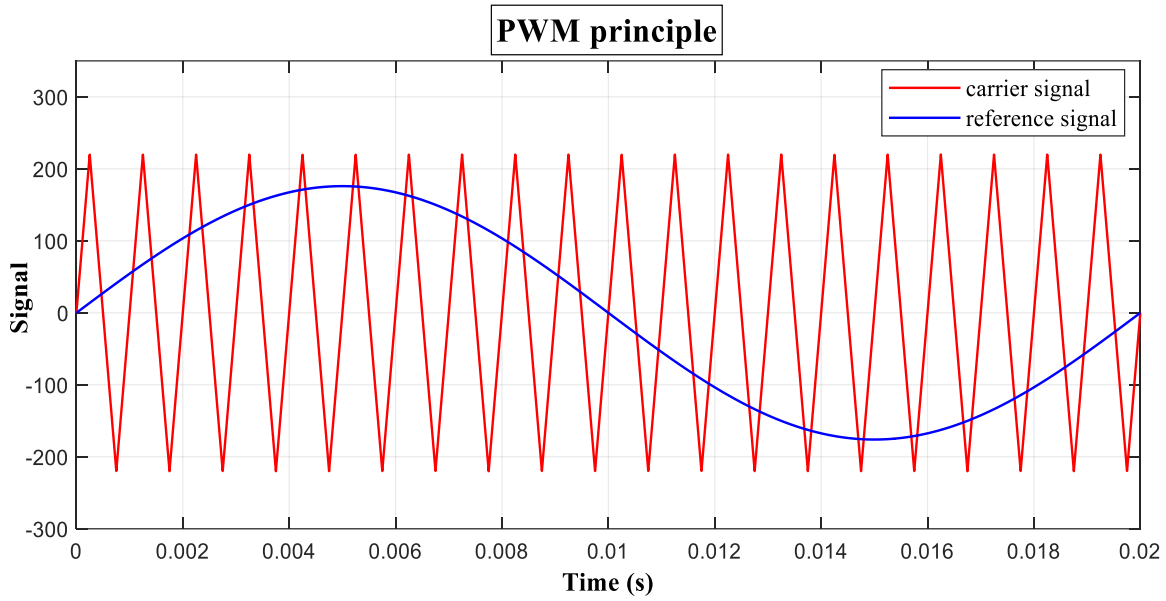


Figure III-5: Principle of current control by PWM

III.7 Simulation results with and without inverter

We have chosen to use MATLAB software to simulate the cage induction motor. The motor parameters used for the simulation are presented in Appendix A. We simulated the squirrel cage induction motor fed from a balanced three-phase network, both without and with a voltage inverter. The simulation conditions are as follows:

- Power supply: $U = 220\ V$ (effective value), frequency 50 Hz.
- Start at no load, then apply a resistive torque of 10 $N.m$ between 4 s and 8 s.

III.7.1 IM results without inverter

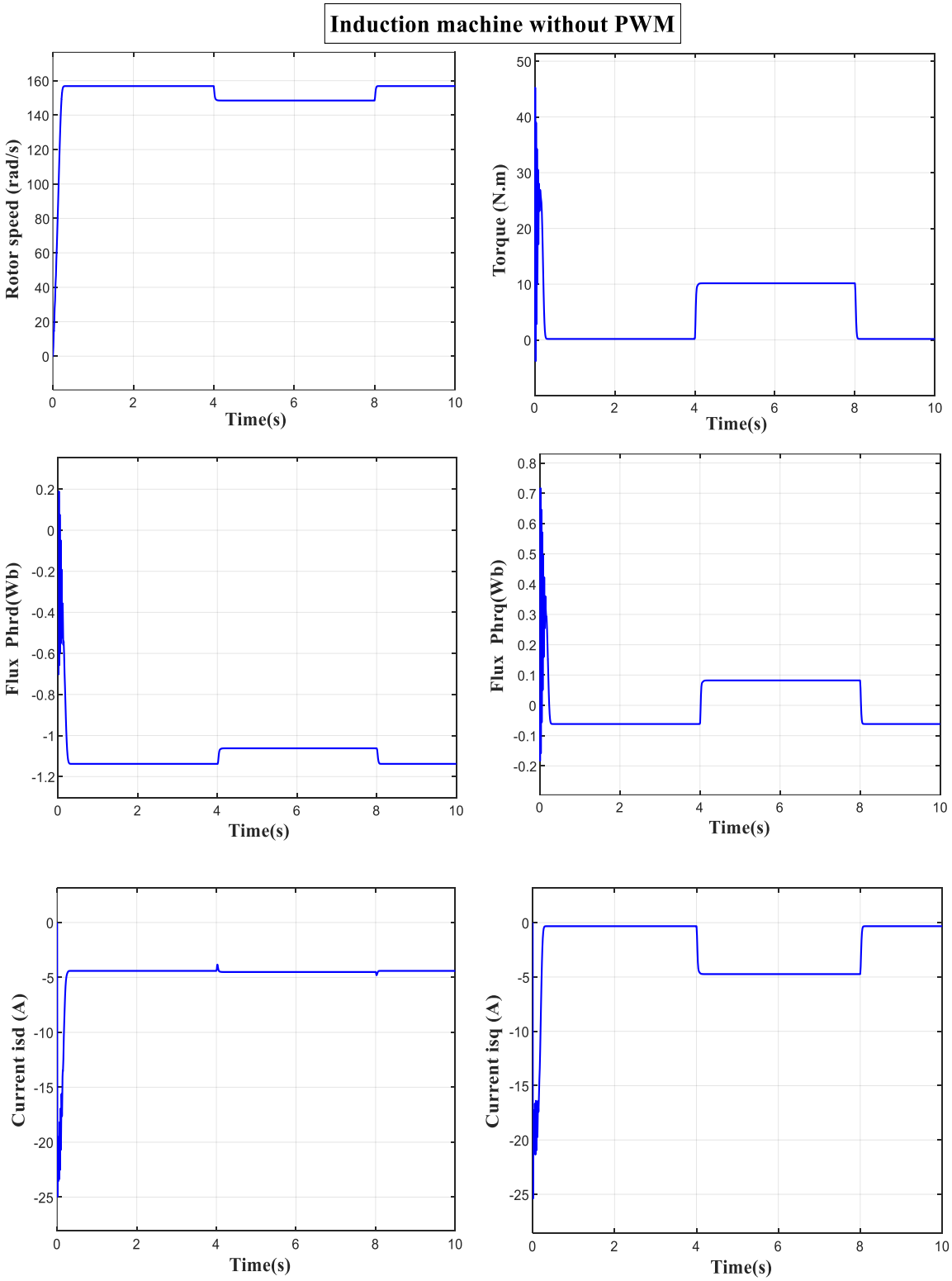


Figure III-6: Simulation results of an induction machine without PWM

III.7.1.1 Interpretation of results without inverter

- **Current**

During startup in the transient regime, significant current spikes are observed that attenuate as the transient regime progresses. Under load, the stator currents evolve according to the load applied to the motor shaft.

- **Speed**

The speed increases linearly, with a tendency to oscillate due to the inertia of the rotating masses. Under load, a decrease in rotor speed is observed, resulting in a very marked slip.

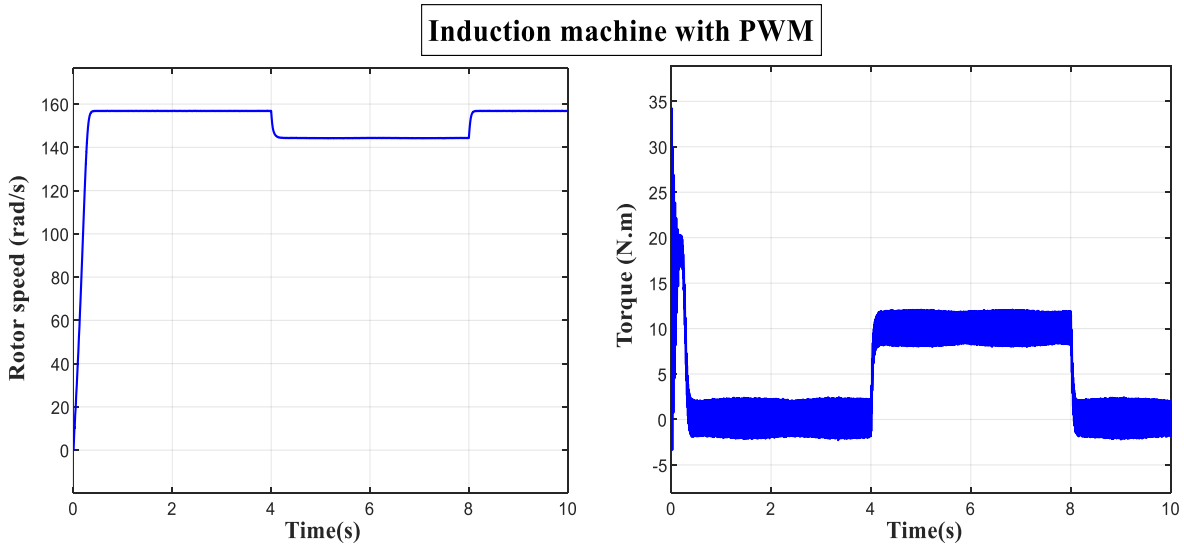
- **Torque**

The evolution of the torque between 0 and 0.2 seconds exhibits a characteristic pattern of squirrel-cage induction machine motors: highly marked pulsations at the beginning, followed by stabilization at the end of the transient regime. When the load is applied, the electromagnetic torque quickly reaches its reference value to compensate for this demand, with an almost instantaneous response before stabilizing at the resistant torque value.

- **The transition from No-load to Load**

It is observed that the transition from no-load to load at time t=4s (or from one load regime to another) occurs almost instantly, without oscillations, with very slight overshoot.

III.7.2 IM results with inverter



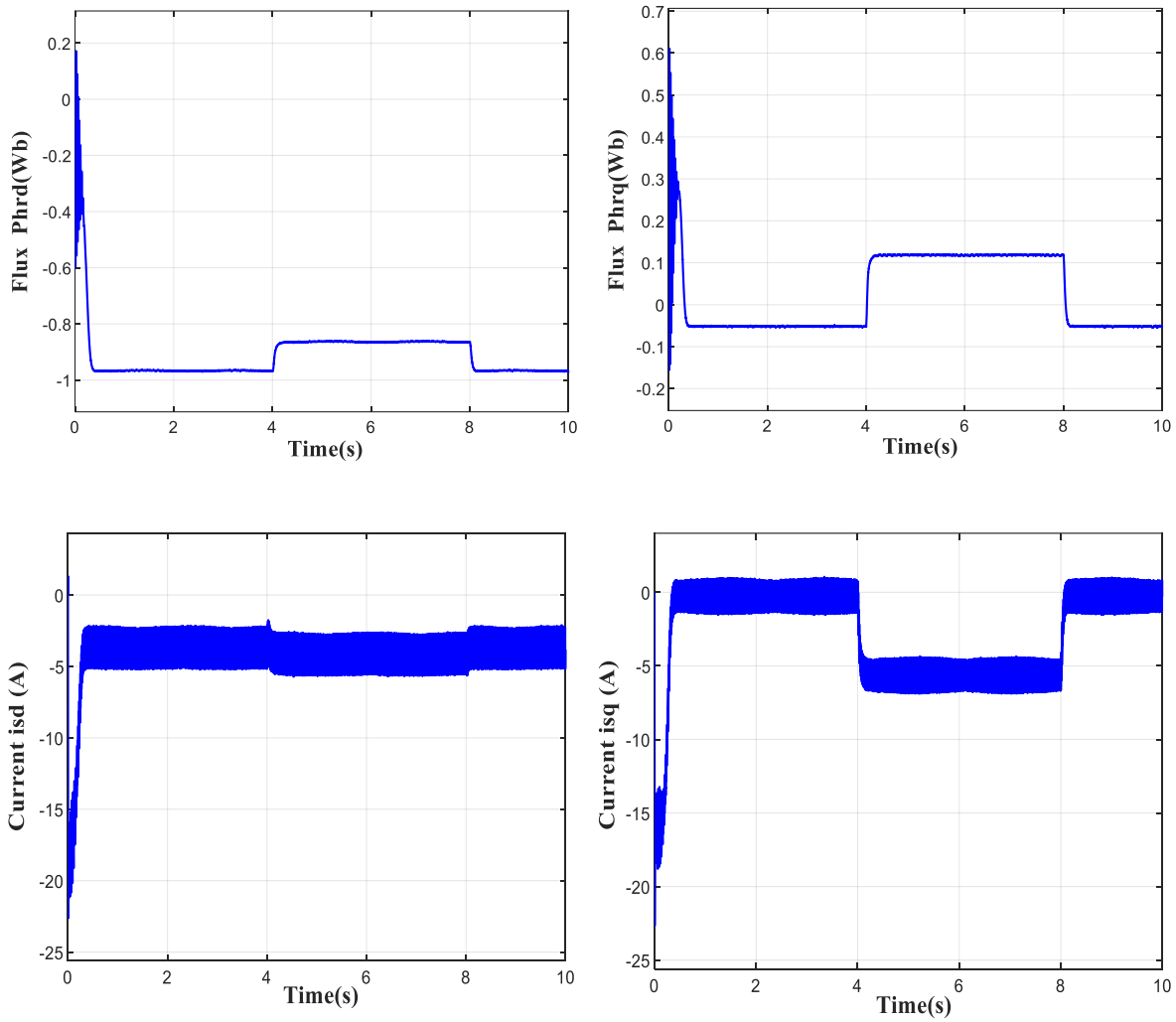


Figure III-7: Simulation results of an induction machine with PWM

III.7.2.1 Interpretation of results with inverter

- **Current**

In the transient regime, significant current spikes are observed, which attenuate as the transient regime progresses. When under load, the currents vary according to the load applied to the motor shaft.

- **Speed**

During no-load startup, the speed curve shows initial oscillations before increasing almost linearly. After about 0.2 seconds, the speed stabilizes at a constant value of 157 rad/s, corresponding to a 2-pole motor. With a load applied, an initial decrease in rotor speed is observed, resulting in a more marked slip before stabilizing at a speed suited to the load.

- **Electromagnetic Torque**

In the initial moments, highly marked pulsations are observed. During the transient regime, the torque is highly pulsative but stabilizes in the permanent regime. When loaded, the electromagnetic torque quickly reaches its reference value to compensate for the demand, with an almost instantaneous response before stabilizing at the resistant torque value.

- **The transition from No-load to Load**

The transition from no-load to load at time t=4s (or from one load regime to another) occurs almost instantly, without oscillations, with very slight overshoot.

III.7.3 Comparison of results obtained with and without inverter

A comparison of these results with those obtained in the case of a direct supply at full voltage shows a difference in the shape of the torque. In the case of an inverter supply. The electromagnetic torque is more damped during the transient regime but exhibits ripples.

The shape of the stator current component is similar to that obtained with a direct supply at full voltage,

III.8 Conclusion

We have seen that the mathematical model of the induction machine is highly non-linear, with varied, high-order dynamics. The expression of the electromagnetic torque also reveals a complex interaction between the stator and rotor fields.

Consequently, this chapter began with a general presentation of the induction machine and then examined its modeling. Park was modified in order to simplify the machine model and analyze its transient behavior. We then simulated the two-level voltage inverter and its management.

Chapter VI:

Direct Torque Control (DTC)

IV.1 Introduction

The direct torque control (DTC) was proposed as an alternative to the vector control in the middle of 1980s, by I. Takahashi. Subsequently, a number of studies have led to an accurate understanding of this control. **[DJA 21]**

Direct torque control, or DTC, is an electrical motor strategy characterized for simplicity and high performance when controlling industrial machines such as induction motors. **[RAF 15]**

In this chapter, we present the principle of direct torque control, analysing in particular the coupling and dynamics of control between stator flux and electromagnetic torque.

We will present the principles of flux and torque control, then we will develop the estimation of the two control quantities which are the stator flux and the electromagnetic torque, then we will develop the model of the hysteresis controllers involved in the general structures of the control. Finally, we present the DTC simulation results for IM using MATLAB/SIMULINK.

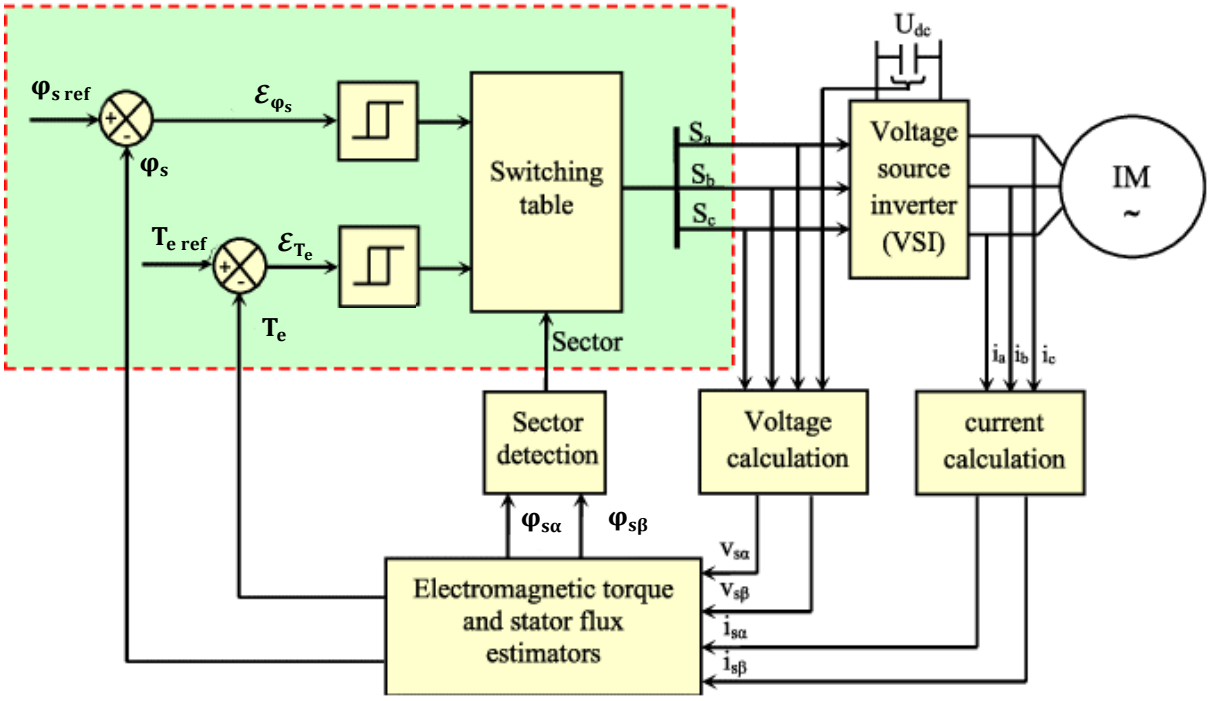


Figure IV-1: General structure of direct torque control.

IV.2 Principle of DTC control

Direct torque control (DTC) techniques involve directly controlling the closing or opening of inverter switches based on calculated stator flux and electromagnetic torque. There is no need for a modulator, tachometer or position encoder to provide speed or position information. The purpose of controlling the switches is to give the vector representing the stator flux the direction specified by the setpoint values. In order to determine the electromagnetic state of the motor, it is necessary to know the control of the inverter switches. The machine model must be established using measurements of the DC voltage at the inverter input and the stator currents, in accordance with: the machine's actual stator flux, couple she develops, its rotation speed.

There is no need to measure shaft speed, which is a major advantage of these methods. The switch actuation times are determined by comparing the flux and torque obtained with their reference values. Normally, the aim is to keep the flux constant.

IV.3 Operation of a three-phase voltage inverter

It is necessary to control the switches of the voltage inverter, so as to ensure the stability of the machine's flux and torque. The voltage vector is generated by the following equation : **[DJA 21]**

$$\overline{V}_s = \sqrt{\frac{2}{3}} U_{dc} \left[S_a + S_b e^{j\frac{2\pi}{3}} + S_c e^{j\frac{4\pi}{3}} \right] \qquad (IV.1)$$

Where (S_a, S_b, S_c) represent the logical state of the three switches: Si=1 means that the top switch is closed and the bottom switch is open, with $V_i = +U_{dc}/2)$ and Si=0 means that the top switch is open and the bottom switch is closed with ($V_i = -U_{dc}/2$).

Flux and torque control will be performed by choosing the appropriate voltage vector, which will be determined by a particular configuration of the inverter switches. With 3 switches, there are 8 possible voltage vectors for Vs, (2^3). Two vectors $V0$ and $V7$ correspond to the zero vector: (S_a, S_b, S_c) = (0,0,0) and (S_a, S_b, S_c)= (1,1,1). V0(0,0,0) is always next to an odd vector; $V1$ (1,0,0); $V3$ (0,1,0); or $V5$ (0,0,1); hence only one switch; $V7$(1,1,1) is always next to an even vector; $V2$ (1,1,0); $V4$ (0,1,1); or $V6$(1,0,1); so only one switch in each modulation period, an arm does not switch twice.

The representation in the complex plane of the six non-zero voltage vectors that can be generated by a two-level three-phase voltage inverter is shown in Figure (IV.3). The method used is as follows:

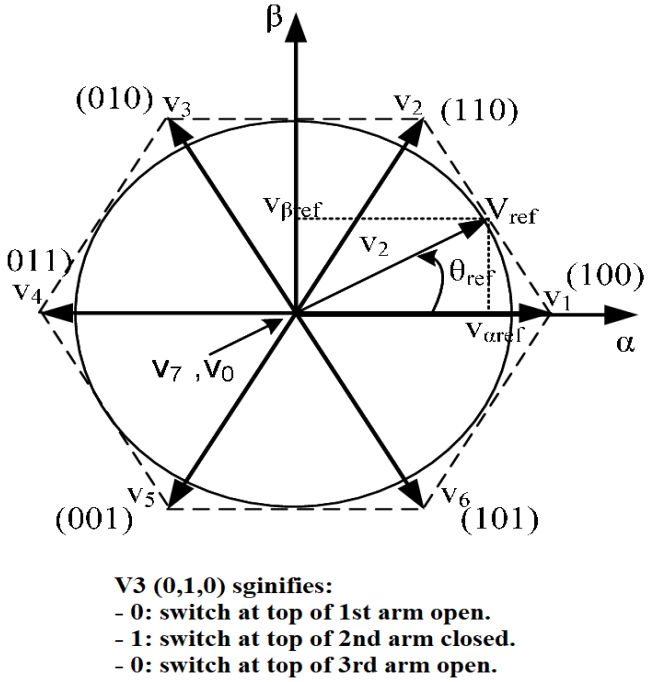


Figure IV-2:Operating sequences of a two-level voltage inverter

IV.4 Control of stator flux and electromagnetic torque

IV.4.1 Stator flux control principle

Using the model of the asynchronous machine in a frame of reference linked to the stator and the expression for the stator voltage:

$$\mathbf{V_s = R_s I_s + \frac{d\varphi_s}{dt}} \qquad \mathbf{(IV.2)}$$

The stator flux is estimated from the following relationship:

$$\boldsymbol{\varphi_s(t) = \int_0^t (V_s - R_s I_s) dt} \qquad \mathbf{(IV.3)}$$

$$\boldsymbol{\varphi_s(t) = \varphi_{s0} + V_s(t) - R_s \int I_s \, dt} \qquad \mathbf{(IV.4)}$$

Assuming that remains constant and that the term ($R_s I_s$) is negligible compared to the voltage V_s over a periodic control interval [0;Ts] corresponding to a sampling period Ts orders (S_a, S_b, S_c) are fixed, so we can write:

$$\boldsymbol{\varphi_s(t) \approx \varphi_{s0} + V_s T_e} \qquad \textbf{(IV.5)}$$

Where

$\boldsymbol{\varphi_{s0}}$: is the flux vector at time t = 0.

In a time interval T_s , the end of the vector φs moves along a straight line whose direction is given by V_s. Figure (IV.3) illustrates this principle, when the vector is selected

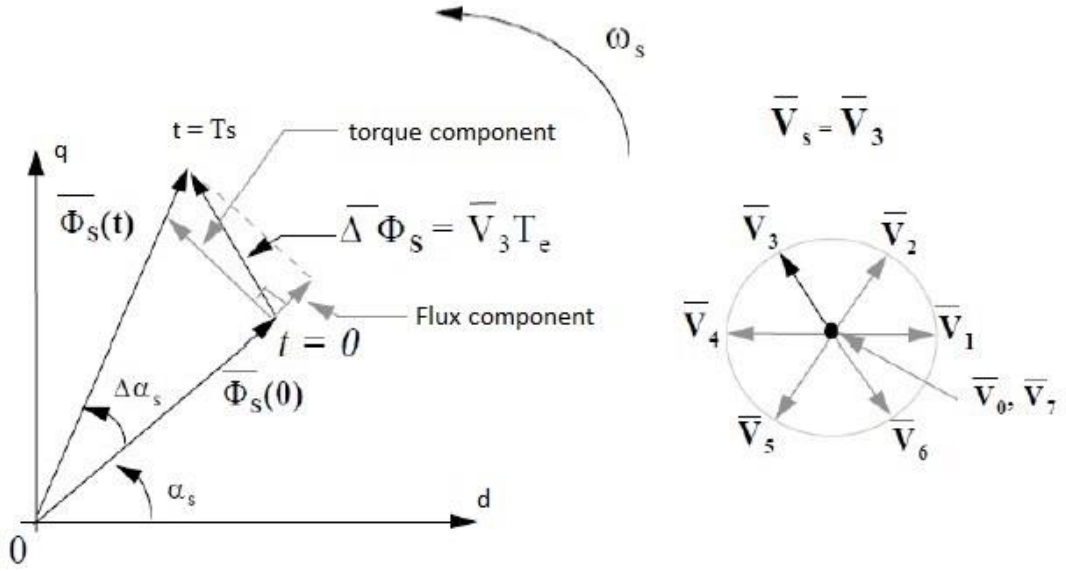


Figure IV-3:Evolution of the end of vector φ_s.

By choosing an appropriate sequence of inverter voltage vectors over successive time intervals of duration "T_s", the end of the stator flux vector (φ_s) can be made to follow the desired trajectory, provided that the control period "T_s" is much smaller than the rotation period of vector φ_s.

The vector φ_s is maintained between two values φ_{max} and φ_{min} the change from one to the other being controlled by V_s. If the control vector is one of the non-zero vectors, φ_s evolves with a constant speed proportional to the control voltage if φ_s is kept approximately constant, the torque depends only on the phase shift between the two fluxes. To meet a demand for rapid variation in torque, it is therefore sufficient to quickly modify the phase shift between the two fluxes.

For example, when φ_s reaches the value φ_{max}, the switch change is triggered so that the new value of V_s causes a decrease in the modulus of φ_s. At the same time, the new phase of

the V_s vector causes I and φs to shift in the direction of rotation, which increases the phase shift and torque.

It is conceivable to maintain a virtually constant stator flux modulus (φ_s) by choosing a circular path for the end of the flux vector. However, this can only be achieved if the control period is significantly smaller than the rotation period of the flux. In addition, the flux component of the applied voltage vectors must be minimal, while the torque component must be maximal.

In this way, the applied vectors change the position of the flux with an almost constant amplitude. When the voltage vector V_s is non-zero, the direction of displacement of the end of the flux φs and given by its derivative ($d\varphi_s/dt$) practically corresponding to the vector V_s.

With regard to the rotor flux φ_r, it can be assumed that given the high time constant of the rotor of the asynchronous machine, its amplitude does not vary during a transient, so the variation in rotor flux is negligible compared with that of the stator flux.

IV.4.2 Principle of electromagnetic torque control

The electromagnetic torque is proportional to the vector product between the stator and rotor flux vectors according to the following expression :

$$\mathbf{T_e = k(\bar{\varphi}_s \cdot \bar{\varphi}_r) = k|\bar{\varphi}_s||\bar{\varphi}_s| \sin(\gamma)} \qquad \mathbf{(IV.6)}$$

With :

$\bar{\varphi}_s$: represents the stator flux vector.

$\bar{\varphi}_r{}'$: represents the rotor flux vector returned to the stator

γ : represents the angle between the stator and rotor flux vectors

According to this expression, the torque therefore depends on the amplitude of the two vectors $\bar{\varphi}_s$ and $\bar{\varphi}_s{}'$ and their relative position.

IV.4.3 Voltage vector selection

The choice of the stator voltage vector $\bar{V}_s$ depends on the position of the stator flux vector in the complex $\alpha\beta$ plane, the desired variation in the modulus of the flux φ_s, the desired

variation in the torque, and the direction of rotation of the flux. desired for the torque, and the direction of rotation of the flux. **[IKR 22]**

The space in which the flux φ_s evolves is divided into six zones called sectors

- When the flux φ_s is in a zone i, control of the flux and torque can be achieved by selecting one of the following six vectors:

- If $\overline{V}_{i+1}$ is selected then $\overline{\boldsymbol{\varphi}}_{\mathbf{s}}$ increases and the $\mathbf{T_e}$ increases;
- If $\overline{V}_{i-1}$ is selected then $\overline{\boldsymbol{\varphi}}_{\mathbf{s}}$ increases and the $\mathbf{T_e}$ decreases;
- If $\overline{V}_{i+2}$ is selected then $\overline{\boldsymbol{\varphi}}_{\mathbf{s}}$ decreases and the $\mathbf{T_e}$ increases;
- If $\overline{V}_{i-2}$ is selected then $\overline{\boldsymbol{\varphi}}_{\mathbf{s}}$ decreases and the $\mathbf{T_e}$ decreases;
- If $\overline{V}_0$ or $\overline{V}_7$ is selected, the $\overline{\varphi}_s$ rotation is stopped, resulting in a decrease in torque while the torque modulus remains unchanged.

The level of efficiency of the applied voltage vectors also depends on the position of the flux vector in zone i.

Indeed, at the beginning of the zone, the $\overline{V}_{i+1}$ and $\overline{V}_{i+2}$ vectors are perpendicular to $\overline{\varphi}_s$, resulting in a rapid change in torque but a slow change in the amplitude of the flux $\overline{\varphi}_s$, whereas at the end of the zone, the change is the opposite. With the $\overline{V}_{i-1}$ and $\overline{V}_{i+2}$ vectors, there is a slow change in torque and a rapid change in the amplitude of $\overline{\varphi}_s$ at the beginning of the zone, whereas the opposite is true at the end of the zone.

Whatever the direction of flux or torque evolution, in zone i, the two vectors $\overline{V}_i$ and $\overline{V}_{i+3}$ are never used. In fact, these two vectors cause a strong increase in flux, but their effect on torque depends on the zone, with a zero effect in the middle of the zone. The stator voltage vector $\overline{V}_s$ at the inverter output is deduced from the estimated torque and flux deviations from their references, as well as from the position of the vector $\overline{\varphi}_s$. A modulus and position estimator of $\overline{\varphi}_s$ and a torque estimator are therefore required.

	$\overline{V}_{i-2}$	$\overline{V}_{i-1}$	$\overline{V}_i$	$\overline{V}_{i+1}$	$\overline{V}_{i+2}$	$\overline{V}_{i+3}$	$\overline{V}_0, \overline{V}_7$
$\overline{\varphi}_s$	$\Downarrow$	$\Uparrow$	$\Uparrow\Uparrow$	$\Uparrow$	$\Downarrow$	$\Downarrow\Downarrow$	$\Uparrow\Downarrow$
$T_e\ (\Omega > 0)$	$\Downarrow\Downarrow$	$\Downarrow\Downarrow$	$\Downarrow$	$\Uparrow$	$\Uparrow$	$\Downarrow$	$\Downarrow$
$T_e\ (\Omega < 0)$	$\Downarrow$	$\Downarrow$	$\Uparrow$	$\Uparrow\Uparrow$	$\Uparrow\Uparrow$	$\Uparrow$	$\Uparrow$

Table IV-1: Evolution of the flux and torque quantities

IV.5 Estimators

The challenge of direct torque and flux control is to obtain a reliable estimate of the instantaneous value of torque, flux and stator flux angle. The performance depends on the accuracy with which these quantities are estimated. **[IKR 22]**

IV.5.1 Stator flux estimation

Stator flux can be estimated from measurements of the machine's stator current and voltage using the following equation

$$\overline{\boldsymbol{\varphi_s}}(\mathbf{t}) = \int_0^t (\bar{\mathbf{V}}_\mathbf{s} - \mathbf{R_s}\bar{\mathbf{I}}_\mathbf{s})\mathbf{dt} \qquad (\mathbf{IV.7})$$

$$\begin{cases} \boldsymbol{\varphi}_{\mathbf{s\alpha}} = \int_0^t (\mathbf{V_{s\alpha}} - \mathbf{R_s I_{s\alpha}})\mathbf{dt} \\ \boldsymbol{\varphi}_{\mathbf{s\beta}} = \int_0^t (\mathbf{V_{s\beta}} - \mathbf{R_s I_{s\beta}})\mathbf{dt} \end{cases} \qquad (\mathbf{IV.8})$$

Where $\varphi_{s\alpha}$ and $\varphi_{s\beta}$ are estimated using the equation above, which requires knowledge of the components of the stator current and voltage vectors: $I_{s\alpha}$, $I_{s\beta}$, $V_{s\alpha}$, $V_{s\beta}$. The components of the stator current vector are obtained by applying the Concordia transformation to the measured three-phase components I_{sa}, I_{sb}, I_{sc}.

$$\begin{cases} \mathbf{I_{s\alpha}} = \sqrt{\dfrac{3}{2}}\mathbf{I_{sa}} \\ \mathbf{I_{s\beta}} = \dfrac{\mathbf{1}}{\sqrt{\mathbf{2}}}\,(\mathbf{I_{sb}} - \mathbf{I_{sc}}) \end{cases} \qquad (\mathbf{IV.9})$$

The components of the stator voltage vector are obtained from the switch states.

$$\begin{cases} \mathbf{V_{s\alpha}} = \sqrt{\dfrac{2}{3}}\mathbf{U_{dc}}(\boldsymbol{S_a} - \dfrac{\mathbf{1}}{\mathbf{2}}(\boldsymbol{S_b} + \boldsymbol{S_c})) \\ \mathbf{V_{s\beta}} = \dfrac{\mathbf{1}}{\sqrt{\mathbf{2}}}\,\mathbf{U_{dc}}(\boldsymbol{S_b} - \boldsymbol{S_c}) \end{cases} \qquad (\mathbf{IV.10})$$

The stator flux module is written as:

$$\boldsymbol{\varphi_s} = \sqrt{(\boldsymbol{\varphi_{s\alpha}}^2 + \boldsymbol{\varphi_{s\beta}}^2)} \qquad (\mathbf{IV.11})$$

The area in which the flux vector $\varphi_s$is determined from the components $\varphi_{s\alpha}$and $\varphi_{s\beta}$.The angle between the stator reference frame and the vector $\varphi_s$is equal to:

$$\measuredangle\boldsymbol{\varphi_s} = \boldsymbol{arctang}\frac{\boldsymbol{\varphi_{s\beta}}}{\boldsymbol{\varphi_{s\alpha}}} \qquad (\mathbf{IV.12})$$

IV.5.2 Electromagnetic torque estimation

Electromagnetic torque can be estimated from estimated fluxes and measured stator currents. It can be formulated as follows:

$$\boldsymbol{T_e} = \boldsymbol{P}(\boldsymbol{\varphi_{s\alpha}}\mathbf{I_{s\beta}} - \boldsymbol{\varphi_{s\beta}}\mathbf{I_{s\alpha}}) \qquad (\mathbf{IV.13})$$

IV.6 Development of the control vector

IV.6.1 Flux corrector

The aim of the flux controller is to keep the end of the flux vector φ_s in a circular forme, As seen in figure (IV.4), the corrector output must indicate the direction of evolution of the $\boldsymbol{\varphi_s}$ modulus, in order to select the corresponding voltage vector. For this purpose, a simple two-level hysteresis controller is perfectly suitable for this, and provides very good dynamic performance. **[IKR 22]**

$$\left|\boldsymbol{\varphi_{s_{ref}}} - \boldsymbol{\varphi_s}\right| \leq \Delta\boldsymbol{\varphi_s} \qquad (\mathbf{IV.14})$$

With:

$\boldsymbol{\varphi_{s_{ref}}}$: The reference stator flux

$\Delta\boldsymbol{\varphi_s}$: Corrector hysteresis width

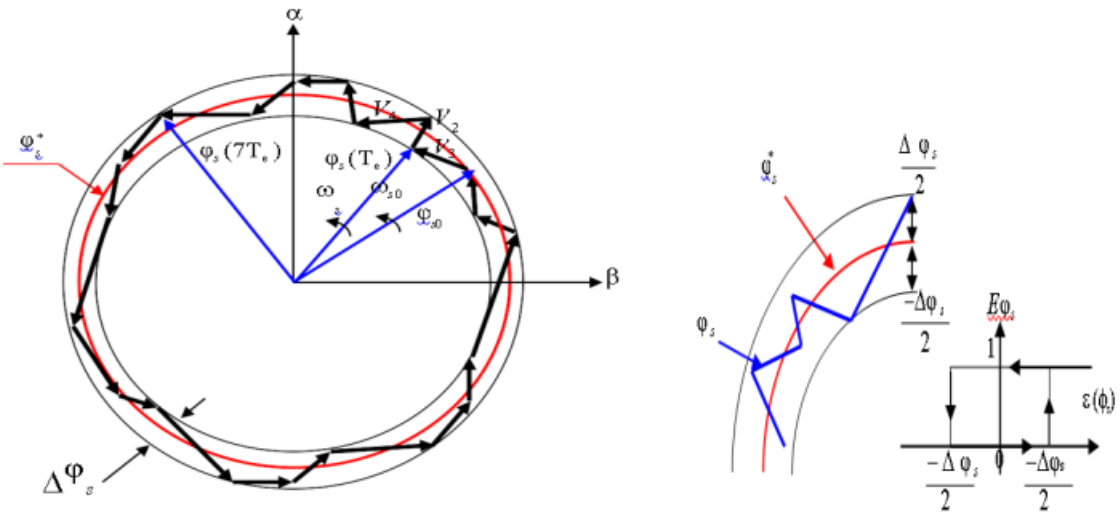


Figure IV-4:Selection of voltages corresponding to stator flux amplitude control.

IV.6.2 Torque corrector

The main role of the torque corrector is to keep the torque within the designated hysteresis band. There by controlling the amplitude of torque ripples and ensuring that it remain within the specified limits.

$$\left|\mathbf{T_{e_{ref}}} - \mathbf{T_e}\right| \leq \Delta\mathbf{T_e} \qquad (\mathbf{IV.15})$$

With :

$\mathbf{T_{e_{ref}}}$: The reference torque.

$\Delta\mathbf{T}$: The hysteresis band of the corrector.

However, an important difference between torque control and flux control, which is that torque can be either positive or negative, depending on the direction of rotation.

- **The two-level corrector**

This corrector is simpler to implement, and by correctly selecting zero vectors along the Ni zones, we can see that for each zone i, there is an inverter arm of the inverter that never switches, thus reducing the average switching frequency, thus reducing switching losses in the inverter. **[DJA 21]**

The model of two-level voltage inverter is shown in Figure IV-5

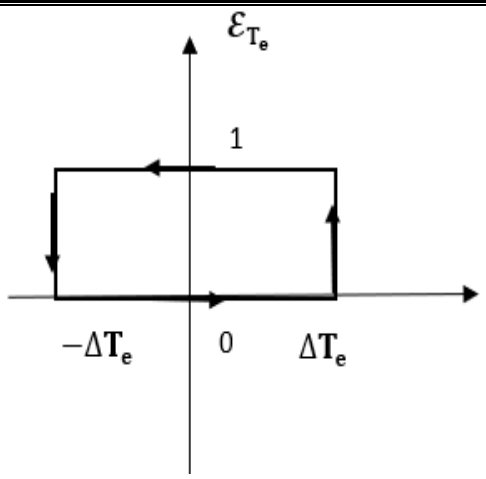


Figure IV-5:The two-level torque corrector

IV.7 Development of switching table:

Depending on the sector and the flux and torque evolution, we can choose the voltage vector Vs to be applied to respect the flux and torque setpoints. The switching table used to select the appropriate vector is based on the flux $\boldsymbol{\varepsilon_{\varphi_s}}$ and torque $\boldsymbol{\varepsilon_{T_e}}$ errors, and on the position of the stator flux vector (i=1,….,6).

To control torque and stator flux, several commutation tables can be used, each of which has an influence on the behavior of the machine in terms of torque, stator flux, current ripple, switching frequency and the ability to operate in two or four quadrants of the torque-speed plane. In the following table IV-2, four tables switching are presented, while Table IV.3 shows the table for the fourth most commonly used strategy, which is also proposed in our work.

	$T_e \Uparrow \varphi_s \Uparrow$	$T_e \Uparrow \varphi_s \Downarrow$	$T_e \Downarrow \varphi_s \Uparrow$	$T_e \Downarrow \varphi_s \Downarrow$
1st Strategy	V_{i+1}	V_{i+2}	V_0, V_7	V_0, V_7
2st Strategy	V_{i+1}	V_{i+2}	V_i	V_0, V_7
3st Strategy	V_{i+1}	V_{i+2}	V_i	V_{i+3}
4st Strategy	V_{i+1}	V_{i+2}	V_{i-1}	V_{i-2}

Table IV-2: Different strategies of switching tables

Flux	Torque	N=1	N=2	N=3	N=4	N=5	N=6	Regulators
$\mathcal{E}_{\varphi_s} = 1$	$\mathcal{E}_{T_e} = 1$	V_2	V_3	V_4	V_5	V_6	V_1	Two Level
	$\mathcal{E}_{T_e} = 0$	V_7	V_0	V_7	V_0	V_7	V_0	
$\mathcal{E}_{\varphi_s} = 0$	$\mathcal{E}_{T_e} = 1$	V_3	V_4	V_5	V_6	V_1	V_2	
	$\mathcal{E}_{T_e} = 0$	V_0	V_7	V_0	V_7	V_0	V_7	

Table IV-3: Control strategy with a two-level hysteresis comparator.

The switching table is a crucial element of this structure, as it allows the Vs vector to be selected without using the rotor position, which would usually require a speed sensor. This switching table, combined with hysteresis comparators, replaces the PWM generator of conventional voltage inverter control structures.

IV.8 Advantages and Drawbacks of DTC control

IV.8.1 The advantages of Direct Torque Control

- Excellent torque dynamics.
- Robustness against variations in machine rotor parameters.
- No decoupling of currents from control voltages.
- No need to know the rotor position angle. Only the sector in which the stator flux is located.
- No need to use a speed sensor to implement it.

IV.8.2 Drawbacks of Direct Torque Control

The disadvantages of DTC can be summarized as follows:

- The existence of often significant torque and flux ripples,
- The switching frequency is not controlled,
- The need to use stator flux and torque estimators,
- Poorly controlled low-speed operation,
- Stator currents are poorly controlled during transients.

IV.9 Simulation results for DTC of IM

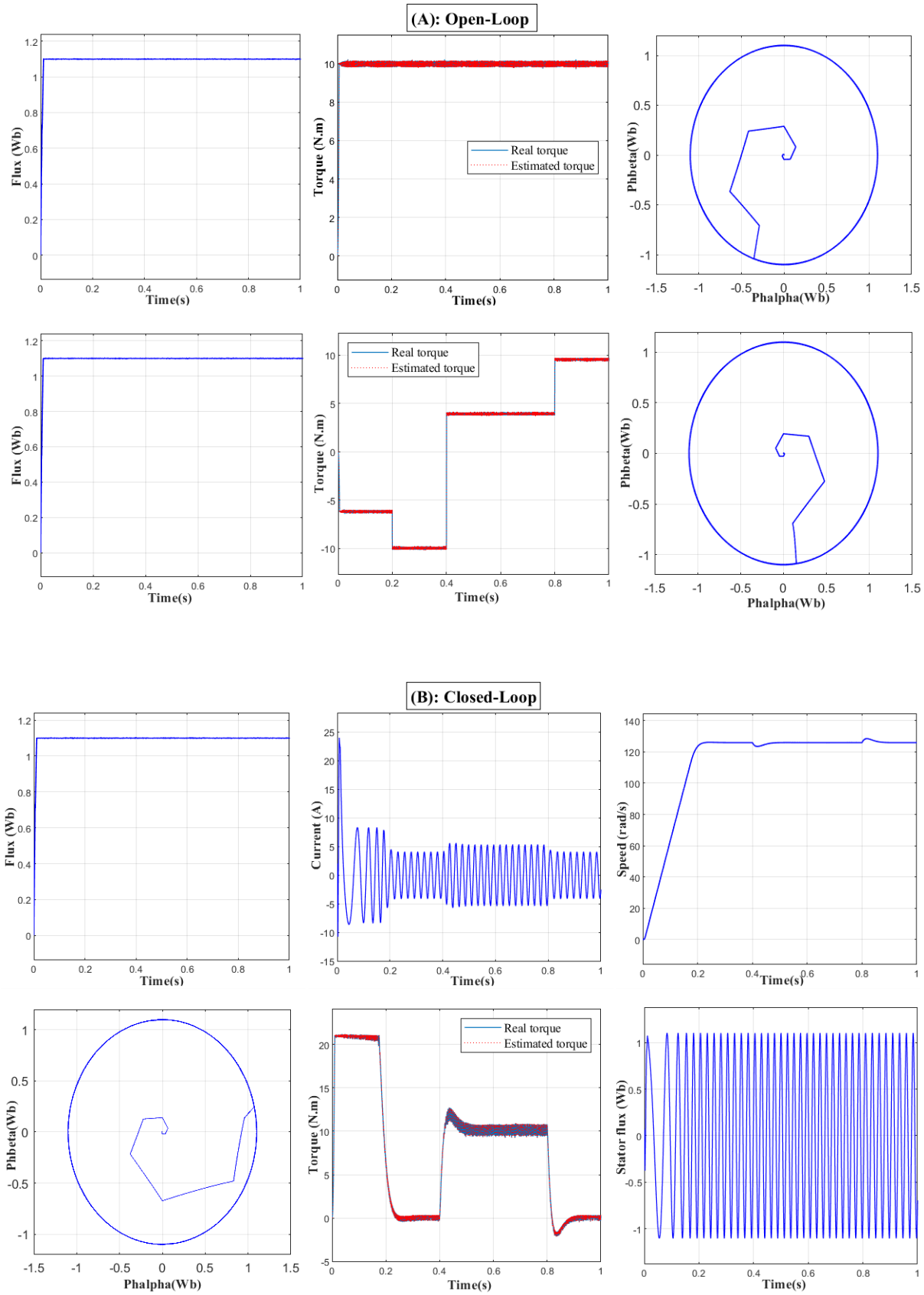


Figure IV-6:Evolution of torque, stator flux and IM-DTC current [(A): open loop, (B): closed loop]

IV.10 Interpretation of results

It can be seen that the speed follows its reference value without overshooting with a response time equal to 0.21S and recovers again when the load torque is applied. The electromagnetic torque follows its reference perfectly before and after the application of the load torque, without any overshoot, but with ripples caused by the hysteresis regulators. The stator current (i_{sa}) has a sinusoidal shape with an increase observed when the load torque is applied, the fluxes $\varphi_{s\beta} = f(\varphi_{s\alpha})$ have a circular shape, which verifies the purpose of the hysteresis comparator which also allows a stator flux with a constant modulus equal to 1.1Wb for all models. The simulation results obtained show that the DTC control is a robust control. Indeed, even in the presence of magnetic saturation, the DTC operates correctly and does not need to be modified.

IV.11 Conclusion

The work presented in this chapter highlights the feasibility and advantages of applying the DTC control technique to an asynchronous machine fed by a two-level voltage inverter.

The results obtained show that direct torque control of the asynchronous machine based on the DTC technique makes it possible to achieve high dynamic performance with a simple structure. It provides a practical solution to the robustness and dynamic problems encountered in the FOC control structure for the same type of machine.

In fact, direct torque control offers several significant advantages, such as simplicity and ease of implementation, robustness, high dynamics, and precision, among others. These results show that the DTC control technique can be considered an interesting alternative for controlling asynchronous machines.

Chapter V:

PV pumping system-DTC based on MPPT-Remora

V.1 Introduction

Renewable energy is a crucial resource, and solar energy is the most abundant form of it. Photovoltaic (PV) cells use the photovoltaic effect to convert sunlight directly into electrical energy. The performance of a photovoltaic system depends on several factors, including sunshine, temperature, shading, and the load being supplied. To optimize efficiency, a Maximum Power Point Tracker (MPPT) is essential to continuously adjust the maximum power extracted from the photovoltaic generator (PVG), as the Maximum Power Point (MPP) varies according to environmental conditions. In the case of partial shading, there may be multiple maximums on the P-V curve, including one global maximum (GMPP) and several local maximums (LMPPs).

Conventional techniques, such as the hill-climbing algorithm and P&O (Perturb and Observe) algorithm, can be limited by the risk of getting stuck in a local optimum that they are not always capable of tracking the global maximum (GMPPT). To improve this, Research is underway to develop more efficient methods, including meta-heuristic algorithms inspired by nature and by the behavior of animals, to find new solutions that adapt to the constraints of the environment.

For this reason, this chapter focuses on a new meta-heuristic called Remora, which aims to optimize GMPPT tracking, demonstrating its effectiveness. It also highlights the importance of the effect of shading and the nature of the load for the performance of a photovoltaic array.

V.2 The proposed photovoltaic system

The study in this chapter is applied to a photovoltaic pumping system based on the MPPT-Remora technique; as shown in Figure (V-1), where firstly we propose the simulation results for a DC load as a resistance and five panels as a source, this configuration is tested under three patterns, the first under zero shading [1000-1000-1000-1000-1000 W/m2], the second under weak partial shading [1000-1000-500-1000-1000 W/m2], and the third under strong shading [500-1000-800-1000-200 W/m2].

Secondly, this load is replaced by a pumping system as an AC load, that contains a DTC-control of the induction machine related to the centrifugal pump.

To get the needed value of DC voltage to feed the induction motor (514V), we use in this case fifteen panels in series, this system is tested under two scenarios, the first without shading and the second scenario under PSC [900-1000-700-900 W/m2].

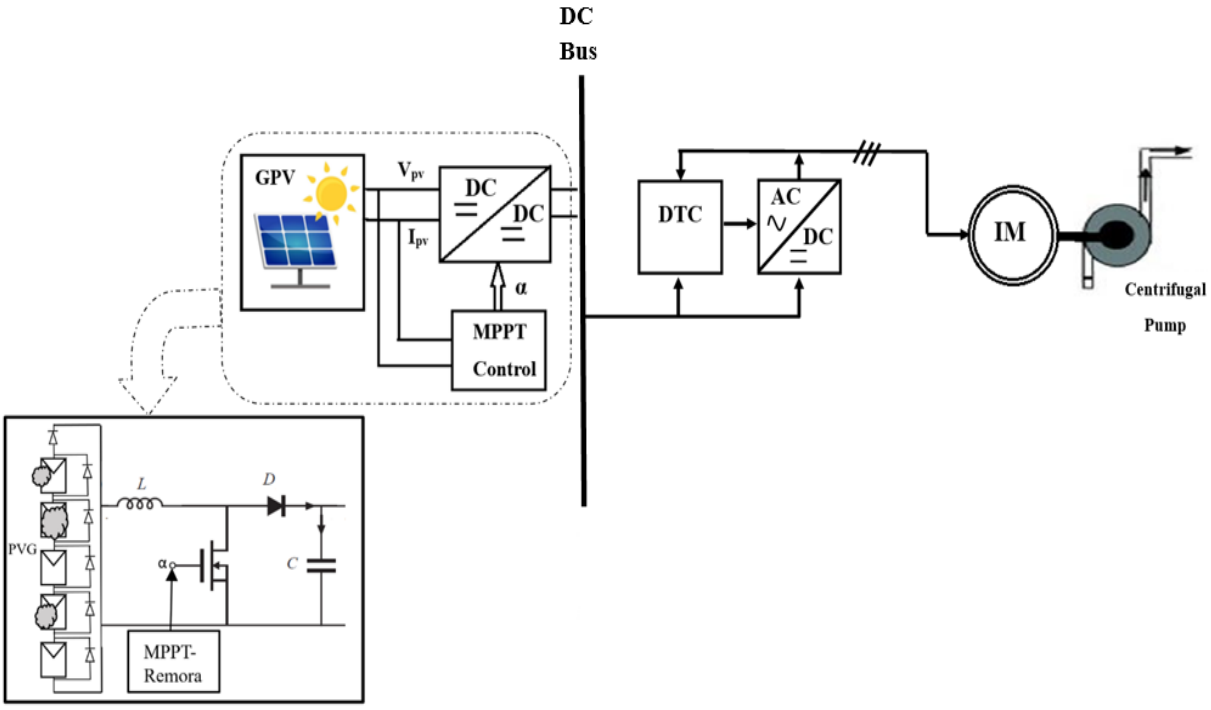


Figure V-1: The proposed system

V.3 Overview of pumps

Pumps are all hydraulic machines that move liquids from a low-pressure region to a high-pressure region. Its operation consists of producing a pressure difference between the suction region and the repulsion region by means of the active organ (piston, wheel, etc.) of the pump. From a physical point of view, the pump transforms mechanical energy into hydraulic energy. **[LEI 16]**

There are two main types of pumps:

- Positive displacement (volumetric) pumps
- Centrifugal pumps

V.3.1 Positive displacement pump

The positive displacement pump transmits the kinetic energy of the motor in a reciprocating motion (back-and-forth movement), allowing the fluid to overcome gravity by successive variations of a volume connected alternately to the suction port and the discharge port. These pumps draw in the fluid by increasing its volume and then discharge it by decreasing the same volume.

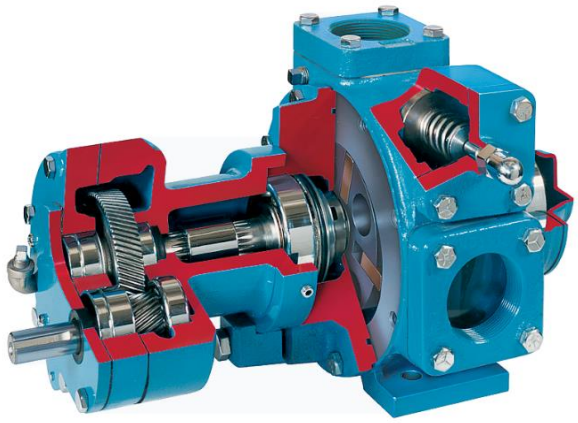


Figure V-2: Positive displacement pump

V.3.2 Centrifugal pump

A centrifugal pump is an open system, a sort of hole or duct, in which a field of centrifugal forces is set up. It transmits the kinetic energy of the motor to the fluid using a rotational movement of impellers or vanes. The water enters the center of the pump and is pushed outwards and upwards by the centrifugal force of the imperllers. They use variations in the speed of the fluid being pumped combined with the effect of centrifugal force to obtain an increase in pressure. Centrifugal pumps are the most common type of water pump. They are coupled with asynchronous motors forming an electro pump unit. **[LEI 16]**

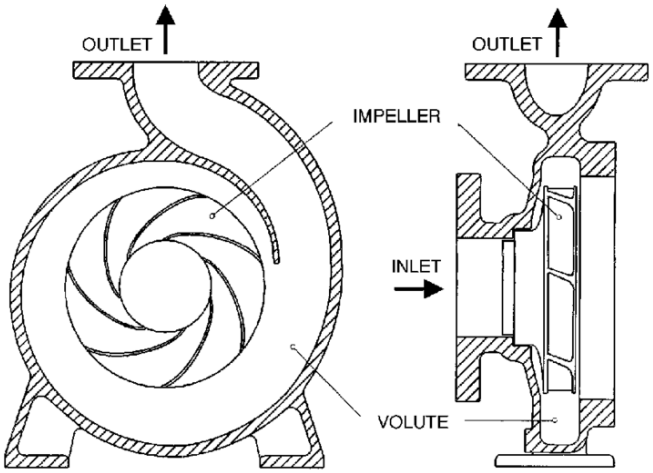


Figure V-3: Centrifugal pump

We employed a centrifugal pump in our pumping system.

V.3.3 Modeling Pump

The operation of a centrifugal pump involves three parameters: head (HMT), flow, and speed. The pumping head is the sum of the static head and the dynamic head. **[LEI 16]**

In this application, the hydraulic power of the centrifugal pump is given by :

$$\mathbf{P_h} = \eta_{\mathbf{mp}}.\mathbf{P_{ele}} = \boldsymbol{\rho}.\mathbf{g}.\mathbf{HMT}.\mathbf{Q} \qquad (\boldsymbol{V}.\mathbf{1})$$

With:

$\mathbf{P_h}$: Power communicated to the fluid by the pump (W)

$\mathbf{P_{ele}}$: Asynchronous motor electrical power (W)

$\eta_{\mathbf{mp}}$: Efficiency of the motor-pump unit (%)

$\mathbf{g}$: Acceleration due to gravity (9.81 m/s2)

$\boldsymbol{\rho}$: Density of water (1000 Kg/m3)

$\mathbf{Q}$: Volume flow (m3/s)

$\mathbf{HMT}$: Total manometric head that the pump must meet (m).

The centrifugal pump opposes a resisting torque$\mathbf{C_r}$.

$$\mathbf{C_r} = \mathbf{K_r}.\Omega^{\mathbf{2}} \qquad (\boldsymbol{V}.\mathbf{2})$$

Where:

Ω : Asynchronous motor speed (rad/s).

$\mathbf{K_r}$: a proportionality coefficient [(Nm/$(rad.s^{-1})^2$] which is expressed by the following equation:

$$\mathbf{K_r} = \frac{\mathbf{P_n}}{\Omega_\mathbf{n}^{\,3}} \qquad (V.3)$$

$\mathbf{P_n}$: Nominal power of the asynchronous motor (W).

$\Omega_\mathbf{n}$: Asynchronous motor rated speed (rad/s).

V.4 MPPT Based on Remora Algorithm

ROA, a new meta-heuristic algorithm proposed by **Heming Jia, Xiaoxu Peng** and **Chunbo Lang** in 2021, is inspired by the intelligent traveler in the ocean, the remora and their random replacement of hosts. **[SHU 22]**

Remora, also known as sucker fish, is warm-water fish that have the particularity of attaching themselves to the skin of sharks using a natural sucker. **[CHA 22]**



Figure V-4: The individual remora

In doing so, they feed on the parasites and bacteria present on the shark's skin, helping to maintain the shark's health by preventing various skin infections. **[HEM 21]**

As part of this mutually beneficial relationship, sharks defend their remora from predators, as they provide them with a valuable service by keeping their bodies clean and free

from parasites. Remora behavior provides the basis for two host algorithms, the Whale Optimisation Algorithm (WOA) and the Swordfish Optimisation Algorithm (SFO), in which remora follows optimization strategies designed for humpback whales and swordfish.**[CHA 22]**



Figure V-5: Remora parasitizes on different hosts

V.5 Remora optimization principle

To enhance the overall optimization capability of ROA. The formulas in ROA involving SFA and WOA were improved on the original form, and a formula that was more suitable for the movement of remora was obtained.

By simulating the whole process of remora's predation, the exploration and exploitation were divided into two processes: “Free travel” and “Eat thoughtfully”, and the “experience” of remora was taken as the main basis for the judgment of phase switching. **[HEM 21]**

V.5.1 Initialization

In the proposed ROA, it is assumed that the candidate solution is the remora. Initialize the population location and memory location $\boldsymbol{X_{pre}}$, initialize the optimal solution $\boldsymbol{X_{best}}$ and corresponding optimal fitness $f(\boldsymbol{X_{best}})$. **[HAM 23]**

V.5.2 Free travel (Exploration)

Free travel” is further divided into “SFO Strategy” and “Experiment attack” global optimization methods, which correspond to “big global” and “small global” respectively in the algorithm. Besides, “Experiment attack” is the main way for Remora to accumulate experience. **[HEM 21]**

V.5.2.1 SFO Strategy.

The remora is stuck to the swordfish, its position can be considered as the swordfish position, the formula of its location update was improved and got the following equation:**[SHU 22]**

$$\mathbf{X(t+1) = X_{best}(t) - (rand.\left(\frac{X_{best} + X_{rand}}{2}\right) - X_{rand})} \qquad (\mathbf{V.5})$$

where t is the number of current iterations, $X_{best}(t)$ represents the best solution obtained so far, X_{rand} indicates a random location, and rand is a uniformly distributed random number between 0 and 1. **[CHA 22]**

V.5.2.2 Experience attack.

To know whether it is necessary to change the host or not, the remora must continuously take small steps around the host, this behavior is modeled by the following equation: **[SHU 22]**

$$\mathbf{X_{att} = X_i(t) + randn.\left(X_i(t) - X_{pre}\right)} \qquad (\mathbf{V.6})$$

X_{pre} represents the previous position wich regarded as an experience, X_{att} represents the tentative position. If the cost function value obtained by the attempted solution is smaller than the current solution. **[HAM 23]**

$$\mathbf{f\left(X_i(t)\right) > f\left(X_{att}(t)\right)} \qquad (\mathbf{V.7})$$

The remora then chooses a different feeding method for local optimization shown in the next section. However, if it is not the case, shown in (V.8), the remora returns back to the host selection, **[HAM 23]**

$$\mathbf{f\left(X_i(t)\right) < f\left(X_{att}(t)\right)} \qquad (\mathbf{V.8})$$

V.5.3 Eat thoughtfully (Exploitation)

Eat thoughtfully" is further divided into two feeding modes which are "WOA Strategy" and "Host feeding". Different convergence methods enhance the stability of the algorithm. **[HEM 21]**

V.5.3.1 WOA Strategy

To update the remora position in the research space for the WOA strategy, we use the following equations: **[HAM 23]**

$$\mathbf{X_i(t+1) = D * e^N * \cos(2\pi b) + X_i(t)} \quad (\mathbf{V.9})$$

$$\mathbf{D = |X_{best}(t) - X_i(t)|} \quad (\mathbf{V.10})$$

$$\mathbf{b = -\left(1 + \frac{t}{M_{ax_T}}\right)} \quad (\mathbf{V.11})$$

$$\mathbf{N = rand * (b - 1) + 1} \quad (\mathbf{V.12})$$

D represents the distance between the best candidate and the Remora, N is a random number in [-1, 1], b is a linear decrease from (-1 to -2) during the iteration, and M_{axT} is the maximum number of iterations. **[CHA 22]**

V.5.3.2 Host Feeding.

The solution space can be minimized to the position space of the host. The movement of the Remora on or around the host can be considered as small steps, which can be presented mathematically as follows: **[HAM 23]**

$$\mathbf{X_i(t+1) = X_i(t) + A} \quad (\mathbf{V.13})$$

$$\mathbf{A = B * (X_i(t) - C * X_{best})} \quad (\mathbf{V.14})$$

$$\mathbf{B = 2 * V * rand - V} \quad (\mathbf{V.15})$$

$$\mathbf{V = 2 * \left(1 - \frac{t}{M_{ax_T}}\right)} \quad (\mathbf{V.16})$$

where A is the moving distance of the remora, which is related to the volume of the remora and the host. The remora factor C is used to limit the position of the remora, and its value is set to 0.1 in ROA. B is used to simulate the host's volume, and V is used to simulate the volume of the remora. **[SHU 22]**

V.6 Proposed ROA-MPPT

The maximum power point tracking by the ROA method is used to get the optimum power, the input of MPPT block is represented by the power $(V_{PV} * I_{PV})$ and the output by the duty cycle of DC-DC converter. Figure (V-6) represents the flowchart of the ROA used in this work with the initial position 0, 0.3, 0.5, 0.9, the population number 50, and the maximum number of iterations 150.

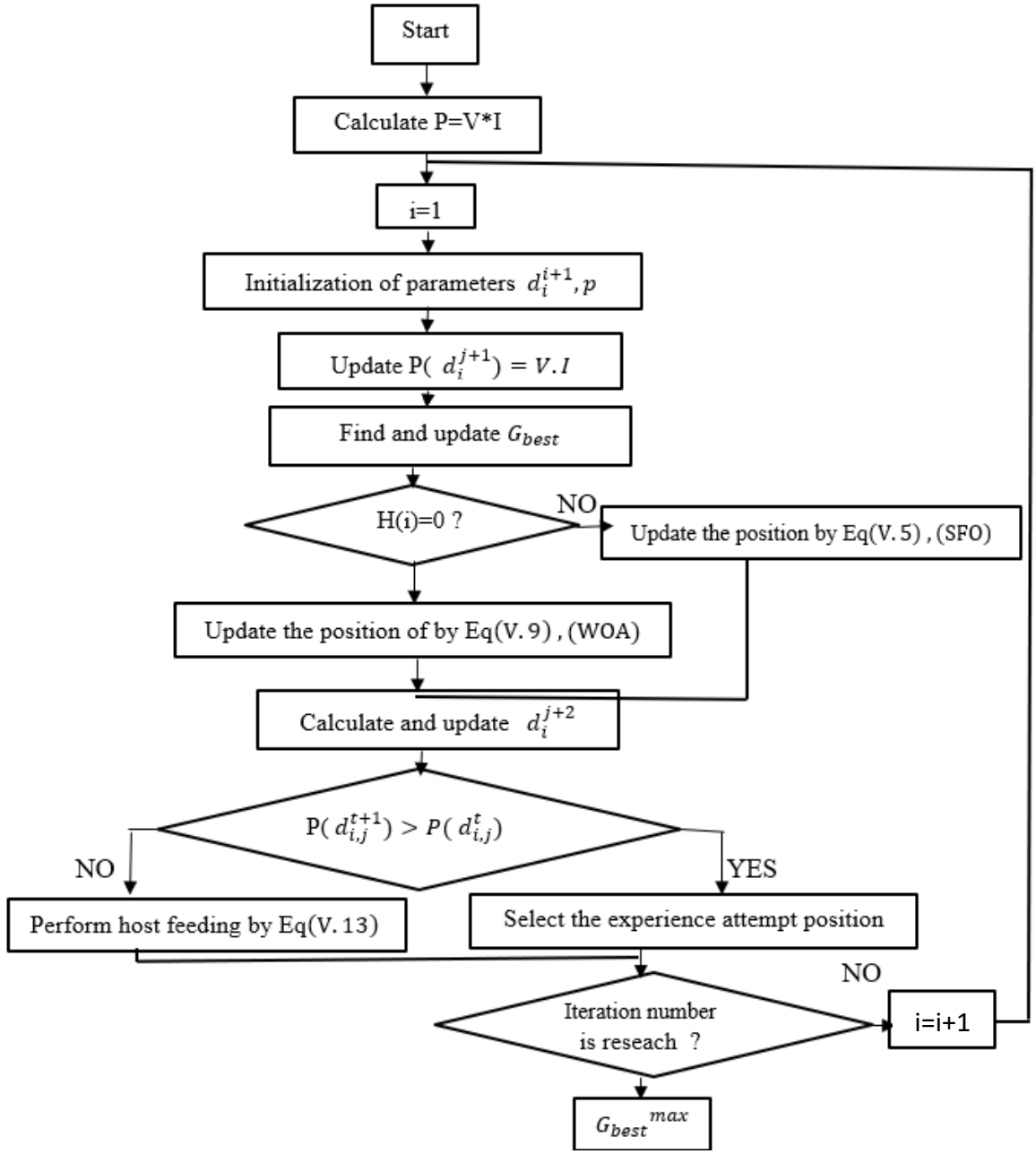


Figure V-6:Flowchart of ROA

V.7 Simulation results

The objective of this study is to test the ability of the proposed method ROA to achieve the global maximum power point (GMPPT) under different shading scenarios. As previously mentioned, the first proposed system consists of DC load and five panels connected in series, with the maximum power of a single panel equal to 200W (see Appendix). As shown in Figure (V-7), we have a single peak (GMMP1) in the first case (Zero Shading), we have two peaks

(GMMP2, LMMP2) in the second (Weak Shading), and in the third (strong Shading) we have four peaks (GMMP3, three LMMP3).

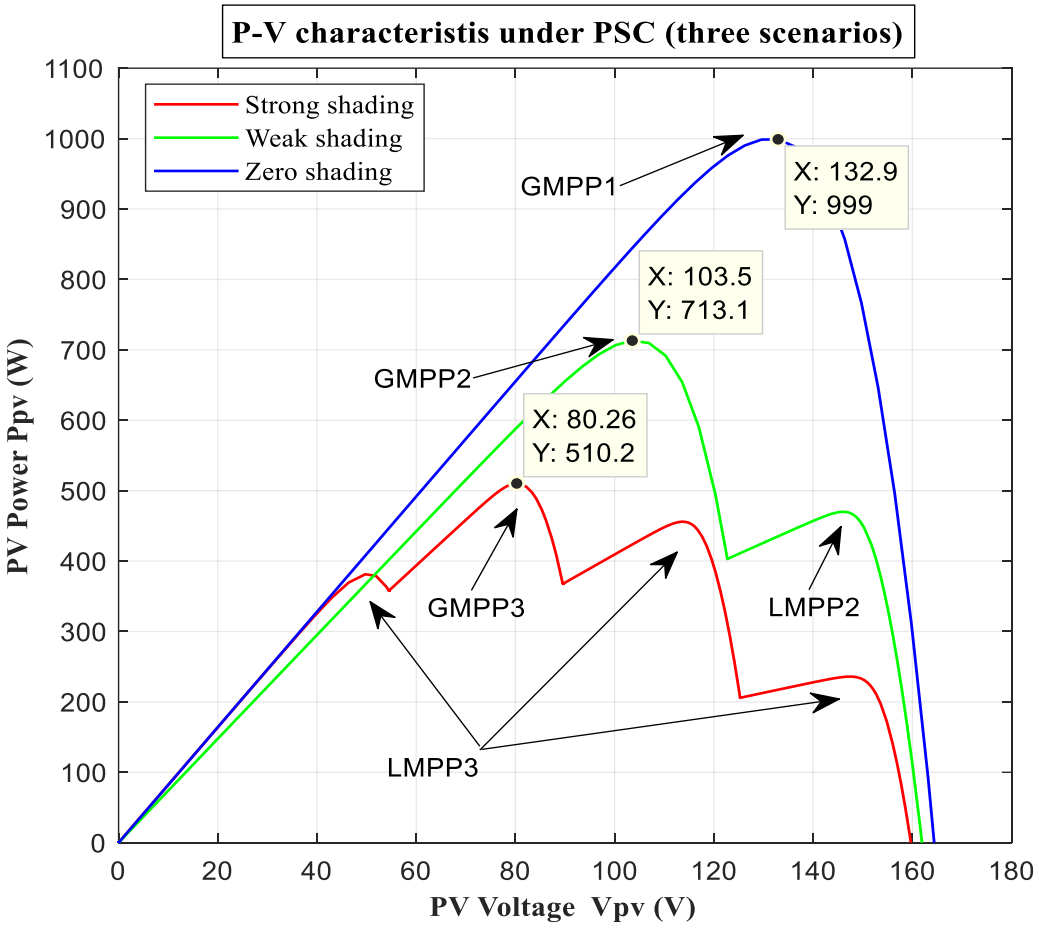


Figure V-7: Impact of partial shading on the P(V) characteristic at T=25 °C

Figure (V-8) shows that the algorithm searches for the GMMP for the three scenarios, and after a while it converges to the global.

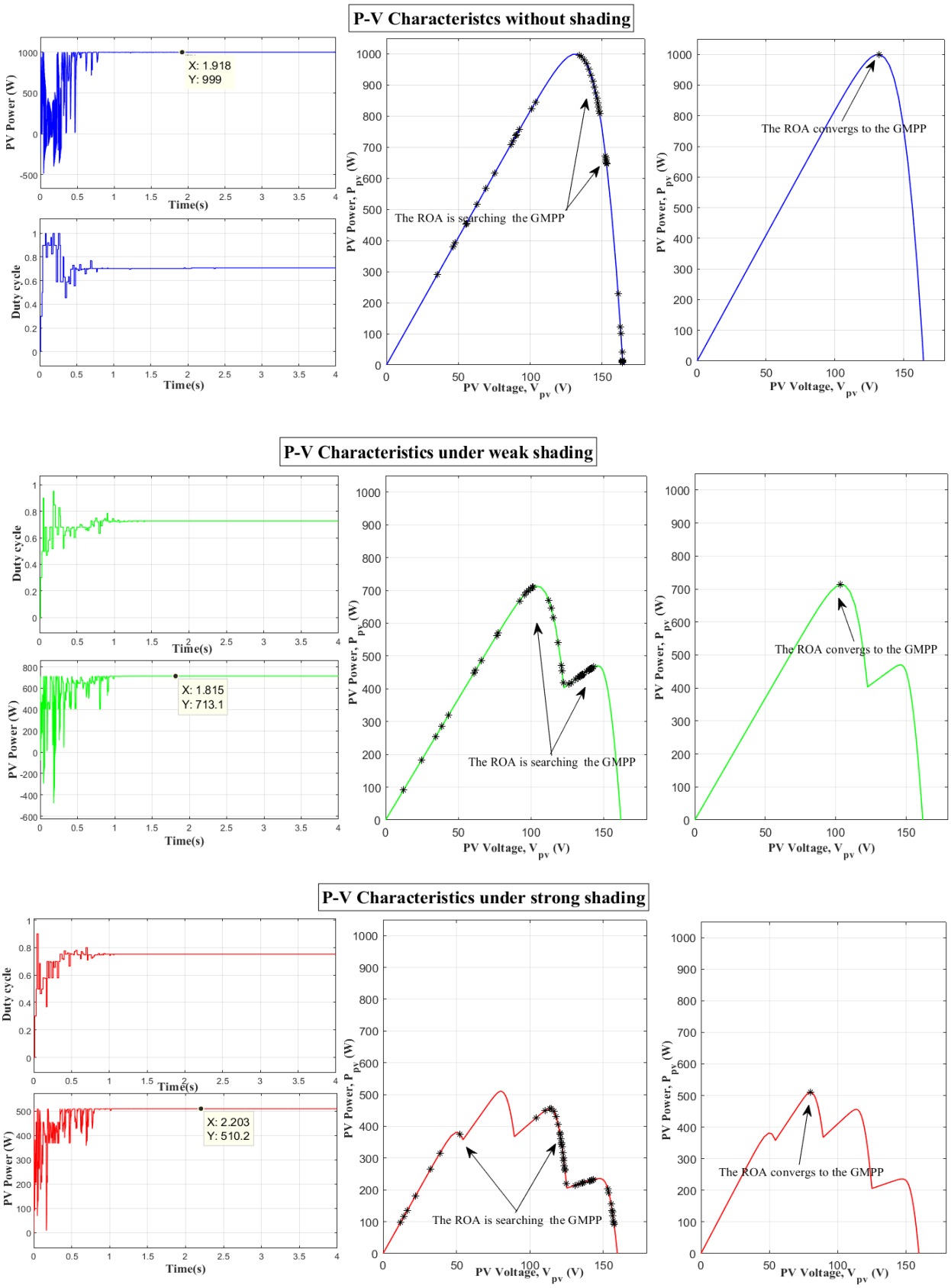


Figure V-8:PV power and duty cycle responses of the PV-resistance load controlled by Remora-MPPT without and under shading with MPPT

According to the panel power response (Figure V-8), the Remora algorithm succeeded in achieving the GMPP in three scenarios as shown in the same figure, the ROA converges to GMMP1 (999W), in case of weak shading, the ROA converges to GMMP2 (713.1W), and in the case of strong shading the ROA converges to GMMP3 (510.2W).

In the second part, the pumping system consists of fifteen PV panels, as previously mentioned, and it is simulated with a constant load torque (10N.m) applied between 0.4 s and 0.8 s these systems are tested without shading and under the PSC.

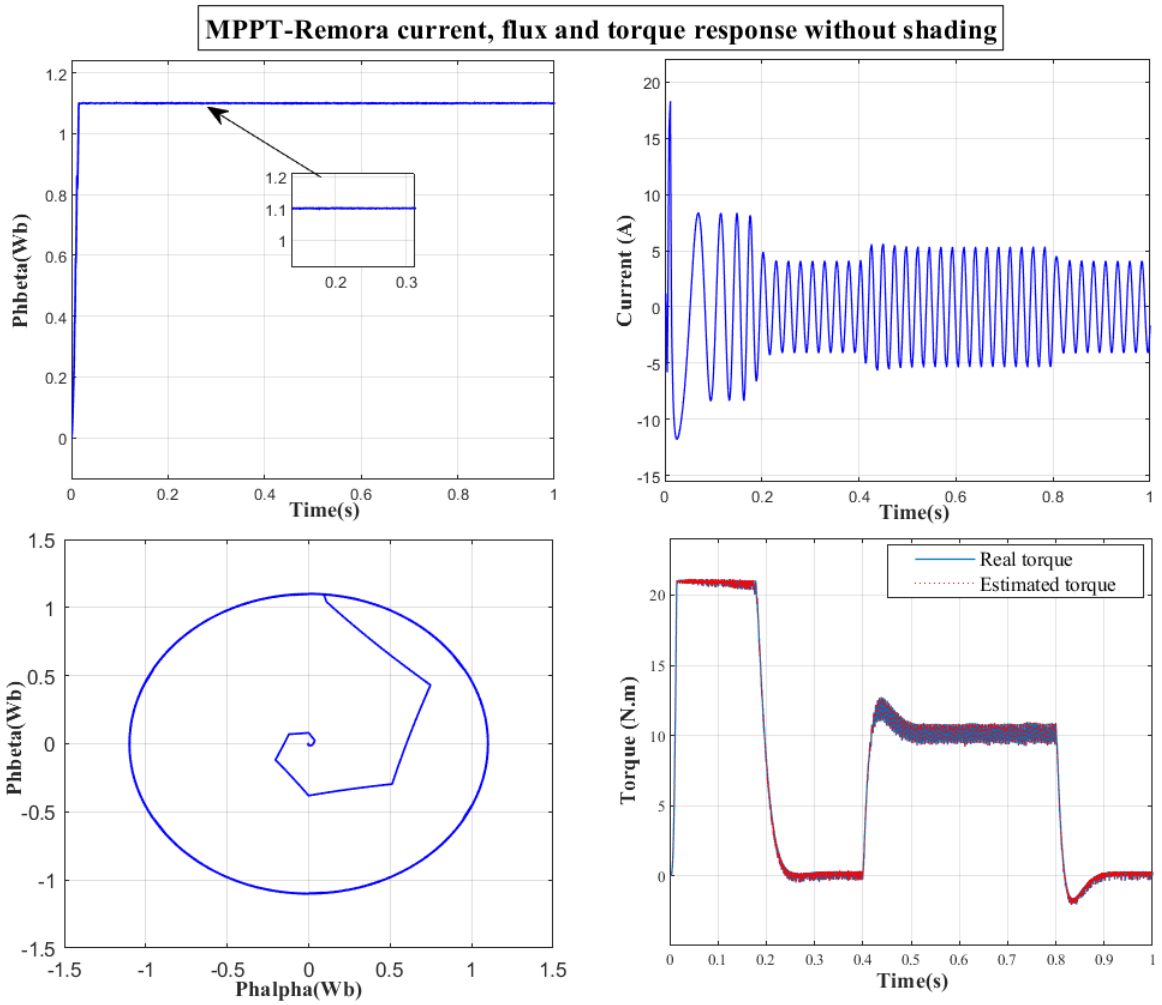


Figure V-9: Flux, torque and current response without shading

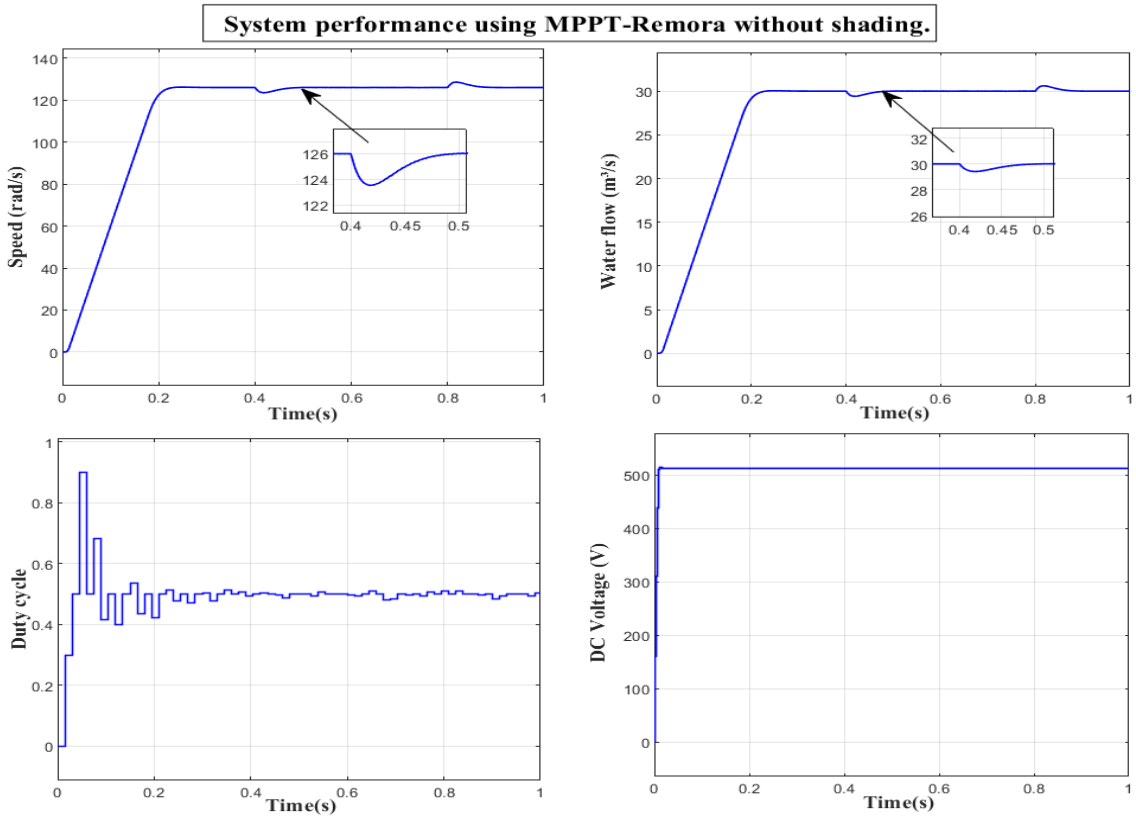


Figure V-10:Performance of the photovoltaic system (PV-IM-Pump) using MPPT-Remora without shading

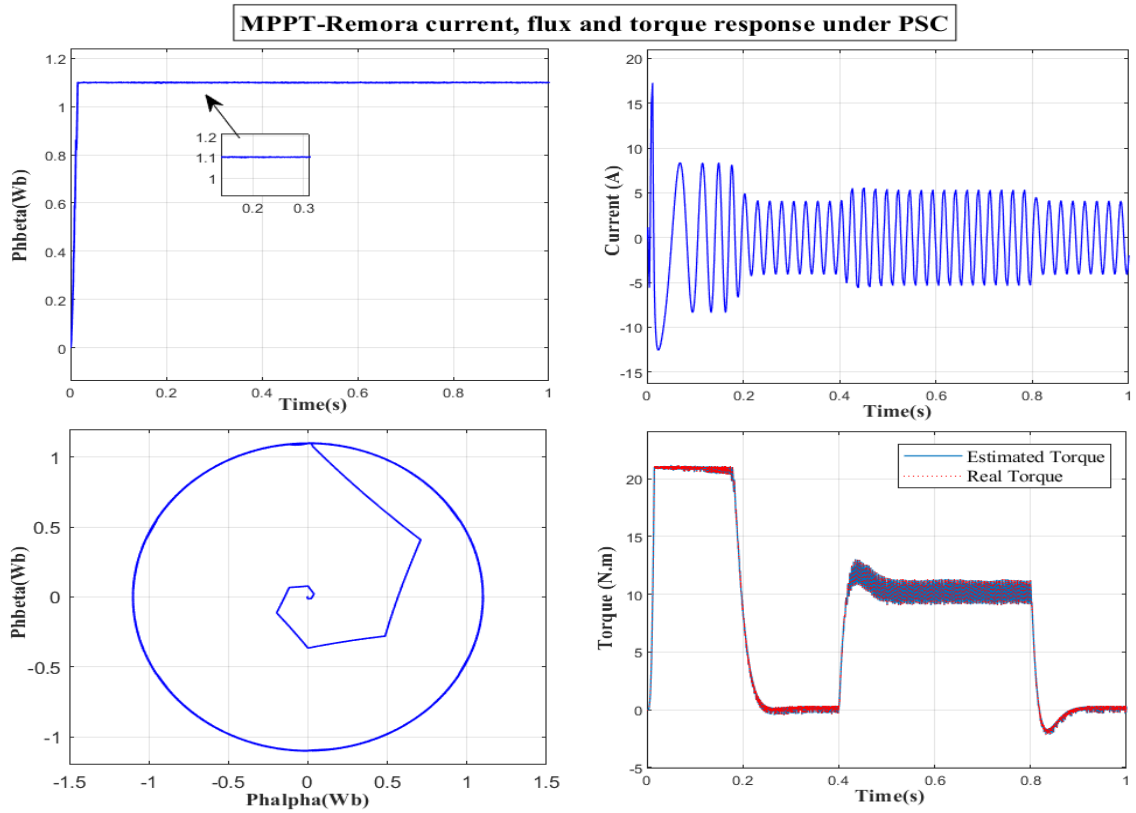


Figure V-11: Flux, torque and current response under PSC

Figure V-11 shows the pumping system response with the same load torque (10N.m) applied between (0,4s and 0.8s) under partial shading conditions.

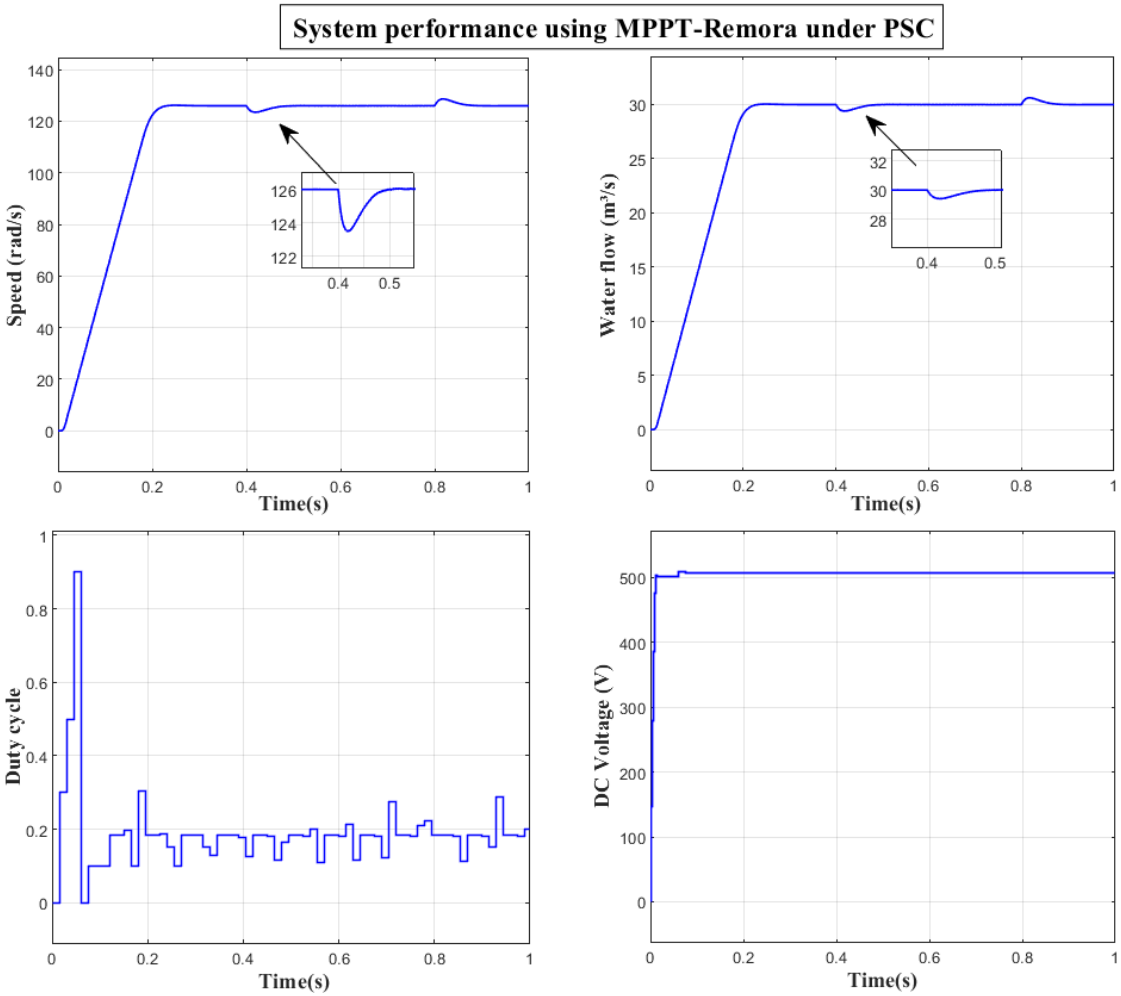


Figure V-12:Performance of the photovoltaic system (PV-IM-Pump) using MPPT-Remora under PSC

The results in Figures (V-9) and (V-11) show the pumping system responses flux follow the reference (φ*=1.1Wb), the flux trajectory in the systems describes a circle and the current is sinusoidal.

Figures (V-10) and (V-12) show the duty cycle response, the DC voltage, and the evolution of the speed for the same load torque between (t=0.4s and 0.8s) where (w*=126 rad/s). Overall, the performance obtained by our photovoltaic system based on MPPT-Remora with and without shading is considered effective and perfect.

V.8 Conclusion

In this chapter, we have given a detailed study of a meta-heuristic technique used in various fields for optimization which is Remora Optimization Algorithm ROA.

The dynamic behavior of the proposed PV system in the case of partial shading has been studied, applying this technique to find the GMPP which aims to replace conventional techniques. According to the simulation results obtained, the proposed method offers satisfactory results.

In conclusion, the Remora method is one of the many optimization methods that are simple and effective, allowing us to improve renewable energy systems.

General Conclusion

General Conclusion

Photovoltaic solar energy is universally recognized as a leading renewable energy source for generating electricity. However, the energy generated by solar panels is closely linked to environmental conditions. It can be said that random variations in these conditions are the major problem that hinders the operation of the PV system at its maximum power point.

For this reason, and as it is essential to design high-performance photovoltaic systems capable of adapting to climatic variations and load fluctuations, we have proposed a hybrid system (PV-IM-Pump) based on a new metaheuristics algorithm called Remora Optimization algorithm under partial shading and follow the response of our system.

We first presented the basic concepts of PV systems and the modeling of a PV cell. Then we have modeled the different types of DC-DC converters, focusing more specifically on boost converter, and we have classified the different methods of MPPT control.

Our study also looked at different aspects of induction machine. We first set out the fundamental principles of this machine and then carried out an in-depth analysis of their modeling using Park's equivalent model, taking into account certain simplifications to obtain a representative model of the machine's behavior.

Simulations carried out on the machine supplied by a three-phase source and controlled by a PWM-controlled voltage inverter revealed a strong coupling between the magnetic flux and the torque of the machine. To remedy this, we introduced a decoupled control called DTC (Direct Torque Control), which allows the machine's flux and torque to be controlled independently, thus improving its performance.

Finally, the intelligent algorithm Remora was used to extract the maximum power point of the photovoltaic generator and the different behaviors of the Remora fish were explained, to allow optimal operation of the photovoltaic system.

The simulation results confirmed the satisfactory efficiency of the system using the Remora Optimization Algorithm (ROA) method in finding the global maximum power point, even in the presence of partial shading or other non-ideal conditions that can cause several local maximum power points. As summered in the following table:

DC load	Zero shading: ROA converges to GMPP1(999 W)
	Weak shading: ROA converges to GMPP2 (713.1W)
	Strong shading: ROA converges to GMPP3 (510.2 W)
AC load	Without shading and under PSC: the flux follows the reference (φ*=1.1Wb), and the DC voltage is nearly equal to the needed value.

This ability is crucial for maintaining the overall efficiency of the photovoltaic system and guaranteeing maximum energy generation.

In conclusion, this research highlights the promising nature of using the ROA search algorithm for MPPT in PV systems. Its rapid convergence, robustness, and simplicity make it a valuable tool for maximizing power extraction from solar panels. Ongoing research and experimentation will help refine the algorithm's parameters and understand its limitations, paving the way for more efficient and reliable solar energy conversion.

Future research should build upon this technique, further developing it and exploring its combination with other methods.

Appendix

- **Induction Machine parameters**

Nominal power	**3.5 Kw**
Nominal torque	**10 N.m**
Nominal flux	**1.1 Wb**
Frequency	**50 HZ**
Stator resistance	**4.85 Ω**
Rotor resistance	**3.805 Ω**
Stator inductance	**0.274 H**
Rotor inductance	**0.274 H**
Mutual inductance (Msr)	**0.258 H**
Moment of inertia	**0.031 Kg/m^2**
Coefficient of friction	**0.001131 IS**
Number of pole pairs	**2**

- **PV Module**

Open circuit voltage Voc	**32.9 V**
Short-circuit current Isc	**8.21A**
MPP current ($Impp$)	**7.4 A**
MPP voltage ($Vmpp$)	**27 V**
Maximum power ($Pmax$)	**200 W**
Parallel resistance (Rp)	**951.9319 Ω**
Series resistor (Rs)	**0.2172 Ω**
Number of cells in series per module	**54**
Number of modules in series	**15**

REFERENCES

[ABA 23] O. Abaidi. "Modélisation et Simulation d'un Onduleur à trois Niveaux NPC alimenter par une machine asynchrone double étoile." MASTER ACADEMIQUE, UNIVERSITE KASDI MERBAH OUARGLA, 2023.

[AGH 22] Aghaei M., Nedaei A., Eskandari A., & Milimonfared J. "Introductory Chapter: Solar Photovoltaic Energy." IntechOpen, 2022. doi: 10.5772/intechopen.106259.

[BEL 23] Belbali, A., Makhloufi, S., Kadri, A., Abdallah, L., & Seddik, Z. "Mathematical Modeling of a Three-Phase Induction Motor." 2023.

[CHA 22] W. Changshen, J. Heming, Di Wu, R. Honghua, L. Shanglong, L. Qingxin, and L. Abualigah. "Modified Remora Optimization Algorithm with Multistrategies for Global Optimization Problem." Mathematics, 2022, 10(19), 3604.

[DAN 19] Dan Chiras. "Solar Electricity Basics - Revised and Updated 2nd Edition: Powering Your Home or Office with Solar Energy." New Society Publishers, Canada, 2019. pp. 39-49.

[DEG 24] Nassir Deghfel, Abd Essalam Badoud, Farid Merahi, Mohit Bajaj, and Ievgen Zaitsev. "A New Intelligently Optimized Model Reference Adaptive Controller Using GA and WOA-Based MPPT Techniques for Photovoltaic Systems." 2024.

[DJA 21] Djamila, C., & Yahia, M. "Direct Torque Control Strategies of Induction Machine." 2021.

[DOU 24] Youssouf Doumbia. "Elaboration and Characterisation of Organic-Inorganic Hybrid Perovskite Thin Films for Photovoltaic Solar Cells." PhD thesis, Universitat Politècnica de València (Spain), 18 January 2024.

[FOR 17] M. Forouzesh, Y. P. Siwakoti, S. A. Gorji, F. Blaabjerg, and B. Lehman. "Step-Up DC–DC Converters: A Comprehensive Review of Voltage-Boosting Techniques, Topologies, and Applications." IEEE Transactions on Power Electronics, vol. 32, no. 12, pp. 9143-9178, Dec. 2017. doi: 10.1109/TPEL.2017.2652318.

[GRA 18] Gary D. Price. "Renewable Power and Energy: Photovoltaic Systems." Volume I, Momentum Press LLC, New York, 2018.

[HAI 17] Haider Ibrahim, Nader Anani. "Variations of PV Module Parameters with Irradiance and Temperature." 9th International Conference on Sustainability in

Energy and Buildings SEB-17, 5-7 July 2017, Chania, Crete, Greece. Energy Procedia, 134, 2017, 276-285.

[HAM 23] F. Hamidia, A. Abbadi, M. Skender, A. Morsli, F. Bettache, A. Medjber, and A. Tlemcani. "Maximum Power Point Tracking Based on Remora Algorithm under PSC." Nonlinear Dynamics and Systems Theory, 23(4), 2023, 381-388.

[HEM 21] J. Heming, Jia P., Xiaoxu, and L. Chunbo. "Remora Optimization Algorithm." Expert Systems With Applications, 185, 2021, 115665.

[IKR 22] Ikram Saady, Mohammed Karim, Badre Bossoufi, Najib El Ouanjli, and Saad Motahhir. "Optimization and Control of Photovoltaic Water Pumping System Using Kalman Filter Based MPPT and Multilevel Inverter Fed DTC-IM." 2022.

[LEI 16] C. Lei, W. Xu, and D. Wei. "Control for the Centrifugal Pump in the Simulation Platform of Power Plants." 2016 International Conference on Industrial Informatics - Computing Technology, Intelligent Technology, Industrial Information Integration (ICIICII), Wuhan, China, 2016, pp. 263-267. doi: 10.1109/ICIICII.2016.0070.

[LYU 24] Lyu Guanghua, Farah Andleeb Siddiqui, Muhammad Mohsin Aman, Syed Hadi Hussain Shah, Aqsa Ali, Arsalan Muhammad Soomar, Shoaib Shaikh. "Improved Maximum Power Point Tracking Algorithms by Using Numerical Analysis Techniques for Photovoltaic Systems." Volume 21, March 2024, 101740.

[MAH 21] R. Mahto and R. John. "Modeling of Photovoltaic Module." Solar Cells - Theory, Materials, and Recent Advances. IntechOpen, Sep. 22, 2021. doi: 10.5772/intechopen.97082.

[RAF 15] Rafael Rodríguez-Ponce, Fortino Mendoza-Mondragón, Moisés Martínez-Hernández, and Marcelino Gutiérrez-Villalobos. "DTC-FPGA Drive for Induction Motors." 2015.

[SAD 23] Sadick Abubakari. "Maximum Power Point Tracking Simulation for Photovoltaic Systems Using Perturb and Observe Algorithm." Solar Radiation - Enabling Technologies, Recent Innovations, and Advancements for Energy Transition [Working Title]. IntechOpen, May 11, 2023. Crossref doi: 10.5772/intechopen.111632.

[SHU 22]	Wang S., Hussien A.G., Jia H., Abualigah L., Zheng R. "Enhanced Remora Optimization Algorithm for Solving Constrained Engineering Optimization Problems." Mathematics, 2022, 10, 1696. doi: 10.3390/math10101696.
[SIT 01]	"PV System: how to ensure safety during normal operation." Electrical Installation Guide, Electrical-Installation.org. [Online]. Available: https://www.electrical-installation.org.
[SIT 20]	"Types de cellules photovoltaïques." Énergie Plus - Le Site. [Online]. Available: https://energieplus-lesite.be/techniques/photovoltaique3/types-de-cellules.
[VAS 90]	Vas, P. "Vector Control of AC Machines." Oxford University Press, 1990, 332p.
[WEN 24]	Wentao Ding. "Comparison Between Perovskite and Silicon for Photovoltaic Cell Applications and Future Industrial Prospects." School of Engineering, The University of Edinburgh, Edinburgh, EH9 3JU, United Kingdom, 2024.
[YEK 23]	S. Yekinni, I. Asiata, O. Hakeem, and L. Mubarak. "Solar Photovoltaic Energy System." Nanogenerators and Self-Powered Systems. IntechOpen, May 24, 2023. doi: 10.5772/intechopen.108958.